Development of Ion Mobility-Mass Spectrometry Methods for Membrane Proteins Incorporated into Nanodiscs

by

Kristine F. Parson

A dissertation submitted in partial fulfillment
of the requirements for the degree of
Doctor of Philosophy
(Chemistry)
in the University of Michigan
2022

Doctoral Committee:

Professor Brandon T. Ruotolo, Chair
Professor Ryan Bailey
Professor Kristina Hakansson
Professor Ayyalusamy Ramamoorthy

Kristine F. Parson

kfparson@umich.edu

ORCID iD: 0000-0002-0194-6629

Dedication

For my Granny Val, whose loving spirit sustains me still and to Bernie Davis for finding me my best friend & teacher, Lightning

Acknowledgements

Obtaining a Ph.D. has been a surreal experience for me, I have many people to thank. First off, I would like to thank my undergraduate advisor, Dr. Lesley Putman for approaching me to do research with you and suggesting that I go to graduate school. Never in my lifetime, would I have applied to the University of Michigan Chemistry Ph.D. program if you didn't believe in me. Thank you for showing me the passion and excitement in a research lab. A massive shout out of appreciation goes towards my current Ph.D. advisor, Professor Brandon Ruotolo. Graduate school is pretty challenging, especially during a global pandemic, and your guidance and relentless commitment has brought me confidence. I lacked confidence and had an overabundance of anxiety when I started graduate school, you have been so kind and supportive, and I just really appreciate you. I am also thankful that you do really cool and interesting research and have allowed me to be creative in my own thesis adventure with membrane proteins and nanodiscs.

Next I would like to thank my thesis committee members, Professor Kristina Hakansson (Kicki) for being a supportive female role model and being so passionate about mass spectrometry, Professor Ryan Bailey for always having a smile on your face and always up for a friendly chat in the hallway or elevator, and Professor Ayyalusamy Ramamoorthy (Rams) for allowing me to do a rotation in your lab and teaching me about nanodiscs and Cytochrome P450s. Each and every one of you have provided me with intellectual feedback throughout each of my Ph.D. milestones.

Additionally, I would like to thank Professor Chuck Sanders and Manuel Castro for the engaging Zoom calls about C99. I would also like to thank Professor Richard Auchus, Neikelyn Burgos and Sang-Choul Im for providing me with the redox partner samples used in Chapter 5. Katie Gentry and Carlo Barnaba for their hard work mentoring me when I rotated in Rams lab and continuing to collaborate with me in the mass spectrometry realm. (chapters 3 and 4) I think of you both as dear friends and I cherish the time we spent together. Finally, Marina Sarcinella and Colleen Riordan from the Bailey lab, working with Colleen in the early days using their microfluidic device was very exciting to be a part of (chapter 3) and Marina, I consider you a close friend too, after your rotation in the Ruotolo lab and our countless conversations about nanodiscs, lipids, and the meaning of life.

Next, I would like to thank all the members in the Ruotolo lab, past and present. Dan and Suggie, you were both my homies when I first started, I was totally intimated by you both, but you both taught me so much in so many ways, thank you for being pivotal for my early success and being close friends even to this day. Grabbing a beer after work at Ashley's was never the same after you both left and you both also made karaoke night a blast. Sarah Fantin, for being my mentor, jamming out to Queens of the Stone Age in lab, going to interesting workout classes, and you taught me a lot about membrane proteins and IM-MS, especially using all the colored sharpies and when experiments failed you always had a good attitude and up for happy hour. Chunyi and Daniel for being my first desk buddies, thank you for the long pep talks of encouragement, you both had your own special way of cheering me up! Cara, for always having a sense of fashion and bringing laughter and joy into the lab even though you did spend most of your days in the Kennedy lab!

Now, I would like to thank the current members, starting with Varun, you and I started the same summer and we were pretty much friends from the very beginning. You, Tracy, and Harvey have been really supportive during my job search and I thank you for the countless conversations we have had when I just needed someone to bounce ideas off of. I am really excited for you and Tracy in your next adventures, you are going to be an amazing PI! Brock, you were doing an REU when I started in the summer and I am so glad you ended up coming back and joining team membrane protein and doing super neat things with the laser on the Lumos! You have also been a great friend to me, and I thank you for always being there when I needed you, especially for all the free cookie alerts (pre-pandemic)! Chae, thank you for all your conversations and help with modeling, it has been nice to have someone to talk to about the modeling stuff and kudos to you for being such a rockstar at it after Suggie graduated. I also appreciate you sharing Camille with me every chance we have. Rosendo, thank you for your fun spirt and always feeling safe to call and talk me, this offer still stands even when I move away. Devin and Anna, the two of you are a lot of fun and I admire both of your drive and willingness to try new things unprompted, Anna diving in deep with RNA and thinking positive about negative mode and Devin for tackling a new instrument, the cyclic IM! Nicole, you have a really positive attitude and ask really good questions, I have no doubt that you will be an amazing asset to the lab. Kate, I am so excited for you to be wandering down the Cryo-EM-Mass Spec interface path, as you know, I think this is the bees knees and I just over the moon that someone from the lab is moving forward with it! Best of luck!

Iliana, I have lots of words for you and I think you know what they are – you are so incredibly brave and smart, keeping pushing ahead, you got this! It has been amazing being able to mentor you and watch you grow as a scientist even in the tricky membrane protein space! You

and I have had a lot of deep conversations as well as laughed so hard that we lost our breath. Thank you for your support when I had my surgery. Last, but certainly not least: Yilin and Carolina! Together we are the three musketeers, gal pals for life! Carolina, your quirkiness and true admiration for mass spec is refreshing, you are so kind and caring you are truly one of a kind. Yilin, you have some of the best metaphors and fun-loving attitude towards everyone. Thank you for showing me new things, like foods and Zumba classes, pretty sure our favorite activities are eating and flailing around. I also want to thank you for all your help and support you gave me when I had my surgery. It really is nice knowing all of you and the friendships and memories will be cherished. You are all truly irreplaceable.

Finally, I would like to take a moment and thank my family. My mom and dad for encouraging me to always to what is right and supporting me in my quest to keep going to school for what seems like forever. This academic journey has been new for all of us and I just really appreciate you both for letting me keep working towards something, even if I didn't know what that was. The lessons I learned growing up on the farm have been invaluable. Thank you for allowing me to be a self-expressive individual. I know I was a little wild as a kiddo. I love you both very much.

Billy, I have so much to thank you for. You have been the most supportive partner I could have ever dreamed of; you have moved with me all over Michigan so that I can chase this crazy dream and now heading to North Carolina together for our next chapter. More importantly, you have fed me. I am pretty sure I would have starved or have become malnourished from eating only popcorn, dill pickles, skittles, and pizza if it wasn't for you.

Next, I want to thank Sprout and Lightning (my cat and horse). Sprout you give the best hugs and have kept me good company as I write this entire thesis document. My horse Lightning,

we grew up together, the past 24+ years have been a blast. You have taught me lessons that shaped who I am today, I have cried into your mane countless evenings and you gave me a sense of belonging when I was younger and struggling. I am positive that I am still on this planet today because of you. Thank you and as you continue to age gracefully, I hope that I can provide with the best care and comfort I possibly can.

This thesis is dedicated to my Granny Val and Bernie Davis. Loosing you both has never hurt so much; I still can't believe you are both gone. I love both so much, thank you both for guiding me into being the person I am today. I also want to thank my Grandpa Bob; I know he would be proud of me today. I remember being so sad when I got accepted into UM Chemistry that I wasn't able to call and tell you. I miss you and Go Blue!

Table of Contents

List of Figures

List of Appendices

Abstract

Membrane proteins (MPs) are vital therapeutic targets which play important roles in a multitude of cellular functions. MPs interact intimately with the cellular membranes in which they embed. Interactions between proteins and ligands such as membranous lipids and other small molecules can affect MP structure and function. Ion mobility-mass spectrometry (IM-MS) has recently emerged as a valuable tool for interrogating the interactions between proteins and ligands, offering direct measurements of protein-complex stoichiometry, ligand binding strengths, and stabilities. This dissertation seeks to extend IM-MS technologies to study the relationships between MPs and their lipid environment, probing directly long-standing questions surrounding the functional role of local lipid environments on MP structure and function.

In chapter 2 we develop a workflow for studying different MP classes using various solubilization techniques and discuss the implications such membrane mimetics carry in the context of the embedded protein structures. We utilize four different MPs that vary in both the way that they span the membrane and in terms of their native oligomeric states. Specifically, we utilize a small multidrug resistance transporter (GDX), a transmembrane protein that has a unique antiparallel orientation, WT and the L16P disease-associated mutant form of peripheral myelin protein (PMP22), a transmembrane protein which occupies both a monomeric and dimeric state, and Cytochrome P450 (CYP), a monotopic membrane-bound enzyme. Each MP system was studied within at least two different mimetics, including: detergent-based micelles, lipid-bicelles, or lipid-nanodiscs (NDs). In general, we find evidence of differences in MP

structure, oligomeric state, and ligand binding that appears to depend strongly on the membrane mimetic used.

In chapters 3, 4 and 5 we focus on CYP and deploy IM-MS and collision induced unfolding (CIU) to study how this centrally important enzyme interacts with binding partners, ligand and its membrane environment in order to carry out essential functions. In chapter 3, we use NDs of carefully designed compositions to study the role of different lipid environments and ND scaffolding proteins on CYP structure. We find that CYP CIU, and by extension its structure, strongly depends on its local environment, and that more native membrane environments can result in more compact and more destabilized CYP forms. In chapter 4 we focus on CYP ligand binding and develop CIU classifiers capable of differentiating CYP binders based on their mode of attachment to the protein and their hydrophilicities. The ability of our CIU assays to differentiate CYP-ligand complexes to discern hydrophobic from hydrophilic binders relates directly to the proximity of the CYP active site to the biological membrane and supports the conclusion that lipids are significantly involved in structure of the CYP active site. In chapter 5 we study the interactions between full length CYP, cytochrome b5 (cytb5), and P450 oxioreductase (POR) within NDs. When we co-incubated these proteins with NDs we observed no direct evidence of stable complexes, but significant alterations in CYP CIU, suggesting changes in CYP structure when present within the same local membrane environment to cytb5 or POR. We observe evidence of additional lipid binding events within POR when reduced by NADPH, suggesting deeper membrane engagement when the protein is in its reduced state. We conclude in Chapter 6 by discussing the future of MP structural biology and how this dissertation works has emphasized the impact that a membrane environment has on the membrane protein structure.

Chapter 1 **Introduction**

The study of protein structure, function, and complex formation is of great importance for advancing our understanding of cellular biochemistry. Proteins comprise the molecular machines that are responsible for performing almost all cellular activity. Therefore, a comprehensive understanding of protein function has the ability to lead to insights into human disease, as well as the downstream development of groundbreaking therapeutics.[1] There are three main types of proteins: fibrous, globular and membrane.[2] Of these main types, and the focus of this thesis are membrane proteins, which are important for many cellular processes, including cell to cell communication, energy production, signal transduction, facilitated/passive diffusion, markers for cell identification, and enzymatic reactions.[3,4] These proteins are unique because they are embedded in the cellular membrane comprised of not only lipids, but sterols, carbohydrates, and other proteins that regulate their function.[5] The study of membrane proteins lags significantly behind that of their soluble analogs, given their hydrophobic nature, making them challenging analytes to work with in standard aqueous solutions.[6,7] In order to enable the study of structurally and functionally sound membrane proteins, a variety of membrane mimetics have been developed to stabilize such proteins outside of cell membranes.[8–10] This chapter will consist of a review of the general properties, challenges, and methods for studying membrane proteins, with an emphasis on development of methods for studying membrane protein structure and stability. Special emphasis will be given to nanodisc (ND) based membrane mimetics and ion mobility-mass spectrometry (IM-MS) technologies, which function as the methodological focus of this thesis.

1.1 Membrane Proteins

Membrane proteins (MPs) are important therapeutic targets which play vital roles in cellular function;[3,11] it is estimated that they represent up to 30% of the eukaryotic proteome, however only 3% of the unique structures in the protein data bank (PDB) are MPs.[11–13] Membrane proteins represent over 60% of therapeutic drug targets, and nearly 80% of drugs approved by the FDA act on membrane proteins.[3,14,15] (Figure 1-1) As the structure of a protein is closely linked to its function, the characterization of MPs is vital to elucidating their involvement in disease and in assessing their potential druggability.[16] Despite this, MPs are underrepresented in structural databases due to challenges associated with their hydrophobicity and with difficulties surrounding the acquisition of high-purity samples.

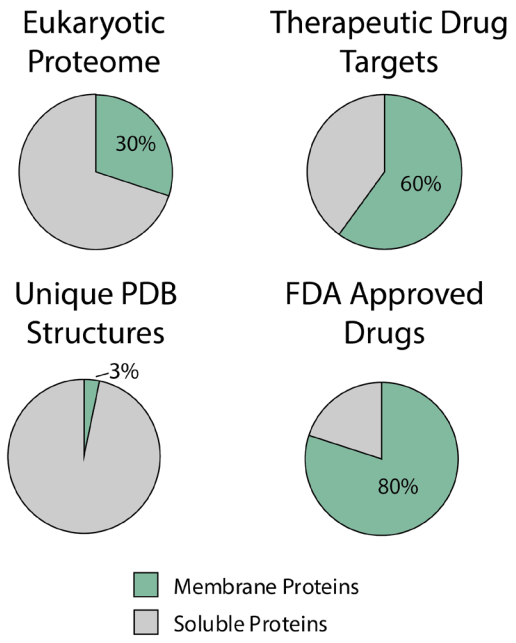

Figure 1-1 Membrane protein stats.Percentage of membrane proteins in the eukaryotic proteome and percentage of membrane proteins in the PDB.

Current structural biology methods, such as cryo-electron microscopy (cryo-EM) and X-ray crystallography have been used to study the high-resolution structures of membrane proteins. However, capturing such data on protein-ligand and protein-protein interactions remains a challenge.[17,18] To circumvent these challenges, MPs are often artificially modified in order to increase their stability.[4,6,19–21] However, these approaches can often alter the native structures or activities of the target proteins.[4,22]

Another drawback of standard structural biology techniques is that information associated with the flexibility of protein structures can difficult to acqauire.[4,23] Methods such as nuclear magnetic resonance (NMR) have been employed to elucidate the dynamic nature of proteins, but NMR is incompatible with high-throughput analysis, and typically requires large amounts of homogenous samples, expensive isotope-labeling reagents, and is limited by the size of the protein being studied.[4] Thus, there is an urgent need in the structural biology space for a method which can rapidly detect, identify, and structurally characterize protein-ligand interactions in a label-free manner, all while using minimal amounts of sample.

1.2 Solubilization methods

To conserve the native structure of MPs outside of cellular membranes, multiple solubilization techniques have been developed. From a historical perspective, detergent micelles have been the most widely used technique for solubilizing purified membrane proteins, and they remain widely used today.[4,24] Detergents vary in terms of their structures and charges, but all possess the ability to form micelles that can encapsulate membrane protein targets. The hydrophobic membrane protein residues interact with the hydrophobic tails of the detergent, and their polar head groups allow the complex to be solubilized in aqueous solutions.[13,24,25] Among the many newer approaches that seek to mimic the native lipid bilayer environment, bicelles and NDs are most commonly used in conjunction with MS.[26–28] In bicelles, detergents are used to surround the edges of the bilayer to create a fluid, yet discrete, structure.[29,30] Within NDs, the lipid bilayer is embraced by an amiphatic scaffolding belt, which can be composed of either protein, peptide or polymer.[31] Other bilayer-based solubilization techniques include styrene maleic acid lipid particles (SMALPs),[32,33] amphipols,[34] and lipid vesicles or liposomes.[35]

The three methods used in this thesis: detergent micelles, bicelles, and nanodiscs, are shown schematically in Figure 1-2**.** The concentration at which detergents form micelles is called the critical micelle concentration (CMC) in membrane protein purification and analysis protocols. MP purification strategies typically involve the optimization of the detergent, its concentration, and the general solution conditions in order to retain native MP structures.[24,25]

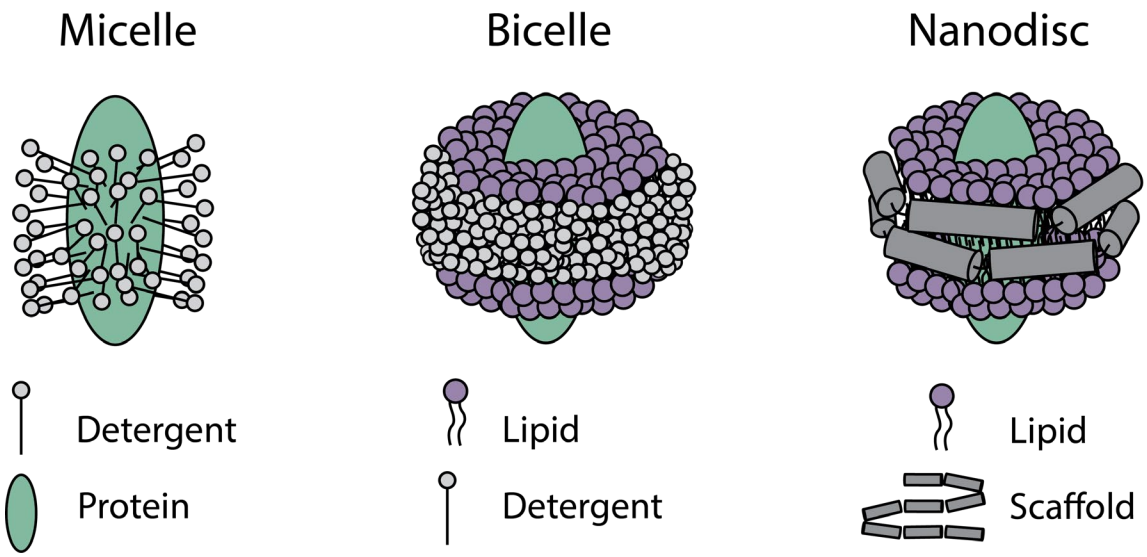

Figure 1-2 Membrane Mimetics.Detergent micelle, bicelles and nanodiscs are all solubilization techniques for membrane proteins employed in this work

In an effort to better mimic the native cellular membrane in which the MPs exist *in vivo* there have been recent developments in methods able to create model lipid bilayers encompassing a wide range of compositions. There are many approaches to create such a bilayer mimic, each with advantages and disadvantages.[26–28] As only bicelles and NDs are utilized in this thesis, they will be the focus of the review provided in this chapter. In both bicelles and NDs, MPs are encapsulated by an amphipathic lipid bilayer, which consists of one or more lipid type. In bicelles, detergents are used to surround the edges of the bilayer to create a fluid, yet discrete, bilayer structure.[29] In NDs, a scaffold protein or peptide is used in lieu of detergents.[36] For both

methods, the thickness of the bilayer,[37] the overall sizes of the particles,[36,38] and the composition of lipids that make up the bilayer[39,40] can be optimized for protein incorporation. The composition of the lipids must be carefully optimized as lipid head and tail properties can affect the bilayer fluidity as well as its curvature.

1.2.1 Nanodiscs

One membrane protein mimetic that has recently gained traction for MS-associated studies are NDs, which were first developed by the Sligar lab.[41,42] As previously described, NDs are a soluble lipid bilayer that is stabilized by a scaffolding belt, the Sligar NDs are composed of two membrane scaffold proteins (MSPs). MSP was derived from Apolipoprotein A1 (ApoA1), the main protein component of human high-density lipoproteins (HDL).[43] This scaffolding protein allows for homogenous size distributions of the NDs.[41] Due to the popularity and utility of MSP based NDs, there have been extensive work done in order to expand the size and

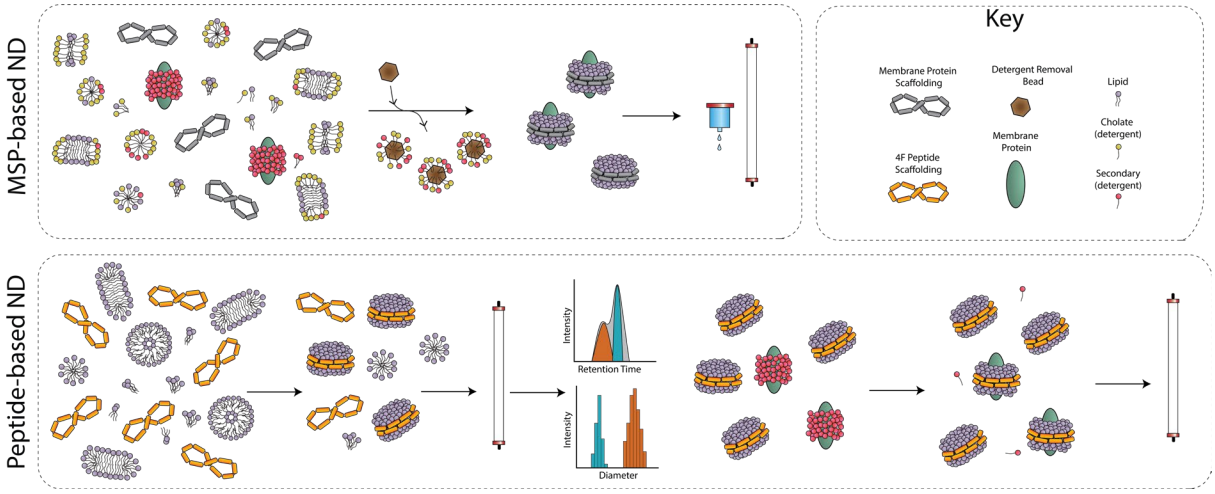

Figure 1-3 Comparative illustration of the two main NDs preparations, MSP based NDs and peptide based NDs. MSP based NDs, membrane protein, scaffolding belt, lipids, secondary detergent and cholate detergent are mixed and incubated, the addition of detergent removal beads allows for self-assembly, the final step is to purify with NiNTA and/or SEC. Peptide based NDs are a detergent free preparation, first mixing peptide scaffolding belt and lipids to form lipid discs which are characterized using SEC and DLS, the appropriate sized disc is chosen and protein is incorporated finishing with SEC purification and subsequent buffer exchange.

dynamics of MSP NDs. For example, the addition of up to three α- helices within the original ApoA1 sequence, allows for an increase in the ND diameter, from 9 nm to 13 nm[36]. This larger diameter allows for the incorporation of larger membrane proteins or protein complexes. In addition, purification tags, such as a 6-histadine tag for Ni-NTA purification, allow for downstream purification to clean up of ND samples[31]. (Figure 1-3)

The Sligar protocol for preparing NDs is performed by mixing lipids and MSP, with or without the MP of interest. This mixture is solubilized in detergent (typically a mixture of cholate and the secondary detergent, which is specifically the detergent the target MP is solubilized within), next the detergent is removed using detergent removal beads or dialysis, which causes spontaneous ND assembly (Figure 1-3).[31,36] The standard bulk bead-based process can take between 2 and 18 hours.[36,41] To expedite the ND formation process, a microfluidic approach has been developed which dramatically decreases the amount of materials and time required for ND assembly.[44] Using these microfluidic devices has been applied to wide range of biological and chemical methods and successfully decreased both the time and the regents used.[45–48] Using lower sample concentrations is important due to the difficulties associated with obtaining samples containing high MP concentrations.

Other types of NDs have also recently gained traction for MP characterization, using scaffolds other than MSP to stabilize the lipid bilayer. These scaffolds include styrene-maleic acid (SMA) and peptide-based belts.[49,50] One of the advantages of the SMA and peptide scaffolds is that they are detergent free preparations.[49,51] One of the concerns with the MSP preparations is that the use of detergents, which can act to destabilize some MPs and disrupt lipid uniformity.[52–55] However, SMA NDs are challenging to construct using multi-lipid compositions, and often require multiple freeze-thaw cycles to form stable NDs, which can also threaten MP

stability and structure. Additionally, SMA NDs are sensitive to changes in pH and divalent ion concentrations, which can be a concern for the application of downstream activity assays that often require buffers other than those used for initial ND formation.[56] Efforts have been made to create more robust SMA membrane mimetics and thus lessen the disadvantages discussed above.[57]

Peptide NDs, such as those based on 4F peptide scaffolds, are peptide mimics of ApoA-I, these peptides have been extensively studied for their anti-inflammatory, antioxidant, and antiatherogenic properties, as they are known to form peptide-lipid complexes that incorporate cholesterol from peripheral tissues and interact with endogenous lipoproteins in the plasma.[58,59] The formation of ApoA-I NDs using MSP require the presence of MP-associated detergent and cholate. Such detergents can be challenging to fully remove from samples following ND assembly, resulting in residual surfactant and dose-limiting toxicity in clinical trials. [60,61] Because peptide based NDs are detergent free they make an attractive platform for cardiovascular therapeutics. Various peptide-based ND scaffolds designed to mimic the ApoA-I protein have been synthesized. 22A peptide NDs were the first ApoA-I mimetic peptide ND to reach clinical development,[62] whereas 4F was created by substituting leucine (Leu) residues for phenylalanines (Phe), to improve ND flexibility and lipid binding affinity [63,64]. The principle drawback associated with using peptide based NDs for MP analysis is that since the disks must be pre-formed, the incorporation of MPs must occur through direct insertion into fully formed NDs rather than through co-assembly (Figure 1-3). In addition, due to the detergent-free nature of this method for ND preparation, diluting the sample volume so that there is less than 1% detergent in solution is a necessary step, and this dilution step can lead to compromised MP structures, especially for multi-pass transmembrane proteins, in some cases.

1.3 Membrane Protein Types

MPs can be classified broadly into two categories, integral and peripheral, this classification is based on formats of their interacts with the cellular membrane.[65,66] Peripheral MPs are attached to the membrane through interactions with the lipids, and are thus not fully embedded into the membrane (pink in Figure 1-4).[67,68] Whereas integral membrane proteins

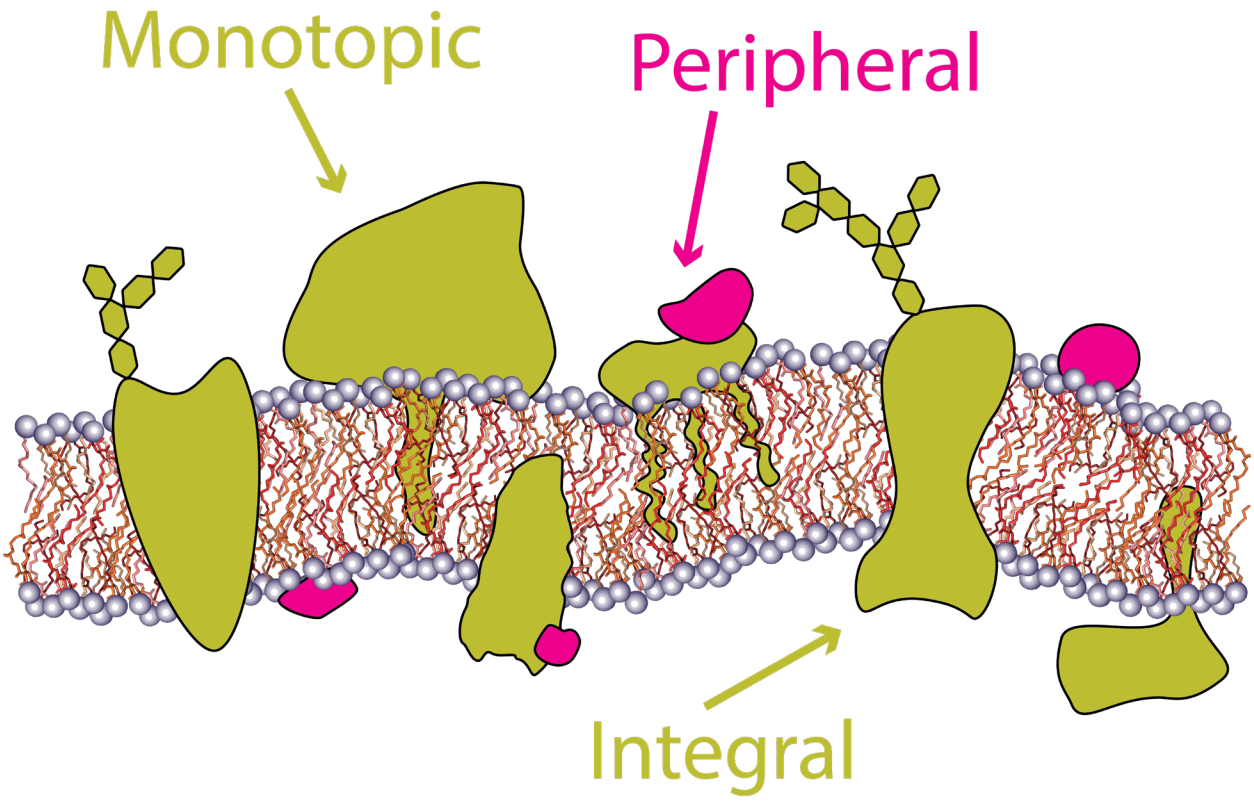

Figure 1-4 Membrane protein types. Peripheral (pink) proteins interact with the surface of the membrane only, while integral (green) MPs are permanently embedded into the biological membrane, integral MPs can span the entire membrane multiple times and monotopic MPS only penetrate part of the bilayer.

(green in Figure 1-4) are permanently attached to the biological membrane, and possess one or more regions that are embedded into the membrane .[69] Integral MPs are known to comprise 33% of all small molecule drugs target.[14] There are various degrees of how integral MPs interact with biological membranes and can be further classfied into additional categories: monotopic,[70,71] bitopic,[72,73] and polytopic.[74–76] For example GPCRs, which possess seven

transmembrane domains, are widely-studied polytopic or multi-pass transmembrane proteins.[77] Monotopic MPs are only embedded into a single face of the membrane and are severely underrepresented in the PDB , as of 2019 only 25 nonredundant structures had been deposited, constituting ~0.06% of identified monotopic sequences.[70,71] Bitopic, or single pass, membrane proteins are those that only pass through the membrane once, and this MP category includes some transmembrane receptor proteins.[78] Additionally, some membrane-bound enzymes have bitopic structures, these include many of the cytochrome P450 monooxygenases (CYPs) that are responsible for metabolizing a wide array small molecules.[79,80] Note that CYPs can also be monotopic (e.g. CYP 3A4),[81] meaning they possess a hydrophobic helix and active site that is embedded into the cellular membrane.

1.3.1 Cytochrome P450

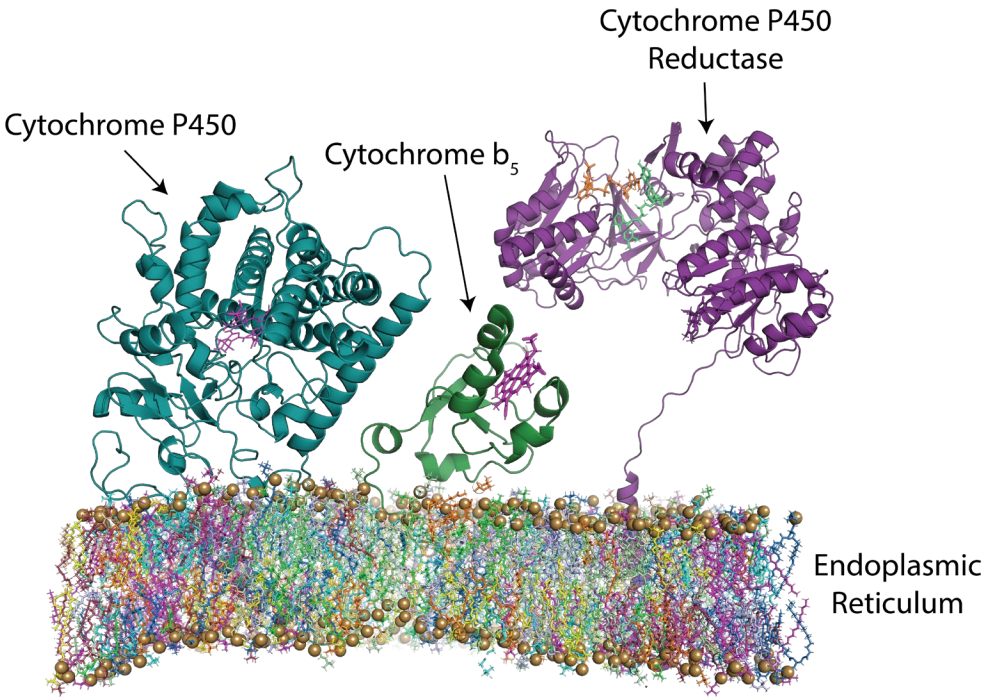

CYPs represent an important class of monotopic/bitopic MP monooxygenases involved in drug metabolism. There are 57 human genes that code various CYP isoforms and about 13

Figure 1-5 Cytochrome P450 and redox partners. Cytochrome P450 (teal) Cytochrome b5 (green)and cytochrome P450 reductase (purple) in a rendition of the endoplasmic reticulum bilayer

human isoforms are responsible for the metabolism of more than 80% of pharmaceutical drugs and are housed in the endoplasmic reticulum (ER).[82–87] The major CYP isoforms which are involved in drug metabolism are mainly located in the liver whereas other CYP isoforms that are in involved in steroid metabolism are located to mainly the adrenals and gonads with smaller amounts expressed in the brain, placenta, and heart.[88] CYPs carry out the first step of metabolism for a variety of hydrophobic compounds. The most common reaction CYP catalyzes is the insertion of a hydroxyl group into a hydrophobic substrate, breaking a C-C or C-H bond. For CYP to fulfill a catalytic function, two electrons or reducing equivalents are required for this catalytic cycle which originates from either NADPH or NADH, depending on which protein redox partner reduces CYP. Either cytochrome P450 oxioreductase (POR) donates both electrons, utilizing NADPH as the cofactor, or cytochrome b5 (cytb5) can provide the second electron needed, also originating from NADH[83,89] (Figure 1-5). By increasing the hydrophilicity of the substrates involved, CYP increases the speed at which some drugs are metabolized and excreted. A better understanding of how CYP metabolizes drugs, specifically multiple drugs or compounds at a time, is crucial to understanding and predicting potentially dangerous drug-drug interactions.[90–93] In addition, CYPs are key targets in the development/treatment of several health conditions including breast cancer, prostate cancer and heart disease.[94–96]

1.4 Mass Spectrometry of Membrane Proteins

MS has recently emerged as a method especially suited for the analysis of native MPs, due in part to its ability to handle complex mixtures and lower sample concentrations.[34,97–105] For the purposes of this work we will focus on ESI (and nESI) methodologies, which dominates the

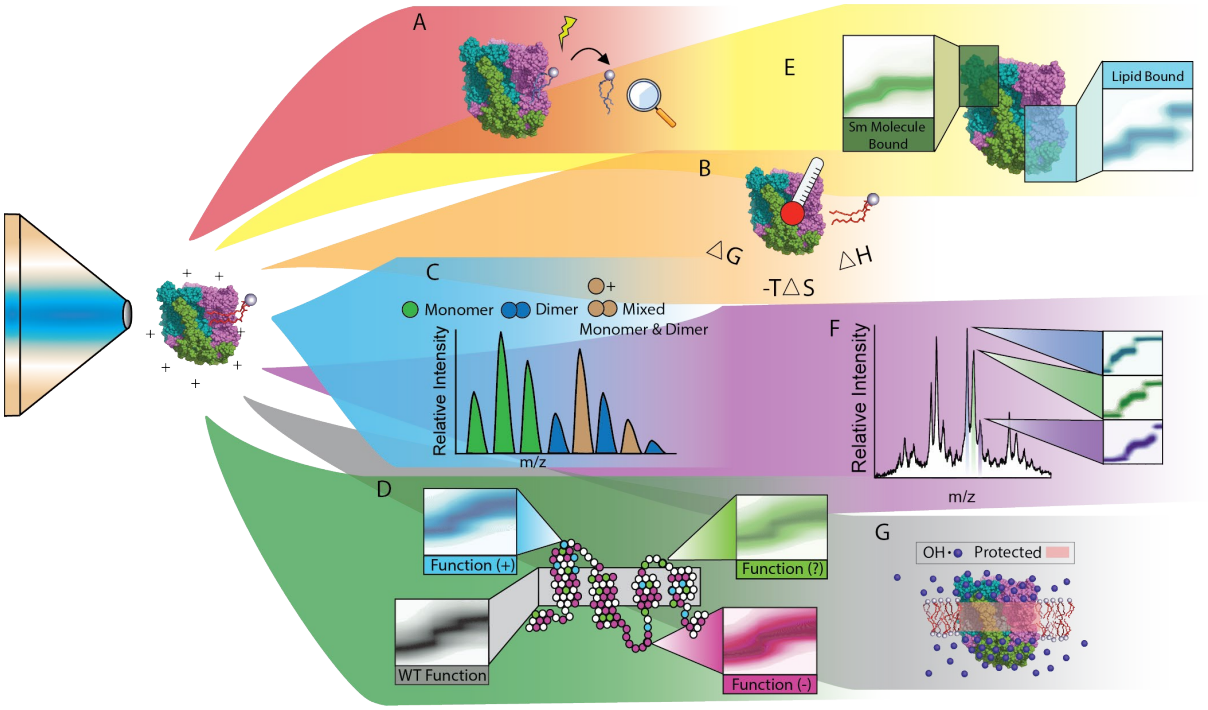

Figure 1-6 Summary of various MS-related measurements associated with MP stability assessments. **A**) Identification of endogenous lipid binding. (B) Thermodynamics of lipid binding to membrane protein. **C**) Oligomeric state assignment. **D**) Evaluation of disease state mutations in the amino acid sequence. **E**) Site-selective ligand binding events. **F**) Resolving multiple simultaneous ligand-bound states. **G**) Oxidative labeling.

native MS (nMS) analysis of MPs, which seeks technology and methods capable of retaining the *in vivo* structures and non-covalent complexes for direct MS measurements and analysis. Membrane protein ions generated through ESI or nESI for nMS analysis are most often still encapsulated in one of the solubilization agents mentioned above, and therefore, collisional activation must be applied to remove bound detergents or lipids from the target membrane protein ion.[100] Additionally, the independent solubilization agents themselves, e.g. detergents/lipids, also ionize and can thus result in an abundance of noise signals in the resulting native mass spectra. While time-of-flight (ToF) mass analyzers have shown great success in this field, higher resolution technologies, such as Orbitrap mass analyzers,[106] can be helpful for resolving the intended membrane protein signal from noise. It is important to note that not all solubilization agents are equally effective in this endeavor, and screening detergents and solution

conditions as well as optimizing instrument parameters are necessities for striking the delicate balance between the removal of solubilization agents and optimizing the stability of the native MP structure.[103] However, with successful optimization, nMS has been used to study discrete lipid[103,107–110] and ligand binding[111] (Figure 1-6A and F) events, as well as to quantify the thermodynamics associated with lipid binding[112–115] (Figure 1-6B) and specific protein−protein interactions associated with a wide range of membrane proteins[40,116,117] and their functional assemblies[30,35,118–121] (Figure 1-6C).

Deeper structural insights can be gained from MPs by deploying liquid chromatography-mass spectrometry (LC-MS) techniques in combination with chemical labeling, where the solvent- accessible sites of native MPs are labeled permanently or reversibly prior to digestion. Hydrogen deuterium exchange (HDX),[122–125] chemical cross linking (CXL),[126–128] and fast photochemical oxidation of proteins (FPOP)[129–132] have all been used to probe MP tertiary structures, as well as the interactions between MPs and both protein binding partners and solubilization agents (Figure 1-6G). Much of the mechanics of MS-based footprinting tools targeting MPs remain similar to those directed toward water-soluble protein systems and typically provide a valuable readout capable of monitoring the conformational responses of MPs upon stimulation, both temporally and spatially. Among the labeling techniques surveyed here, FPOP has most often been applied to assess MP structure and stability. Favorable attributes of FPOP for MP-associated applications include its fast labeling times, the irreversible nature of the chemical modifications generated, the neutrality of pH maintained during the measurement, and its ability to access nonpolar residues for labeling.

1.4.1 Ion Mobility-Mass Spectrometry

In recent years, native ion mobility-mass spectrometry (IM-MS), has emerged as a robust structural biology tool capable of handling complex mixtures in a high-throughput manner. With the use of membrane mimetics such as NDs the native conformation of MPs is retained and

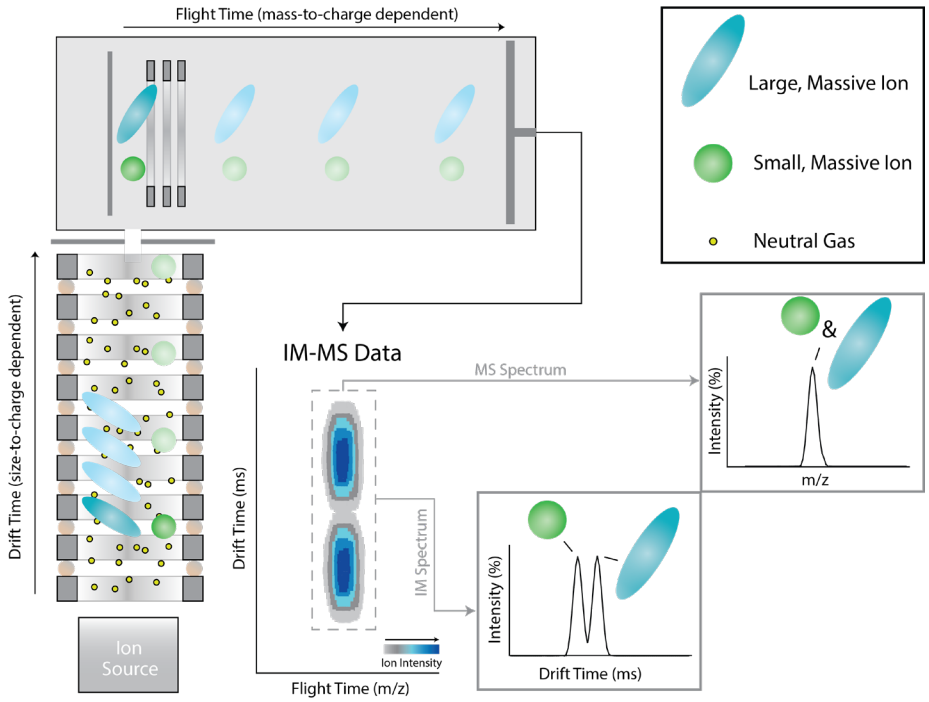

Figure 1-7 IM-MS Instrumentation. After the nESI process, ions are generated in the source and enter the drift cell filled with inert buffer gas where the ions are allowed to traverse the drift tube under the influence of a weak electric field. Ions are separated based on the ions shape, charge, and size, The more elongated (blue) ions collide with buffer gas more frequently compared to the smaller compact (green) ions, the larger ions are therefore slowed down by the inelastic collisions and have a longer arrival drift time. To extract m/z information, ions are injected into an orthogonal acceleration time-of-flight mass analyzer. A 3-D data set is achieved by plotting the drift time (ms) as a function of m/z ratio, and the third dimension being ion intensity values displayed as colorimetric intensity.

studied using IM-MS[34,133–136] IM separates the ions based on their size, shape, and charge. In native IM-MS experiments, we can seperate different protein ion conformations, as shown in Figure 1-7.

The IM-MS data included in this thesis was collected using a Waters Synapt G2 Q-IM-ToF system, utilizing a travelling wave (T-wave) ion mobility (TWIM) separator. Briefly, in our IM-MS experiments nESI is used to ionize and desolvate intact protein complexes,[137] the ions then travel through a quadrupole filter and into a T-wave ion guide that functions as an ion trap,

where collision induced unfolding (CIU) and collision induced dissociation (CID) experiments can be performed.

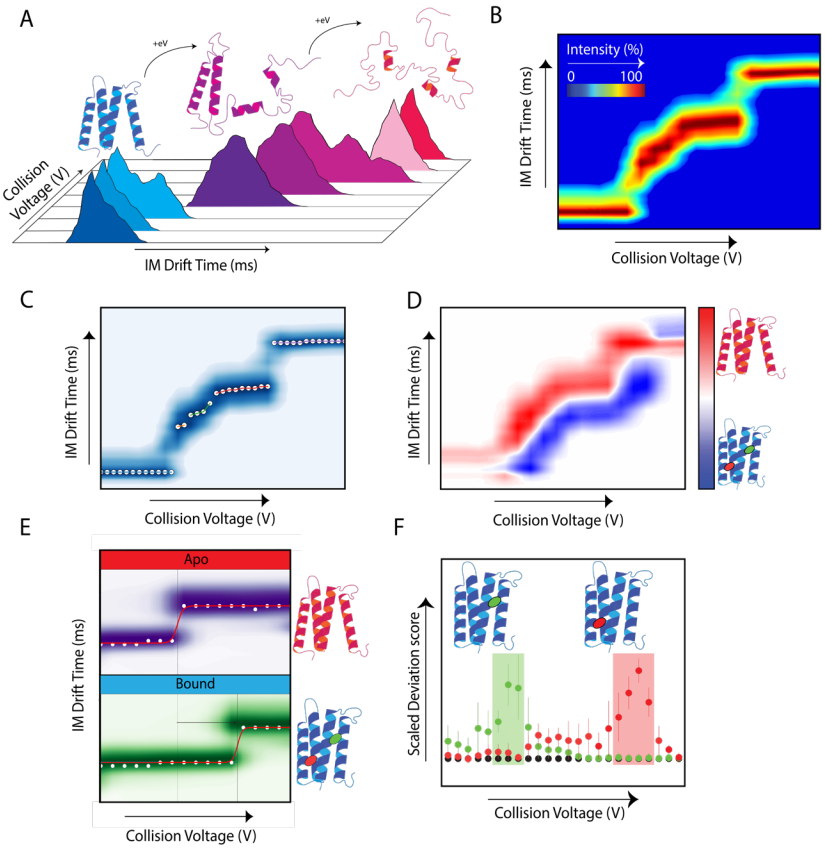

Figure 1-8 Collision Induced Unfolding. A) CIU is the stepwise activation of a protein or other macro-biomolecule as the protein unfolds, arrival time distributions can capture the resulting shift in conformation) using CIUSutie2 these can be converted in a CIU fingerprint with intensity as a heat plot C) feature detection D) RSMD plots illustrating unfolding differences between ligand bound and apo E) Stability shift analysis (CIU50) to illustrate stability shifts upon ligand binding and F) Classification

The addition of IM separation coupled to MS is beneficial for nMS of MPs. Additionally, IM- MS platforms include supplemental trapping regions that can provide opportunities to perform collisional activation aimed at both the liberation of MPs from their solubilization agents as well as the dissociation of detergent or lipid clusters, which can greatly increase signal quality. The energy experienced by ions in these trapping regions is a function of an accelerating potential (collision voltage, CV), and ideally, optimized solubilization systems can be removed

at relatively low CVs. At CVs higher than the threshold for removal of the solubilization agents, the MP can experience CIU, and this unfolding can be tracked through the resulting IM arrival time distribution.[138] These CIU experiments are valuable for assessing the relative gas-phase stability of MP complexes[110,139] and have been used in the past to classify soluble protein systems.[140] The addition of IM to nMS allows for the elucidation of protein stability as a function of lipid and or ligand binding[7,139,141,142] (Figure 1-6F), amino acid sequence in relationship to disease pathologies[121,143] (Figure 1-6D), and lipid and/or ligand binding locations[141] (Figure 1-6E). The study of MPs represents an exciting, high- risk, high-reward area of research with the potential for groundbreaking medical discoveries. Methods to study MP stability in native-like environments are essential to understanding how they perform their cellular functions and, as many MPs are implicated in human disease, how pharmaceuticals may be developed to correct their dysfunction. Due to their relative insolubility in aqueous solutions and the complex environments in which they exist natively, MPs are challenging analytes, and MS has emerged as a frontier tool for determining their stabilities.

1.5 Summary

NDs are an appealing construct for MP characterization due to their ability to stabilize native MP structure by mimicking a membrane bilayer environment. However, there are multiple variables in ND construction that have the potential to impact the structure and function of MPs, including lipid composition and scaffold material. While this is a promising technology for MP solubilization, questions remain about the effects of these variables on MP dynamics and how the ND composition might alter function, such as drug binding.

CYP enzymes play key roles in the synthesis of a broad range of bio-active molecules and are primarily responsible for the metabolism of both pharmaceutical and cytotoxic

compounds.[82,144–146] Despite the pharmacological importance of this class of enzymes, many unanswered questions persist regarding the relationship between the dynamic structure of CYP and its myriad of functions. While atomic-resolution structures of many CYP isoforms are available, all lack the hydrophobic α-helix region of the protein (Figure 1-5), which is critical for the association of CYPs with biological membranes.[147–149] Much regarding the impact of lipid binding and membrane composition on this CYP region is currently unknown, including the presence of allosteric networks that may link the local membrane environment to ultimate enzyme activity. To extract structural information from full length CYP isoforms, in the context of chemical mixtures that include drugs and the constituents of biological membranes, this thesis aims to develop approaches that utilize lipid NDs as constructs for gas-phase ion IM-MS analysis.

We focus on IM-MS and CIU to study MPs in NDs, utilzing a state-of-the-art IM separator in combination with an MS device optimized for the detection and measurement of high molecular weight proteins. IM-MS thus produces a robust dataset that informs the dynamic structure of proteins, as well as potential ligand binding, or drug binding events. Chapter 2 focuses on the effects of the following solubilization techniques: detergent micelles, bicelles, and nanodiscs has on the gas phase unfolding on membrane protein structure. We were able to detect significant differences in protein oligomeric state, charge state distribution and unfolding trajectories for each mimetic chosen. Chapters 3, 4, and 5 are focused primarly on CYP. In chapter 3 we illustrate, using NDs, how the local lipid environment in which the CYP is housed can significantly impact the stabilities and structures of the embedded proteins. In this chapter we use a mixed lipid ND that reflects the composition of the endoplasmic reticulum, as well as compare other various ND design aspects such as belt types and disc size. Chapter 4 focuses on

CYP ligand binding, using CIU methods to detect changes in ligand binding were not straightforward, but when machine learning based classification was utilized, we were able to detect changes in ligand binding differentiating type I substrates from type II inhibitors, as well as based on ligand hydrophobicity. Chapter 5 brings together the CYP redox partners and observed changes with NADPH. When redox partners POR and b5 are co-inserted into NDs with CYP, the latter protein undergoes dramatic changes in stability and structure. Furthermore, POR membrane engagement is observed to be dependent upon NADPH binding to the protein. In Chapter 6, we conclude by summarizing our findings and discuss their impacts on the MP and IM-MS communities. In this last chapter we will also propose future directions related to membrane protein drug design, pushing boundaries on obtaining valuable structure information by combining nMS with cryoEM, as well as pairing and expanding currently available solubilization techniques.

Bibliography

(1) Osadchy, M.; Kolodny, R. Maps of Protein Structure Space Reveal a Fundamental Relationship between Protein Structure and Function. *Proc. Natl. Acad. Sci. U. S. A.* **2011**, *108* (30), 12301–12306.

(2) Chan, H. S.; Dill, K. A. The Protein Folding Problem. *Phys. Today* **2008**, *46* (2), 24.

(3) Fagerberg, L.; Jonasson, K.; von Heijne, G.; Uhlén, M.; Berglund, L. Prediction of the Human Membrane Proteome. *Proteomics* **2010**, *10* (6), 1141–1149.

(4) Lacapère, J.-J.; Pebay-Peyroula, E.; Neumann, J.-M.; Etchebest, C. Determining Membrane Protein Structures: Still a Challenge! *Trends Biochem. Sci.* **2007**, *32* (6), 259–270.

(5) Nicolson, G. L. The Fluid—Mosaic Model of Membrane Structure: Still Relevant to Understanding the Structure, Function and Dynamics of Biological Membranes after More than 40years. *Biochim. Biophys. Acta - Biomembr.* **2014**, *1838* (6), 1451–1466.

(6) Hendrickson, W. A. *Atomic-Level Analysis of Membrane-Protein Structure*; 2016; Vol. 23.

(7) Konijnenberg, A.; Van Dyck, J. F.; Kailing, L. L.; Sobott, F. Extending Native Mass Spectrometry Approaches to Integral Membrane Proteins. *Biological Chemistry*. 2015.

(8) Majeed, S.; Ahmad, A. B.; Sehar, U.; Georgieva, E. R. Lipid Membrane Mimetics in Functional and Structural Studies of Integral Membrane Proteins. *Membranes (Basel).* **2021**, *11* (9).

(9) Klöpfer, K.; Hagn, F. Beyond Detergent Micelles: The Advantages and Applications of Non-Micellar and Lipid-Based Membrane Mimetics for Solution-State NMR. *Prog. Nucl. Magn. Reson. Spectrosc.* **2019**, *114–115*, 271–283.

(10) Thoma, J.; Burmann, B. M. Fake It 'Till You Make It-The Pursuit of Suitable Membrane Mimetics for Membrane Protein Biophysics. *Int. J. Mol. Sci.* **2020**, *22* (1), 1–22.

(11) Wallin, E.; Heijne, G. Von. Genome-Wide Analysis of Integral Membrane Proteins from Eubacterial, Archaean, and Eukaryotic Organisms. *Protein Sci.* **2008**, *7* (4), 1029–1038.

(12) Shimizu, K.; Cao, W.; Saad, G.; Shoji, M.; Terada, T. Comparative Analysis of Membrane Protein Structure Databases. *Biochim. Biophys. Acta - Biomembr.* **2018**, *1860* (5), 1077–1091.

(13) Moraes, I.; Evans, G.; Sanchez-Weatherby, J.; Newstead, S.; Stewart, P. D. S. Membrane Protein Structure Determination-The next Generation ☆☆. **2014**.

(14) Santos, R.; Ursu, O.; Gaulton, A.; Patrícia Bento, A.; Donadi, R. S.; Bologa, C. G.; Karlsson, A.; Al-Lazikani, B.; Hersey, A.; Oprea, T. I.; Overington, J. P. A Comprehensive Map of Molecular Drug Targets. **2017**.

(15) Yıldırım, M. A.; Goh, K.-I.; Cusick, M. E.; Barabási, A.-L.; Vidal, M. Drug—Target Network. *Nat. Biotechnol.* **2007**, *25* (10), 1119–1126.

(16) Dowhan, W.; Vitrac, H.; Bogdanov, · Mikhail. Lipid-Assisted Membrane Protein Folding and Topogenesis. *Protein J.* **1234**, *38*, 274–288.

(17) Pyle, E.; Kalli, A. C.; Amillis, S.; Hall, Z.; Lau, A. M.; Hanyaloglu, A. C.; Diallinas, G.; Byrne, B.; Politis, A. Structural Lipids Enable the Formation of Functional Oligomers of

the Eukaryotic Purine Symporter UapA. *Cell Chem. Biol.* **2018**, *25* (7), 840-848.e4.
(18) Peng, T.; Yuan, X.; Hang, H. C. Turning the Spotlight on Protein–Lipid Interactions in Cells. *Curr. Opin. Chem. Biol.* **2014**, *21*, 144–153.
(19) Bai, X.; Yan, C.; Yang, G.; Lu, P.; Ma, D.; Sun, L.; Zhou, R.; Scheres, S. H. W.; Shi, Y. An Atomic Structure of Human γ-Secretase. *Nature* **2015**, *525* (7568), 212–217.
(20) Thonghin, N.; Kargas, V.; Clews, J.; Ford, R. C. Cryo-Electron Microscopy of Membrane Proteins. *Methods* **2018**, *147*, 176–186.
(21) Parker, J. L.; Newstead, S. 5 Membrane Protein Crystallisation: Current Trends and Future Perspectives. *Adv. Exp. Med. Biol.* **2016**, *922*, 61–72.
(22) Kermani, A. A.; Macdonald, C. B.; Burata, O. E.; Ben Koff, B.; Koide, A.; Denbaum, E.; Koide, S.; Stockbridge, R. B. The Structural Basis of Promiscuity in Small Multidrug Resistance Transporters. *Nat. Commun. 2020 111* **2020**, *11* (1), 1–9.
(23) Alfonso-Garrido, J.; Garcia-Calvo, E.; Luque-Garcia, J. L. Sample Preparation Strategies for Improving the Identification of Membrane Proteins by Mass Spectrometry. *Anal. Bioanal. Chem.* **2015**, *407* (17), 4893–4905.
(24) Haffke, M.; Duckely, M.; Bergsdorf, C.; Jaakola, V. P.; Shrestha, B. Development of a Biochemical and Biophysical Suite for Integral Membrane Protein Targets: A Review. *Protein Expr. Purif.* **2020**, *167*, 105545.
(25) Cheng, X.; Kim, J.-K.; Kim, Y.; Bowie, J. U.; Im, W. Molecular Dynamics Simulation Strategies for Protein-Micelle Complexes. *Biochim. Biophys. Acta* **2016**, *1858* (7 Pt B), 1566.
(26) Warschawski, D. E.; Arnold, A. A.; Beaugrand, M.; Gravel, A.; Chartrand, É.; Marcotte, I. Choosing Membrane Mimetics for NMR Structural Studies of Transmembrane Proteins. *Biochim. Biophys. Acta - Biomembr.* **2011**, *1808* (8), 1957–1974.
(27) Cross, T. A.; Sharma, M.; Yi, M.; Zhou, H.-X. Influence of Solubilizing Environments on Membrane Protein Structures. *Trends Biochem. Sci.* **2011**, *36* (2), 117.
(28) Lyukmanova, E. N.; Shenkarev, Z. O.; Khabibullina, N. F.; Kopeina, G. S.; Shulepko, M. A.; Paramonov, A. S.; Mineev, K. S.; Tikhonov, R. V.; Shingarova, L. N.; Petrovskaya, L. E.; Dolgikh, D. A.; Arseniev, A. S.; Kirpichnikov, M. P. Lipid–Protein Nanodiscs for Cell-Free Production of Integral Membrane Proteins in a Soluble and Folded State: Comparison with Detergent Micelles, Bicelles and Liposomes. *Biochim. Biophys. Acta - Biomembr.* **2012**, *1818* (3), 349–358.
(29) Dürr, U. H. N.; Gildenberg, M.; Ramamoorthy, A. The Magic of Bicelles Up Membrane Protein Structure. *Chem. Rev.* **2012**, *112* (11), 6054.
(30) Hutchison, J. M.; Shih, K. C.; Scheidt, H. A.; Fantin, S. M.; Parson, K. F.; Pantelopulos, G. A.; Harrington, H. R.; Mittendorf, K. F.; Qian, S.; Stein, R. A.; Collier, S. E.; Chambers, M. G.; Katsaras, J.; Voehler, M. W.; Ruotolo, B. T.; Huster, D.; McFeeters, R. L.; Straub, J. E.; Nieh, M. P.; Sanders, C. R. Bicelles Rich in Both Sphingolipids and Cholesterol and Their Use in Studies of Membrane Proteins. *J. Am. Chem. Soc.* **2020**, *142* (29), 12715–12729.
(31) Sligar, S. G.; Denisov, I. G. Nanodiscs: A Toolkit for Membrane Protein Science. *Protein Sci.* **2021**, *30* (2), 297–315.
(32) Lyons, J. A.; Bøggild, A.; Nissen, P.; Frauenfeld, J. Saposin-Lipoprotein Scaffolds for Structure Determination of Membrane Transporters. *Methods Enzymol.* **2017**, *594*, 85–99.
(33) Jamshad, M.; Grimard, V.; Idini, I.; Knowles, T. J.; Dowle, M. R.; Schofield, N.; Sridhar, P.; Lin, Y.; Finka, R.; Wheatley, M.; Thomas, O. R. T.; Palmer, R. E.; Overduin, M.;

Govaerts, C.; Ruysschaert, J.-M.; Edler, K. J.; Dafforn, T. R. Structural Analysis of a Nanoparticle Containing a Lipid Bilayer Used for Detergent-Free Extraction of Membrane Proteins. *Nano Res.* **2015**, *8* (3), 774–789.

(34) Marty, M. T.; Hoi, K. K.; Robinson, C. V. Interfacing Membrane Mimetics with Mass Spectrometry. *Acc. Chem. Res.* **2016**, *49* (11), 2459–2467.

(35) Chorev, D. S.; Tang, H.; Rouse, S. L.; Reddy Bolla, J.; Von Kügelgen, A.; Baker, L. A.; Wu, D.; Gault, J.; Grünewald, K.; Bharat, T. A. M.; Matthews, S. J.; Robinson, C. V. The Use of Sonicated Lipid Vesicles for Mass Spectrometry of Membrane Protein Complexes. *Nat. Protoc.*

(36) Bayburt, T. H.; Sligar, S. G. Membrane Protein Assembly into Nanodiscs. *FEBS Lett.* **2010**, *584* (9), 1721–1727.

(37) Arnold, A.; Labrot, T.; Oda, R.; Dufourc, E. J. Cation Modulation of Bicelle Size and Magnetic Alignment as Revealed by Solid-State NMR and Electron Microscopy. *Biophys. J.* **2002**, *83* (5), 2667.

(38) Whiles, J. A.; Glover, K. J.; Vold, R. R.; Komives, E. A. Methods for Studying Transmembrane Peptides in Bicelles: Consequences of Hydrophobic Mismatch and Peptide Sequence. *J. Magn. Reson.* **2002**, *158* (1–2), 149–156.

(39) C, B.; A, R. Picturing the Membrane-Assisted Choreography of Cytochrome P450 with Lipid Nanodiscs. *Chemphyschem* **2018**, *19* (20), 2603–2613.

(40) Henrich, E.; Peetz, O.; Hein, C.; Laguerre, A.; Hoffmann, B.; Hoffmann, J.; Dötsch, V.; Bernhard, F.; Morgner, N. Analyzing Native Membrane Protein Assembly in Nanodiscs by Combined Non-Covalent Mass Spectrometry and Synthetic Biology. *Elife* **2017**, *6*.

(41) Denisov, I. G.; Sligar, S. G. NANODISCS IN MEMBRANE BIOCHEMISTRY AND BIOPHYSICS.

(42) Denisov, I. G.; Grinkova, Y. V.; Lazarides, A. A.; Sligar, S. G. Directed Self-Assembly of Monodisperse Phospholipid Bilayer Nanodiscs with Controlled Size. *J. Am. Chem. Soc.* **2004**, *126* (11), 3477–3487.

(43) Oda, M. N. Lipid-Free ApoA-I Structure - Origins of Model Diversity. *Biochim. Biophys. Acta - Mol. Cell Biol. Lipids* **2017**, *1862* (2), 221–233.

(44) Wade, J. H.; Jones, J. D.; Lenov, I. L.; Riordan, C. M.; Sligar, S. G.; Bailey, R. C. Microfluidic Platform for Efficient Nanodisc Assembly, Membrane Protein Incorporation, and Purification. *Lab Chip* **2017**, *17* (17), 2951–2959.

(45) Beverung, S.; Wu, J.; Steward, R. Lab-on-a-Chip for Cardiovascular Physiology and Pathology. *Micromachines* **2020**, *11* (10).

(46) Khan, N. I.; Song, E. Lab-on-a-Chip Systems for Aptamer-Based Biosensing. *Micromachines* **2020**, *11* (2), 1–30.

(47) Staicu, C. E.; Jipa, F.; Axente, E.; Radu, M.; Radu, B. M.; Sima, F. Lab-on-a-Chip Platforms as Tools for Drug Screening in Neuropathologies Associated with Blood-Brain Barrier Alterations. *Biomolecules* **2021**, *11* (6).

(48) Manz, A.; Lee, A. P.; Wheeler, A. R. Lab on a Chip- Past, Present, and Future. *Lab Chip* **2021**, *21* (7), 1197–1198.

(49) Di Mauro, G. M.; La Rosa, C.; Condorelli, M.; Ramamoorthy, A. Benchmarks of SMA-Copolymer Derivatives and Nanodisc Integrity. *Langmuir* **2021**, *37* (10), 3113–3121.

(50) Mahajan, M.; Ravula, T.; Prade, E.; Anantharamaiah, G. M.; Ramamoorthy, A.; Li, R.; Chemcomm, /; Communication, C. Probing Membrane Enhanced Protein-Protein Interactions in a Minimal Redox Complex of Cytochrome-P450 and P450-Reductase †.

Chem. Commun **2019**, *55*, 5777.
(51) Hall, S. C. L.; Clifton, L. A.; Tognoloni, C.; Morrison, K. A.; Knowles, T. J.; Kinane, C. J.; Dafforn, T. R.; Edler, K. J.; Arnold, T. Adsorption of a Styrene Maleic Acid (SMA) Copolymer-Stabilized Phospholipid Nanodisc on a Solid-Supported Planar Lipid Bilayer. *J. Colloid Interface Sci.* **2020**, *574*, 272–284.
(52) Lichtenberg, D.; Ahyayauch, H.; Goñi, F. M. The Mechanism of Detergent Solubilization of Lipid Bilayers. *Biophys. J.* **2013**, *105* (2), 289–299.
(53) Lichtenberg, D.; Ahyayauch, H.; Alonso, A.; Goñi, F. M. Detergent Solubilization of Lipid Bilayers: A Balance of Driving Forces. *Trends Biochem. Sci.* **2013**, *38* (2), 85–93.
(54) Salvador, D.; Glavier, M.; Schoehn, G.; Phan, G.; Taveau, J. C.; Decossas, M.; Lecomte, S.; Mongrand, S.; Garnier, C.; Broutin, I.; Daury, L.; Lambert, O. Minimal Nanodisc without Exogenous Lipids for Stabilizing Membrane Proteins in Detergent-Free Buffer. *Biochim. Biophys. Acta - Biomembr.* **2019**, *1861* (4), 852–860.
(55) Camp, T.; Sligar, S. G.; Sligar, S. G.; Sligar, S. G. Nanodisc Self-Assembly Is Thermodynamically Reversible and Controllable. *Soft Matter* **2020**, *16* (24), 5615–5623.
(56) Grethen, A.; Oluwole, A. O.; Danielczak, B.; Vargas, C.; Keller, S. Thermodynamics of Nanodisc Formation Mediated by Styrene/Maleic Acid (2:1) Copolymer. *Sci. Rep.* **2017**, *7* (1).
(57) Ravula, T.; Hardin, N. Z.; Ramadugu, S. K.; Cox, S. J.; Ramamoorthy, A. Formation of PH-Resistant Monodispersed Polymer-Lipid Nanodiscs. *Angew. Chem. Int. Ed. Engl.* **2018**, *57* (5), 1342–1345.
(58) Mishra, V. K.; Palgunachari, M. N.; McPherson, D. T.; Anantharamaiah, G. M. Lipid Complex of Apolipoprotein A-I Mimetic Peptide 4F Is a Novel Platform for Paraoxonase-1 Binding and Enhancing Its Activity and Stability. *Biochem. Biophys. Res. Commun.* **2013**, *430* (3), 975–980.
(59) Patel, H.; Ding, B.; Ernst, K.; Shen, L.; Yuan, W.; Tang, J.; Drake, L. R.; Kang, J.; Li, Y.; Chen, Z.; Schwendeman, A. Characterization of Apolipoprotein A-I Peptide Phospholipid Interaction and Its Effect on HDL Nanodisc Assembly. *Int. J. Nanomedicine* **2019**, *14*, 3069.
(60) Degoma, E. M.; Rader, D. J. Novel HDL-Directed Pharmacotherapeutic Strategies. *Nat. Rev. Cardiol.* **2011**, *8* (5), 266–277.
(61) Krause, B. R.; Remaley, A. T. Reconstituted HDL for the Acute Treatment of Acute Coronary Syndrome. *Curr. Opin. Lipidol.* **2013**, *24* (6), 480–486.
(62) Li, D.; Gordon, S.; Schwendeman, A.; Remaley, A. T.; Li, D.; Schwendeman, • A; Gordon, S.; Remaley, • A T. Apolipoprotein Mimetic Peptides for Stimulating Cholesterol Efflux. *Apolipoprotein Mimetics Manag. Hum. Dis.* **2015**, 29–42.
(63) Livingstone, J. R.; Spolar, R. S.; Thomas Record, M. Contribution to the Thermodynamics of Protein Folding from the Reduction in Water-Accessible Nonpolar Surface Area. *Biochemistry* **1991**, *30* (17), 4237–4244.
(64) Mishra, V. K.; Palgunachari, M. N.; Krishna, N. R.; Glushka, J.; Segrest, J. P.; Anantharamaiah, G. M. Effect of Leucine to Phenylalanine Substitution on the Nonpolar Face of aClass A Amphipathic Helical Peptide on Its Interaction with Lipid: HIGH SOLUTION NMR STUDIES OF 4F-DIMYRISTOYLPHOSPHATIDYLCHOLINE DISCOIDAL. *J. Biol. Chem.* **2008**, *283* (49), 34393.
(65) Smith, S. M. Strategies for the Purification of Membrane Proteins. *Methods Mol. Biol.* **2017**, *1485*, 389–400.

(66) Von Heijne, G. Membrane-Protein Topology. *Nat. Rev. Mol. Cell Biol.* **2006**, *7* (12), 909–918.
(67) Siaw, H. M. H.; Raghunath, G.; Dyer, R. B. Peripheral Protein Unfolding Drives Membrane Bending. *Langmuir* **2018**, *34* (28), 8400–8407.
(68) Sahin, C.; Reid, D. J.; Marty, M. T.; Landreh, M. Scratching the Surface: Native Mass Spectrometry of Peripheral Membrane Protein Complexes. **2020**.
(69) Fleishman, S. J.; Unger, V. M.; Ben-Tal, N. Transmembrane Protein Structures without X-Rays. *Trends Biochem. Sci.* **2006**, *31* (2), 106–113.
(70) Allen, K. N.; Entova, S.; Ray, L. C.; Imperiali, B. Monotopic Membrane Proteins Join the Fold. *Trends in Biochemical Sciences*. Elsevier Ltd January 1, 2019, pp 7–20.
(71) Entova, S.; Billod, J. M.; Swiecicki, J. M.; Martín-Santamareda, S.; Imperiali, B. Insights into the Key Determinants of Membrane Protein Topology Enable the Identification of New Monotopic Folds. *Elife* **2018**, *7*.
(72) Vincent, M. S.; Cascales, E. Probing Inner Membrane Protein Topology by Proteolysis. *Methods Mol. Biol.* **2017**, *1615*, 97–103.
(73) Lane, J. R.; Sexton, P. M.; Christopoulos, A. Bridging the Gap: Bitopic Ligands of G-Protein-Coupled Receptors. *Trends Pharmacol. Sci.* **2013**, *34* (1), 59–66.
(74) Patching, S. G. NMR Structures of Polytopic Integral Membrane Proteins. *Mol. Membr. Biol.* **2011**, *28* (6), 370–397.
(75) Cymer, F.; Schneider, D. Oligomerization of Polytopic α-Helical Membrane Proteins: Causes and Consequences. *Biol. Chem.* **2012**, *393* (11), 1215–1230.
(76) Hamasaki, N.; Abe, Y.; Tanner, M. J. A. Flexible Regions within the Membrane-Embedded Portions of Polytopic Membrane Proteins. *Biochemistry* **2002**, *41* (12), 3852–3854.
(77) Latorraca, N. R.; Venkatakrishnan, A. J.; Dror, R. O. GPCR Dynamics: Structures in Motion. *Chem. Rev.* **2017**, *117* (1), 139–155.
(78) Almén, M. S.; Nordström, K. J.; Fredriksson, R.; Schiöth, H. B. Mapping the Human Membrane Proteome: A Majority of the Human Membrane Proteins Can Be Classified According to Function and Evolutionary Origin. **2009**.
(79) Monk, B. C.; Tomasiak, T. M.; Keniya, M. V.; Huschmann, F. U.; Tyndall, J. D. A.; O'Connell, J. D.; Cannon, R. D.; McDonald, J. G.; Rodriguez, A.; Finer-Moore, J. S.; Stroud, R. M. Architecture of a Single Membrane Spanning Cytochrome P450 Suggests Constraints That Orient the Catalytic Domain Relative to a Bilayer. *Proc. Natl. Acad. Sci. U. S. A.* **2014**, *111* (10), 3865–3870.
(80) Šrejber, M.; Navrátilová, V.; Paloncýová, M.; Bazgier, V.; Berka, K.; Anzenbacher, P.; Otyepka, M. Membrane-Attached Mammalian Cytochromes P450: An Overview of the Membrane's Effects on Structure, Drug Binding, and Interactions with Redox Partners. *J. Inorg. Biochem.* **2018**, *183*, 117–136.
(81) Wright, W. C.; Chenge, J.; Chen, T. Structural Perspectives of the CYP3A Family and Their Small Molecule Modulators in Drug Metabolism. *Liver Res.* **2019**, *3* (3–4), 132–142.
(82) Denisov, I. G.; Makris, T. M.; Sligar, S. G.; Schlichting, I. Structure and Chemistry of Cytochrome P450. **2005**.
(83) Barnaba, C.; Gentry, K.; Sumangala, N.; Ramamoorthy, A.; Denisov, I.; Melacini, G. Open Peer Review The Catalytic Function of Cytochrome P450 Is Entwined with Its Membrane-Bound Nature [Version 1; Referees: 4 Approved]. **2017**.

(84) Cheng, Q.; Sohl, C. D.; Guengerich, F. P. High-Throughput Fluorescence Assay of Cytochrome P450 3A4. *Nat. Protoc.* **2009**, *4* (9), 1258–1261.
(85) Wienkers, L. C.; Heath, T. G. Predicting in Vivo Drug Interactions from in Vitro Drug Discovery Data. *Nat. Rev. Drug Discov.* **2005**, *4* (10), 825–833.
(86) Williams, J. A.; Ring, B. J.; Cantrell, V. E.; Jones, D. R.; Eckstein, J.; Ruterbories, K.; Hamman, M. A.; Hall, S. D.; Wrighton, S. A. Comparative Metabolic Capabilities of CYP3A4, CYP3A5, and CYP3A7. *Drug Metab. Dispos.* **2002**, *30* (8), 883–891.
(87) Barnaba, C.; Sahoo, B. R.; Ravula, T.; Medina-Meza, I. G.; Im, S.-C.; Anantharamaiah, G. M.; Waskell, L.; Ramamoorthy, A. Cytochrome-P450-Induced Ordering of Microsomal Membranes Modulates Affinity for Drugs. *Angew. Chemie Int. Ed.* **2018**, *57* (13), 3391–3395.
(88) Yoshimoto, F. K.; Auchus, R. J. The Diverse Chemistry of Cytochrome P450 17A1 (P450c17, CYP17A1). **2014**.
(89) Kandel, S. E.; Lampe, J. N. Role of Protein−Protein Interactions in Cytochrome P450-Mediated Drug Metabolism and Toxicity. *Chem. Res. Toxicol.* **2014**, *27*, 1474–1486.
(90) Ogu, C. C.; Maxa, J. L. Drug Interactions Due to Cytochrome P450.
(91) Hersh, E. V.; Moore, P. A. Drug Interactions in Dentistry: The Importance of Knowing Your CYPs. *J. Am. Dent. Assoc.* **2004**, *135* (3), 298–311.
(92) Denisov, I. G.; Grinkova, Y. V.; Baylon, J. L.; Tajkhorshid, E.; Sligar, S. G. Mechanism of Drug-Drug Interactions Mediated by Human Cytochrome P450 CYP3A4 Monomer. *Biochemistry* **2015**, *54* (13), 2227–2239.
(93) Denisov, I. G.; Baylon, J. L.; Grinkova, Y. V.; Tajkhorshid, E.; Sligar, S. G. Drug-Drug Interactions between Atorvastatin and Dronedarone Mediated by Monomeric CYP3A4. *Biochemistry* **2018**, *57* (5), 805–816.
(94) Nebert, D. W.; Russell, D. W. Clinical Importance of the Cytochromes P450. *Lancet (London, England)* **2002**, *360* (9340), 1155–1162.
(95) Fleming, I. Cytochrome P450-Dependent Eicosanoid Production and Crosstalk. *Curr. Opin. Lipidol.* **2011**, *22* (5), 403–409.
(96) El-Sherbeni, A. A.; El-Kadi, A. O. S. Microsomal Cytochrome P450 as a Target for Drug Discovery and Repurposing. *Drug Metab. Rev.* **2017**, *49* (1), 1–17.
(97) Bender, J.; Schmidt, C. Mass Spectrometry of Membrane Protein Complexes. *Biol. Chem.* **2019**, *400* (7), 813–829.
(98) Barrera, N. P.; Robinson, C. V. Advances in the Mass Spectrometry of Membrane Proteins: From Individual Proteins to Intact Complexes. *Annu. Rev. Biochem.* **2011**, *80* (1), 247–271.
(99) Barrera, N. P.; Isaacson, S. C.; Zhou, M.; Bavro, V. N.; Welch, A.; Schaedler, T. A.; Seeger, M. A.; Miguel, R. N.; Korkhov, V. M.; van Veen, H. W.; Venter, H.; Walmsley, A. R.; Tate, C. G.; Robinson, C. V. Mass Spectrometry of Membrane Transporters Reveals Subunit Stoichiometry and Interactions. *Nat. Methods 2009 68* **2009**, *6* (8), 585–587.
(100) Borysik, A. J.; Hewitt, D. J.; Robinson, C. V. Detergent Release Prolongs the Lifetime of Native-like Membrane Protein Conformations in the Gas-Phase. *J. Am. Chem. Soc.* **2013**, *135* (16), 6078–6083.
(101) Barrera, N. P.; Zhou, M.; Robinson, C. V. The Role of Lipids in Defining Membrane Protein Interactions: Insights from Mass Spectrometry.
(102) Hellwig, N.; Peetz, O.; Ahdash, Z.; Tascó, I.; Booth, P. J.; Mikusevic, V.; Diskowski, M.;

Politis, A.; Hellmich, Y.; Hä, I.; Reading, E.; Morgner, N. Native Mass Spectrometry Goes More Native: Investigation of Membrane Protein Complexes Directly from SMALPs †. *Chem. Commun* **2018**, *54*, 13702.
(103) Laganowsky, A.; Reading, E.; Hopper, J. T. S.; Robinson, C. V. Mass Spectrometry of Intact Membrane Protein Complexes. *Nat. Protoc.* **2013**.
(104) Robinson, C. V.; V., C. From Molecular Chaperones to Membrane Motors: Through the Lens of a Mass Spectrometrist. *Biochem. Soc. Trans.* **2017**, *45* (1), 251–260.
(105) AN, C.; SE, R. Mass Spectrometry-Enabled Structural Biology of Membrane Proteins. *Methods* **2018**, *147*, 187–205.
(106) Campuzano, I. D. G.; Li, H.; Bagal, D.; Lippens, J. L.; Svitel, J.; Kurzeja, R. J. M.; Xu, H.; Schnier, P. D.; Loo, J. A. Native MS Analysis of Bacteriorhodopsin and an Empty Nanodisc by Orthogonal Acceleration Time-of-Flight, Orbitrap and Ion Cyclotron Resonance. *Anal. Chem* **2016**, *88*.
(107) I, L.; MT, D.; S, L.; TD, N.; J, G.; E, R.; JTS, H.; NG, H.; P, W.; M, C.; A, S.; BA, W.; C, K.; PJ, S.; H, B.; JLP, B.; TM, A.; CV, R. Lipid Binding Attenuates Channel Closure of the Outer Membrane Protein OmpF. *Proc. Natl. Acad. Sci. U. S. A.* **2018**, *115* (26), 6691–6696.
(108) Kliman, M.; May, J. C.; McLean, J. A. Lipid Analysis and Lipidomics by Structurally Selective Ion Mobility-Mass Spectrometry. *Biochim. Biophys. Acta - Mol. Cell Biol. Lipids* **2011**, *1811* (11), 935–945.
(109) Gault, J.; Liko, I.; Landreh, M.; Shutin, D.; Reddy Bolla, J.; Jefferies, D.; Agasid, M.; Yen, H.-Y.; Ladds, M. J. G. W.; Lane, D. P.; Khalid, S.; Mullen, C.; Remes, P. M.; Huguet, R.; Mcalister, G.; Goodwin, M.; Viner, R.; Syka, J. E. P.; Robinson, C. V. Brief CommuniCation Combining Native and "omics" Mass Spectrometry to Identify Endogenous Ligands Bound to Membrane Proteins.
(110) Bolla, J. R.; Agasid, M. T.; Mehmood, S.; Robinson, C. V. Membrane Protein–Lipid Interactions Probed Using Mass Spectrometry. *https://doi.org/10.1146/annurev-biochem-013118-111508* **2019**, *88*, 85–111.
(111) Gault, J.; Donlan, J. A. C.; Liko, I.; Hopper, J. T. S.; Gupta, K.; Housden, N. G.; Struwe, W. B.; Marty, M. T.; Mize, T.; Bechara, C.; Zhu, Y.; Wu, B.; Kleanthous, C.; Belov, M.; Damoc, E.; Makarov, A.; Robinson, C. V. High-Resolution Mass Spectrometry of Small Molecules Bound to Membrane Proteins.
(112) Cong, X.; Liu, Y.; Liu, W.; Liang, X.; Russell, D. H.; Laganowsky, A. Determining Membrane Protein-Lipid Binding Thermodynamics Using Native Mass Spectrometry. *J. Am. Chem. Soc.* **2016**.
(113) Bechara, C. C.; Robinson, C. V. Different Modes of Lipid Binding to Membrane Proteins Probed by Mass Spectrometry. *J. Am. Chem. Soc* **2015**, *137*, 33.
(114) Cong, X.; Liu, Y.; Liu, W.; Liang, X.; Laganowsky, A. Allosteric Modulation of Protein-Protein Interactions by Individual Lipid Binding Events. *Nat. Commun.* **2017**, *8* (1), 2203.
(115) ZM, M.; JD, Z.; WA, D.; JS, P. Gas-Phase Protonation Thermodynamics of Biological Lipids: Experiment, Theory, and Implications. *Anal. Chem.* **2020**, *92* (15), 10365–10374.
(116) Keener, J. E.; Zambrano, D. E.; Zhang, G.; Zak, C. K.; Reid, D. J.; Deodhar, B. S.; Pemberton, J. E.; Prell, J. S.; Marty, M. T. Chemical Additives Enable Native Mass Spectrometry Measurement of Membrane Protein Oligomeric State within Intact Nanodiscs. *J. Am. Chem. Soc.* **2019**, *141* (2), 1054–1061.
(117) Sipe, S. N.; Patrick, J. W.; Laganowsky, A.; Brodbelt, J. S. Enhanced Characterization of

Membrane Protein Complexes by Ultraviolet Photodissociation Mass Spectrometry. *Anal. Chem.* **2020**, *92* (1), 899–907.
(118) Reading, E.; Hall, Z.; Martens, C.; Haghighi, T.; Findlay, H.; Ahdash, Z.; Politis, A.; Booth, P. J. Interrogating Membrane Protein Conformational Dynamics within Native Lipid Compositions. *Angew. Chemie Int. Ed.* **2017**, *56* (49), 15654–15657.
(119) Reading, E.; Walton, T. A.; Liko, I.; Marty, M. T.; Laganowsky, A.; Rees, D. C.; Robinson, C. V. The Effect of Detergent, Temperature, and Lipid on the Oligomeric State of MscL Constructs: Insights from Mass Spectrometry. *Chem. Biol.* **2015**, *22* (5), 593–603.
(120) A, K.; L, B.; D, Y.; A, K.; C, V.-B.; F, S. Top-down Mass Spectrometry of Intact Membrane Protein Complexes Reveals Oligomeric State and Sequence Information in a Single Experiment. *Protein Sci.* **2015**, *24* (8), 1292–1300.
(121) SM, F.; KF, P.; P, Y.; B, J.; GC, L.; CR, S.; MD, O.; BT, R. Ion Mobility-Mass Spectrometry Reveals the Role of Peripheral Myelin Protein Dimers in Peripheral Neuropathy. *Proc. Natl. Acad. Sci. U. S. A.* **2021**, *118* (17).
(122) Khakinejad, M.; Ghassabi Kondalaji, S.; Donohoe, G. C.; Valentine, S. J. Ion Mobility Spectrometry-Hydrogen Deuterium Exchange Mass Spectrometry of Anions: Part 3. Estimating Surface Area Exposure by Deuterium Uptake. *J. Am. Soc. Mass Spectrom.* **2016**.
(123) Lau, A. M.; Jia, R.; Bradshaw, R. T.; Politis, A. Structural Predictions of the Functions of Membrane Proteins from HDX-MS. *Biochem. Soc. Trans.* **2020**, *48* (3), 971.
(124) Giladi, M.; Khananshvili, D. Hydrogen-Deuterium Exchange Mass-Spectrometry of Secondary Active Transporters: From Structural Dynamics to Molecular Mechanisms. *Front. Pharmacol.* **2020**, *0*, 70.
(125) DP, O.; V, H.; A, C.; S, B. Hydrogen/Deuterium Exchange Mass Spectrometry for the Structural Analysis of Detergent-Solubilized Membrane Proteins. *Methods Mol. Biol.* **2020**, *2127*, 339–358.
(126) Weerasekera, R.; Schmitt-Ulms, & G. Crosslinking Strategies for the Study of Membrane Protein Complexes and Protein Interaction Interfaces. *Biotechnol. Genet. Eng. Rev.* **2006**, *23* (1), 41–62.
(127) Debelyy, M. O.; Waridel, P.; Quadroni, M.; Schneiter, R.; Conzelmann, A. Chemical Crosslinking and Mass Spectrometry to Elucidate the Topology of Integral Membrane Proteins. *PLoS One* **2017**, *12* (10).
(128) Corgiat, B. A.; Nordman, J. C.; Kabbani, N. Chemical Crosslinkers Enhance Detection of Receptor Interactomes. *Front. Pharmacol.* **2014**, *0*, 171.
(129) Johnson, D. T.; Stefano, L. H. Di; Jones, L. M. Fast Photochemical Oxidation of Proteins (FPOP): A Powerful Mass Spectrometry–Based Structural Proteomics Tool. *J. Biol. Chem.* **2019**, *294* (32), 11969.
(130) Watkinson, T. G.; Calabrese, A. N.; Ault, J. R.; Radford, S. E.; Ashcroft, A. E. FPOP-LC-MS/MS Suggests Differences in Interaction Sites of Amphipols and Detergents with Outer Membrane Proteins. *J. Am. Soc. Mass Spectrom 28*, 50–55.
(131) Lu, Y.; Zhang, H.; Niedzwiedzki, D. M.; Jiang, J.; Blankenship, R. E.; Gross, M. L. Fast Photochemical Oxidation of Proteins Maps the Topology of Intrinsic Membrane Proteins: Light-Harvesting Complex 2 in a Nanodisc. *Anal. Chem.* **2016**, *88* (17), 8827–8834.
(132) Zhou, F.; Yang, Y.; Chemuru, S.; Cui, W.; Liu, S.; Gross, M.; Li, W. Footprinting Mass Spectrometry of Membrane Proteins: Ferroportin Reconstituted in Saposin A Picodiscs.

Anal. Chem. **2021**, acs.analchem.1c02325.
(133) Abhinav Nath, ‡; William M. Atkins, *,‡ and; Stephen G. Sligar*, §. Applications of Phospholipid Bilayer Nanodiscs in the Study of Membranes and Membrane Proteins†. **2007**.
(134) Marty, M. T.; Hoi, K. K.; Gault, J.; Robinson, C. V. Probing the Lipid Annular Belt by Gas-Phase Dissociation of Membrane Proteins in Nanodiscs. *Angew. Chemie Int. Ed.* **2016**, *55* (2), 550–554.
(135) Li, J.; Fan, X.; Kitova, E. N.; Zou, C.; Cairo, C. W.; Eugenio, L.; Ng, K. K. S.; Xiong, Z. J.; Privé, G. G.; Klassen, J. S. Screening Glycolipids Against Proteins in Vitro Using Picodiscs and Catch-and-Release Electrospray Ionization-Mass Spectrometry. *Anal. Chem.* **2016**, *88* (9), 4742–4750.
(136) Han, L.; Kitova, E. N.; Li, J.; Nikjah, S.; Lin, H.; Pluvinage, B.; Boraston, A. B.; Klassen, J. S. Protein–Glycolipid Interactions Studied in Vitro Using ESI-MS and Nanodiscs: Insights into the Mechanisms and Energetics of Binding. *Anal. Chem.* **2015**, *87* (9), 4888–4896.
(137) Wilm, M.; Mann, M. Analytical Properties of the Nanoelectrospray Ion Source. *Anal. Chem.* **1996**.
(138) Dixit, S. M.; Polasky, D. A.; Ruotolo, B. T. Collision Induced Unfolding of Isolated Proteins in the Gas Phase: Past, Present, and Future. *Curr. Opin. Chem. Biol.* **2018**, *42*, 93–100.
(139) Liu, Y.; Cong, X.; Liu, W.; Laganowsky, A. Characterization of Membrane Protein–Lipid Interactions by Mass Spectrometry Ion Mobility Mass Spectrometry. *J. Am. Soc. Mass Spectrom* **2017**, *28*, 579–586.
(140) Rabuck, J. N.; Hyung, S.-J.; Ko, K. S.; Fox, C. C.; Soellner, M. B.; Ruotolo, B. T. An Activation State-Selective Kinase Inhibitor Assay Based on Ion Mobility-Mass Spectrometry. *Anal. Chem.* **2013**, *85* (15), 6995.
(141) Fantin, S. M.; Parson, K. F.; Niu, S.; Liu, J.; Polasky, D. A.; Dixit, S. M.; Ferguson-Miller, S. M.; Ruotolo, B. T. Collision Induced Unfolding Classifies Ligands Bound to the Integral Membrane Translocator Protein (TSPO). *Anal. Chem.* **2019**, acs.analchem.9b03208.
(142) X, C.; Y, L.; W, L.; X, L.; A, L. Allosteric Modulation of Protein-Protein Interactions by Individual Lipid Binding Events. *Nat. Commun.* **2017**, *8* (1).
(143) Fantin, S. M.; Huang, H.; Sanders, C. R.; Ruotolo, B. T. Collision-Induced Unfolding Differentiates Functional Variants of the KCNQ1 Voltage Sensor Domain. *J. Am. Soc. Mass Spectrom* **2020**, *31*, 44.
(144) *Cytochrome P450*; Ortiz de Montellano, P. R., Ed.; Springer US: Boston, MA, 2005.
(145) Guengerich, F. P. Cytochrome P450s and Other Enzymes in Drug Metabolism and Toxicity. *AAPS J.* **2006**, *8* (1), E101-11.
(146) Guengerich, F. P.; Wu, Z.-L.; Bartleson, C. J. Function of Human Cytochrome P450s: Characterization of the Orphans. *Biochem. Biophys. Res. Commun.* **2005**, *338* (1), 465–469.
(147) Prade, E.; Mahajan, M.; Im, S.-C.; Zhang, M.; Anantharamaiah, G. M.; Waskell, L.; Ramamoorthy, A.; Gentry, K. A. Angewandte International Edition Title: A Minimal Functional Complex of Cytochrome P450 and FBD of Cytochrome P450 Reductase in Nanodiscs A Minimal Functional Complex of Cytochrome P450 and FBD of Cytochrome P450 Reductase in Nanodiscs. *Angew. Chem. Int. Ed. Angew. Chem* **2018**, *10* (10).

(148) Im, S.-C.; Waskell, L. The Interaction of Microsomal Cytochrome P450 2B4 with Its Redox Partners, Cytochrome P450 Reductase and Cytochrome B5. *Arch. Biochem. Biophys.* **2011**, *507*, 144–153.
(149) Dürr, U. H. N.; Waskell, L.; Ramamoorthy, A. The Cytochromes P450 and b 5 and Their Reductases-Promising Targets for Structural Studies by Advanced Solid-State NMR Spectroscopy. **2007**.

Chapter 2 **An Evaluation of Membrane Mimetics for Ion Mobility – Mass Spectrometry Measurements of Membrane Protein Structure**

2.1 Introduction

A cell is the most basic unit of life.[1] Membranes are a key component of cellular life, as they provide a barrier between neighboring cells and their outside environment. These boundaries are what define organelles all with a particular function.[1,4] The diversity of cells and their membranes are defined, in part, by the large variety of chemically diverse lipid compositions arrayed on their surface.[5,6] These membranes are also replete with a large variety of different membrane proteins (MPs) which act as receptors, channels, and enzymes that all carryout critical cellular tasks. MP quantities in the average cell membrane varies considerably, and highly specialized eukaryotic membranes are estimated to contain up to 70% MP and make up 30% of the human proteome.[7–10]

MPs are important biological and pharmacological analytes that play key roles in maintaining cellular homeostasis and represent 60% of current therapeutic targets.[11,12] MPs exist in the context of a complex cellular environment where their function can be modulated by interactions with other proteins and lipids.[13,14] Due to their complex native environments and intrinsic hydrophobicity, the purification of MPs requires the use of solubilization agents and often results in low MP yields.[15–18] These factors make obtaining high resolution structural information for MPs difficult, and as a result, they are currently underrepresented in structural databases in comparison to their soluble counterparts.[10,19] Furthermore, the function and structure of MPs has been shown to be sensitive to the solubilization technique used,[20–22] resulting in the

increased use of more native-like lipid mimetics for MP solubilization. A substantial effort in the last 15-20 years has been focused on the development and implementation of membrane mimetics which can more accurately represent the cellular membrane environment in order to study MPs in a more relevant context.

Recently, native mass spectrometry (nMS) has demonstrated powerful capabilities of analyzing MP samples from a variety of solubilization methods to reveal structural and functional information.[23,24] In nMS workflows, MPs are lifted into the gas phase using nano-electrospray ionization (nESI). During this process, they are still protected by their solubilization agents before collisional heating causes them to shed these protective molecules inside the instrument. This process creates MP ions, as well as ions associated with the mimetics, they are housed in. In the past, most nMS experiments have been performed by liberating gas-phase MPs from detergent micelles;[25–33] however, MPs housed in other solubilization vehicles such as amphipols,[34,35] bicelles,[4,36,37] nanodiscs (NDs),[38–42] styrene maleic acid lipid particles (SMALPs),[43] and biological membrane vesicles[44] have all been successfully utilized for MP nMS. The use of these agents with nMS has enabled the study MPs, proving insights into annular lipid binding,[45] oligomerization pathways,[36] and complex formation which span both the inner and outer leaflet cellular membranes.[46]

The addition of ion mobility (IM) separations to nMS allows for the measurement of the orientationally averaged size of gas phase MPs,[47] and also enables collision induced unfolding experiments (CIU). In CIU, the protein ions are collisionally activated through the stepwise ramping of an accelerating potential, or collision voltage (CV), causing ion heating and subsequent unfolding. The CIU pathway adopted protein ions can be tracked through IM separation, and recent advancements have provided automated workflows for the analysis of CIU

fingerprints to provide information on their relative stabilities.[48] While multiple studies have used IM-MS and CIU to elucidate the structural changes and relative stabilities of MP complexes,[26,32,49–52] to our knowledge the use of CIU on MPs has been primarily limited to those ejected from detergent micelles.

Here, we employ IM-MS and CIU to systematically study MPs housed within multiple categories solubilization agents: detergent micelles, bicelles, and NDs. We first describe the use of IM-MS to probe the ability of CIU to capture differences in the MP structure associated the solubilization agents to encapsulate the MPs prior their analysis. We primarily accomplish this by collecting CIU fingerprints for a range of model MP systems which have been solubilized using at least three different methods, including detergent micelles, sphingomyelin and cholesterol rich (SCOR) bicelles[37] and POPC bicelles, and finally POPC lipid nanodiscs. Our three model protein systems, chosen in order to represent a range of MP structures, include the monotopic cytochrome P450 3A4 (CYP3A4) MP, the dimeric L16P variant of the integral peripheral myelin protein (L16P PMP22), a form of WT PMP22 which contains a large, 11 kDa soluble tag (WTtag PMP22), and the small multidrug resistance transporter (GDX). We find evidence of significant differences across all CIU datasets collected for these MPs as a function of the solubilization agents used in their preparation. Further, we find that these differences emphasize the importance of carrying out a careful evaluation of solubilization agents and their impact on MP structure as part of IM-MS workflow development. We conclude by discussing the general role of local environment on MP structure and stability. We also propose further experiments to elucidate the role of solubilization agents in defining structural MS data and MP protein structures.

2.2 Methods

2.2.1 Membrane Protein Sample Preparation

CYP3A4 was expressed in *E. Coli* and purified using protocols described elsewhere.[53–55] PMP22 WT_{tag} and the L16P mutant variant were expressed in *E. coli*. using protocols adapted from Schlebach et al.[56] For WT_{tag} PMP22, the protein did not undergo the final thrombin cleavage step. GDX-Clo (*Clostridiales bacterium oral taxon 876*) was expressed in *E. coli* and purified using protocols previously described.[57] (Octaethylene glycol monododecyl ether (C12E8), n-Dodecyl-β-D-Melibioside (DDMB), and n-dodecyl-β-D-maltoside (DDM) were purchased from Anatrace, Octyl β-D-glucopyranoside (OG), membrane scaffold protein 1D1(-), ammonium acetate, sodium chloride, tris(hydroxymethyl)aminomethane (tris), sodium azide, and ethylenediaminetetraacetic acid (EDTA) were purchased from Sigma Aldrich (St. Louis, MO). The lipids 1-palmitoyl-2-oleoyl-glycero-3-phosphocholine [POPC], dimyristoylphosphatidylcholine [DMPC], egg sphingomyelin [eSM] and cholesterol, were purchased from Avanti Polar Lipids (Alabaster, AL). All membrane proteins were screened for appropriate detergent conditions.[58]

Samples housed in detergent micelles were simultaneously detergent and buffer exchanged using 10 kDa Amicon Ultra-0.5 centrifugal filter units (MilliporeSigma, Burlington, MA). Starting and ending buffers and detergents conditions prior to native MS are as follows: 50 μM PMP22 was exchanged from 50 mM Tris, 0.15% DM, 15 mM imidazole, and 1 mM TCEP, and 0.1% DDM, pH 8.0, into 0.02% C12E8 (~4 x CMC), 200 mM ammonium acetate, pH 8.0, 36 μM CYP3A4 was exchanged from 40 mM potassium phosphate, 20% glycerol, pH 7.4 into 40 mM OG, 200 mM ammonium acetate, pH 7.4. 50 μM GDX was exchanged from 100 mM NaCl, 10 mM HEPES, pH 8.0 buffer with 4 mM DM, into 0.3mM DDM, 200 mM Ammonium acetate, pH 8.0. Samples housed in SCOR bicelles were prepared as described in the supplemental methods

and were then buffer exchanged using 10 kDa Amicon Ultra-0.5 centrifugal filter units. Bicelle samples were not detergent exchanged and the DDMB concentration was held at 1 x CMC to preserve the bicelles q ratio (0.33) Specifically, 40 μM PMP22-wt, PMP-22 L16P or GDX in 10 mM acetate buffer (pH 5.0) containing 100 mM NaCl, 0.2 % SCOR bicelle or (PMP22-wt only) 0.2% POPC bicelles (q = 0.33), 1 mM EDTA, 5 mM TCEP, and 0.3 mM DDMB was exchanged into 200 mM ammonium acetate, 0.3 mM DDMB, pH 8.0 using 10 kDa Amicon Ultra-0.5 centrifugal filter units. PMP22-wt and GDX were incorporated in MSP1D1 NDs and CYP3A4 were incorporated into MSPE3D1 nanodiscs as described by the Sligar lab[59,60] with the final purification SEC step buffer exchanging into 200 mM Ammonium acetate.

2.2.2 Native-MS and CIU Experiments

All IM-MS and CIU data were collected using a Synapt G2 HDMS IM-Q-ToF mass spectrometer (Waters, Milford, MA), with a direct infusion nESI source set to positive ion mode. Our instrument settings were tuned for each protein system and mimetic to generate intact protein ions while completely dissociating detergents, lipids and scaffold protein prior to the IM separator, including appropriately tuned settings for the source temperature (30-40° C), source gas flow (50 mL/min), and the sampling cone (120 V). The traveling wave height and wave velocities in the trap, IM, and transfer region, as well as the helium cell flow rate, were identical for each protein system across mimetics. For PMP, GDX and CYP, trapping cell wave velocity and height were 115 m/s and 0.1 V, IMS wave velocity and height were 250 m/s and 15 V, transfer cell wave velocity and height were 300 m/s and 10 V. An accelerating potential of 70 V in the transfer region was used to dissociate empty solubilization agents for all systems except CYP in nanodiscs, which only required 10 V. Experimental collision cross section analysis was performed by using IMSCal-19v4, a program written in C, and, where possible, theoretical cross sections were calculated from

crystal structures[61] and homology models[62] using IMPACT.[63,64] All CIU analyses were performed by increasing the trap collision voltage in 5 V increments across ranges tuned for each system. CIU data from selected charge states were extracted into a text-based format using TWIMExtract,[65] then processed and analyzed using CIUSuite 2.[66,67] Data processing included two or three rounds of 2D Savitzky-Golay smoothing with a window of five bins and interpolation of the collision voltage axis by a factor of four.

2.3 Results and Discussion

2.3.1 Comparing CIU of transmembrane protein complexes liberated from bicelles and detergent micelles

Appendix Figure I-1 contains example nMS and IM-MS data sets acquired for GDX liberated from DDM micelles and POPC-DDMB bicelles. In both spectra, signals corresponding to monomeric and dimeric GDX are detected. For GDX liberated from the POPC-DDMB bicelles, signals for lower charge states dominate (8+ to 4+) versus those detected for GDX contained within DDM micelles, which adopt higher charge states (10+ to 5+). We selected GDX 6+ and 7+ monomer ions for CIU analysis due to their intensity and minimal overlap with chemical noise signals. A CCS analysis of 6+ GDX monomers indicates that the protein liberated from POPC-DDMB bicelles to 1,404.1 ± 5 $Å^2$, versus a value of 1,350.2 ± 5 $Å^2$ recorded from the same ions prepared in DDM micelles (N = 3). This CCS comparison suggests that GDX-Clo monomers adopt a different

conformation when liberated from POPC-DDMB bicelles when compared to those liberated from DDM micelles.

CIU data collected for 6+ GDX monomers exhibits three features, while CIU data extracted from the same ions released from bicelles reveals four features, further illustrating that the GDX

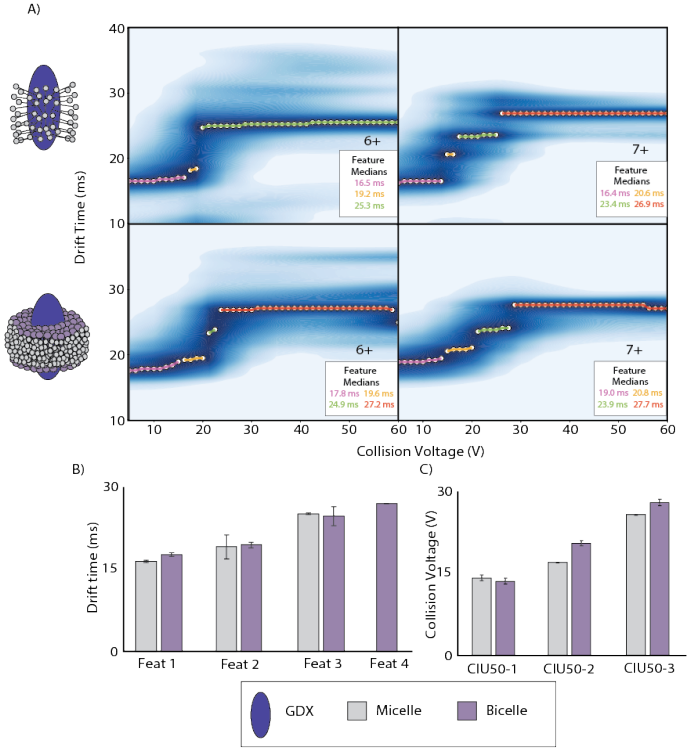

Figure 2-1 GDX CIU micelle vs bicelles. **A)** the 6+ and 7+ charge state CIU of GDX liberated from DDM detergent micelle N=3 (on top) shows features for the 6+ 16.6 ± 0.2, 19.2 ± 2.2, and 25.3 ± 0.1 ms and for the 7+ charge state features at 16.4 ± 0.1, 20.6 ± 0.2, 23.4 ±0.1, and 26.9 ± 0.1 ms and POPC-DDMB bicelles N= 3 (on bottom) shows features 17.8 ± 0.3, 19.6 ± 0.5, 24.9 ± 1.7, and 27.2 ± 0.1 ms and the 7+ charge state 18.0 ± 0.1, 20.8 ± 0.2, 23.9 ± 0.2, and 27.7 ±0.2 ms, **B)** 6+ median drift time analysis comparing micelles vs bicelles unfolding and **C)** CIU50 values for the 7+ charge state illustrating that bicelles (purple) exhibit a stabilizing effect on GDX with micelles CIU50 transitions of 14.1 ± 0.5, 16.9 ± 0.1, and 25.6 ± 0.1 V and the bicellular CIU50 transitions of 13.5 ±0.5, 20.4 ± 0.5, and 27.8 ± 0.6 V.

adopts different conformations when released differently constructed mimetic environments. Given the dramatic differences between these two GDX CIU fingerprints, granular quantitative comparisons are challenging; however, we note that the final CIU50 for GDX ions ejected from bicelles is larger than that recorded for the same ions produced from micelles, 24.0 ± 1.3 and 19.3 ± 0.1 respectively, suggesting a relative stabilization of GDX in the bicelle environment. CIU data recorded for 7+ GDX ions produced from micelle and bicelle samples each contain four features.

CIU50 values produced for GDX liberated from bicelles (CIU50-1 13.5 ± 0.5 V, CIU50-2 20.4 ± 0.5 V, and CIU50-3 27.8 ± 0.6 V) are consistently higher than those from extracted from equivalent ions measured from micelle containing samples (CIU50-1 14.1 ± 0.5 V, CIU50-2 16.9 ± 0.01 V, and CIU50-3 25.6 ± 0.1 V) again confirming the stabilizing effect of bicelles on GDX.

To further evaluate the ability of bicelles to produce stabilized MP structures when compared to those produced from micelles, we elected to perform CIU analysis on 13+ dimeric L16P PMP22 ions due to the intensity and minimal noise overlap of the signals detected (Appendix Figure I-2).

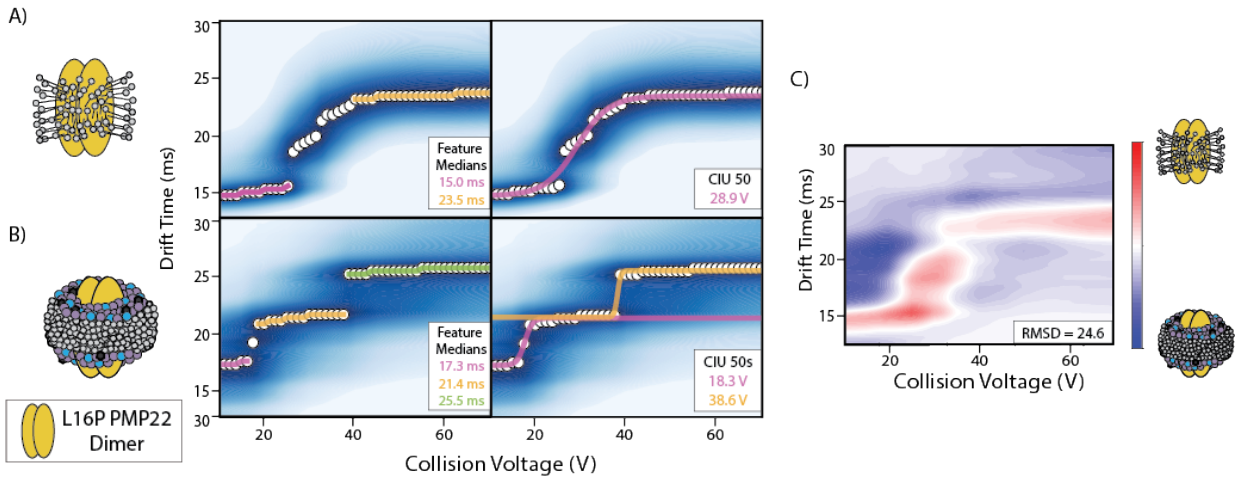

Figure 2-2 CIU of L16P PMP22 dimeric complexes liberated from detergent micelles and SCOR bicelles. All fingerprints shown are for the 13+ dimeric charge state. **A**). Feature detection analysis of L16P PMP22 dimers liberated from C12E8 micelles, N = 3, shows two features of 15.0 ± 0.3 ms and 23.5 ± 0.7 ms. CIU 50 transitions fit to these features occur at 28.9 ± 0.8 V. **B)**. Feature detection analysis of L16P PMP22 dimers liberated from SCOR bicelles, N = 3, show three features of 17.3 ± 0.4 ms, 21.4 ± 0.2 ms, and 25.5 ± 0.2 ms. CIU50 transitions fit to these features occur at 18.3 ± 0.9V and 38.6 ± 0.8 V. **C)**. RMSD plot of the averaged bicellar replicate subtracted from the averaged micellar fingerprint for L16P PMP22 dimers shows an RMSD of 24.6%, which is almost 2x the replicate baseline RMSDs of 13.2% for L16P PMP22 dimers liberated from micelles and 4.5% for bicelles.

CIU data shown in Figure 2-2 for L16P PMP22 dimers reveals significantly different features and CIU50 transitions for samples prepared in micelles and bicelles (N=3). The micellar L16P PMP22 dimer fingerprint contains two features, at 15.0 ± 0.3 ms and 23.5 ± 0.7 ms, and the bicellar L16P PMP22 fingerprint includes three features, at 17.3 ± 0.4 ms, 21.4 ± 0.2 ms, and 25.5 ± 0.2 ms. A CCS analysis of 13+ micellular L16P PMP22 was 2,953 1 ± 9 versus the same ion liberated from

bicelles of 2,654 1 ± 13 Å^2.bicellar L16P PMP22 dimers are more compact that micellar L16P PMP22 dimers. A comparison of CIU50 values reveals that L16P PMP22 dimers produced from micelles are stabilized when compared to their bicelle encapsulated analogs, with CIU501 shifting from 28.9V to 18.3V respectively, a result that contrasts our GDX data discussed above. Overall, our L16P PMP22 CCS and CIU data indicates that bicelle and micelle environments promote significantly different dimer structures, with the former producing more compact structures and the latter generating a more stabilized conformational state.

2.3.2 Tracking the Influence of Membrane Memetic on the Monotopic Membrane Protein CYP3A4

While prior reports of MP nMS experiments have largely focused on multi-pass integral proteins, such as GDX, recent efforts have explored how these techniques can be extended to peripheral proteins.[77] These proteins possess large aqueous domains in addition to regions which interact with, but do not span, the lipid bilayer and their dual nature can complicate their biophysical characterization.[78] For this reason, single pass and monotopic membrane proteins, which are embedded in the membrane with a single alpha helix, are commonly studied in truncated forms excluding the membrane-associated alpha helix.[78] However, to study the more biologically-relevant sequence, solubilization agents are needed that replicate the lipid bilayer found in cellular membranes in order to preserve the overall structure of monotopic MPs.

The CYP family of proteins are enzymes important for the process of drug metabolism.[53] They bind a wide variety of drugs and have been noted in the past to also bind detergent molecules.[79] We therefore screened CYP samples by nMS in order to identify detergent conditions that avoided the formation of CYP-detergent complexes, leading us to select the detergent OG for IM-MS analysis of CYP3A4. The data shown in Appendix Figure I-3 includes signals

corresponding to the 13-17+ charge states for monomeric CYP3A4 liberated from OG micelles, and while the peaks are broad relative to soluble systems of comparable size,[80] no distinct detergent binding is observed. A mass analysis of these peaks reveals that they correspond to the mass of CYP3A4 plus its heme cofactor, indicating we mainly detect the holo protein state under these conditions. CYP3A4 has been previously studied in NDs, and multiple incorporation protocols have been published previously.[81,82] In Figure S-2, we show CYP3A4 incorporated into POPC NDs assembled using the MSP3ED1 scaffold protein by means of a microfluidic device.[55] Signals associated with CYP3A4 liberated from NDs appear significantly more resolved than those recorded under micellar conditions, and allow for the identification of apo and holo CYP3A4, as well as its retained lipid bound states. We assigned these signals to monomeric CYP3A4 charge states identical to those observed for the protein ions produced under micellar data, 13-17+, and both IM-MS data sets show compact signals indicating native-like CYP ions. We detect small differences in holo CYP 16+ CCS values, with micellar CYP3A4 producing 3,451.5 ± 18 $Å^2$ and those from NDs having a value of 3,318.4 ± 17 $Å^2$. Calculated CCS estimates for CYP CCS range from (PA) 3,383.8 ± 8 $Å^2$to (TJM) 4,325.4 ± 11 $Å^2$ indicating that both conditions produced compacted CYP ions when compared to X-ray data, with NDs producing a more collapsed state.

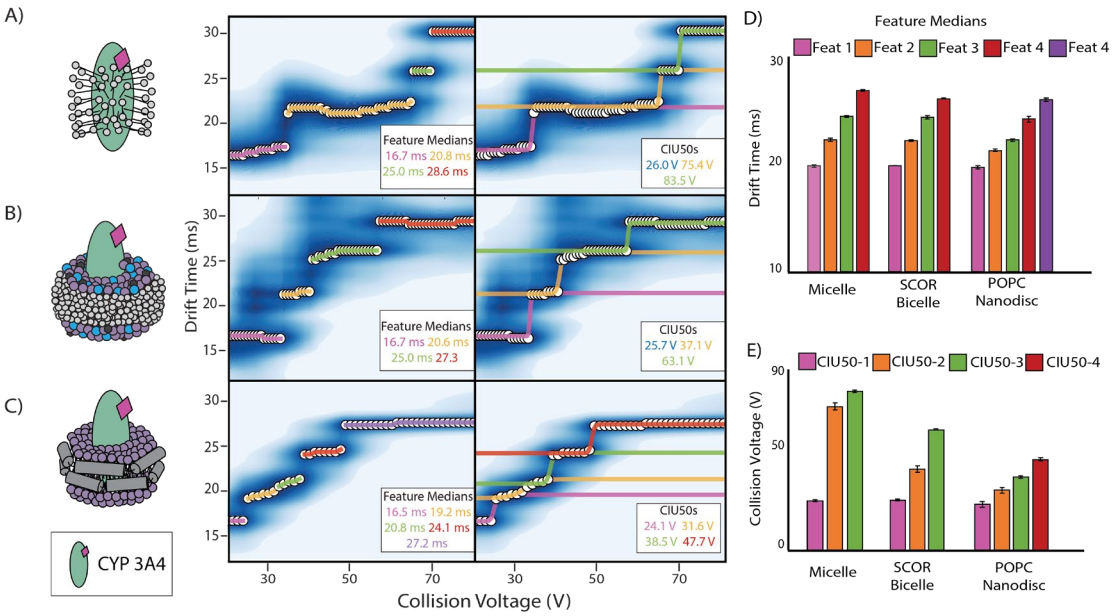

Figure 2-3 CIU of CYP3A4 liberated from detergent micelles, bicelles and nanodiscs. All fingerprints shown are for the 16+ holo state. **A)**. Feature detection analysis of CYP liberated from OG micelles, N = 3, shows features of 16.7 ± 0.2, 20.8 ± 0.2, 24.6 ± 0.1, 28.6 ± 0.1 ms. CIU50 transitions fit to these features occur at 26.0 ± 0.5, 75.4 ± 1.8, and 83.5 ± 0.6 V. **B)**. CYP liberated from SCOR bicelles, N=3, shows features of 16.7 ± 0.1, 20.6 ± 0.1, 25.0 ± 0.3, and 27.3 ± 0.1 ms. CIU 50 transitions fit to these features occur at 25.7 ± 0.6, 37.1 ± 1.6, and 63.1 ± 0.1V **C)**. Feature detection analysis of CYP liberated from POPC nanodiscs with the MSPE3D1 scaffold, N = 3, show features of 16.5 ± 0.3, 19.2 ± 0.2, 20.8 ± 0.2, 24.1 ± 0.5, and 27.2 ± 0.3 ms. CIU 50 transitions fit to these features occur at 24.1 ± 1.5, 31.6 ± 1.5, 38.5 ± 0.7, and 47.7 ± 0.7 V. **D)** comparison of feature drift time medians, **E)** comparison of CUI50 values from CYP3A4 liberated out of various mimetics

To further investigate the differences between CYP3A4 solubilized in micelles, bicelles and NDs, we next performed CIU experiments on 16+ holo ions (Figure 2-3, N = 3). CIU data shown in Figure 2-3A includes five features and four transitions observed for the CYP3A4 micellar replicates, with features beginning at 16.7 ms and a first transition from the most native-like state occurring at 26.0 V. In Figure 2-3B, CIU fingerprint data collected for CYP3A4 liberated from a SCOR bicelles, N=3, contains 4 features of 16.7 ± 0.1, 20.6 ± 0.1, 25.0 ± 0.3, and 27.3 ± 0.1 ms. CIU 50 values fit to these features are 25.7 ± 0.6, 37.1 ± 1.6, and 63.1 ± 0.1V. Figure 2-3C shows the average fingerprint for CYP3A4 generated from the three POPC nanodisc replicates, where we detect five features and four transitions. These data show that CYP3A4 adopts different structures when solubilized in OG micelles, SCOR bicelles, or POPC NDs. Such differences can also be observed in our CIU data through comprehensive difference analyses, as shown in Figure S-3. We

observe different levels of adduction throughout the MS data recorded for ions generated under these conditions, and such adduct population differences have been previously reported to alter CIU data.[84]

2.3.3 CIU Data Indicates Structural Changes in PMP22 Liberated from Micelles, Bicelles, and NDs

Noting the marked differences between PMP22-L16P dimers and GDX monomers liberated from micelles and bicelles, we next aimed to compare additional mimetics and continue to expand our MP survey. We next incorporated a POPC-DDMB bicelles into our comparative workflows. We wanted to continue studying monomeric protein ions to facilitate comparisons across all three solubilization techniques and avoid challenges we encountered in generating sufficient signal intensities for CIU. For these reasons we chose to study a version of WT PMP22 which includes an 11 kDa soluble tag, denoted throughout as WT_{tag} PMP22. The WT_{tag} PMP22 also proved more amenable to ND sample preparation for nMS, as the penta-histidine tag included in the sequence allowed us to use a nickel affinity resin to purify the ND-associated protein. Note that for this reason, the histag free construct of MSP1D1(-) was utilized in these experiments.

As shown in Appendix Figure I-4, WT_{tag} PMP22 can be successfully liberated and detected from C12E8 micelles, SCOR bicelles, POPC-DDMB bicelles, and POPC MSP1D1(-) NDs. We observe signals corresponding to 7-15+ ions of monomeric WT_{tag} PMP22 when the protein is solubilized in both micelles and bicelles, but WT_{tag} PMP22 housed within NDs, IM-MS data indicates significant overlap with MSP1D1(-) signals, reducing the observable charge states to 7-12+ (Figure S5). Ultimately, we determined that the 9+ charge state of WT_{tag} PMP22 was the most suitable for CIU analysis due to its lack of overlap with MSP1D1(-) signals. A CCS analysis of 9+ WT_{tag} PMP22 ions produced from samples containing all mimetics discussed

above were found to yield similar values. Specifically, CCS values recorded for WT_{tag} PMP22 for samples containing micelles: 1,932.1 ± 9 $Å^2$, SCOR bicelles: 1,918.8 ± 9 $Å^2$, POPC-DDMB bicelles: 1,905.4 ± 9 $Å^2$, and POPC NDs: 1,996.5 ± 9 $Å^2$. While we observe that POPC-DDMB bicellar WT_{tag} PMP22 monomers to possess the most compact CCS values, there is no available high-resolution structure for the WT_{tag} PMP22 construct to which we can compare our CCS values in order to assess their proximity to its native fold.

CIU fingerprints recorded for 9+ WT_{tag} PMP22 monomers solubilized in micelles, bicelles, and NDs were generated in triplicate and their averages with detected features and CIU50 transitions are shown in Figure 2-4. The WT_{tag} PMP22 fingerprints produced from samples containing micelles and SCOR bicelles possess three similar features at approximately 17.0 ms, 19.9 ms, and 21.7 ms (Figure 2-4 A, B). However, the most unfolded feature which occurs at 26.4 ms in the bicelle fingerprints is not detected in the micelle fingerprint, as it does not reach the necessary relative intensity within the bounds of the collision voltage range probed. This information can be combined with the CIU50-1 and CIU50-2 values to illustrate that the WT_{tag} PMP22 liberated from detergent micelles is more stabilized relative to SCOR bicelles. Interestingly, there are no apparent differences in the level of adduction of the ions probed in these data as there were for the CYP3A4 data (discussed above) in Figure 2-3. To further explore the solubilization agent dependent changes in the CIU fingerprints collected for monomeric WT_{tag} PMP22, comprehensive difference analysis was performed across all four CIU datasets as shown in Appendix Figure I-5. The micellar and bicellar WT_{tag} PMP22 monomer fingerprints were found to be the most similar between the three solubilization techniques, with an RMSD of 16.0%. On the other hand, RMSD is remains three times higher than our greatest baseline replicate RMSD of 5.8%.

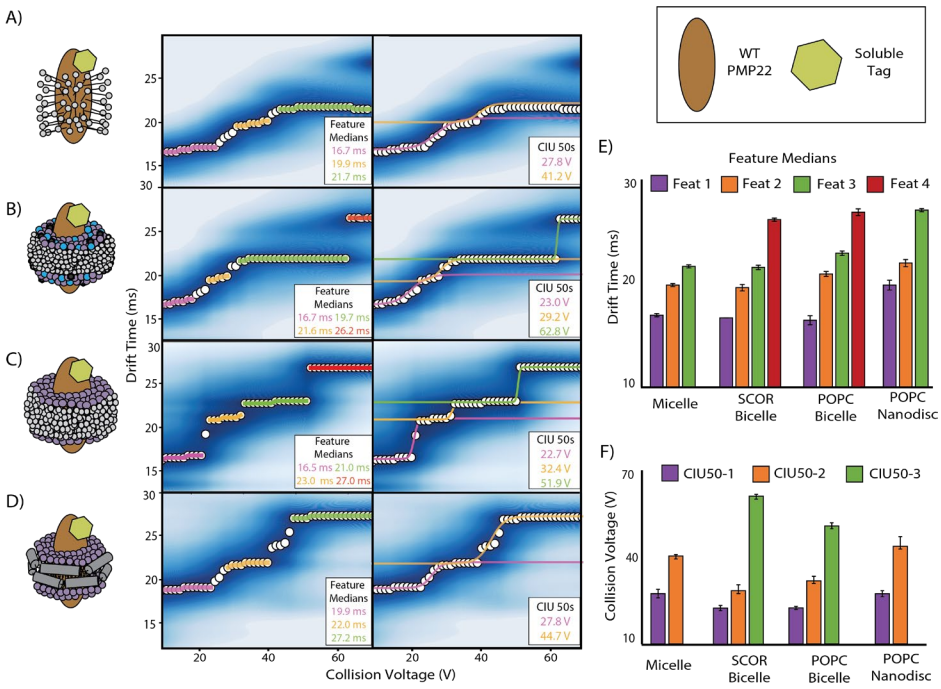

Figure 2-4 . CIU of WT_{tag} PMP22 monomers liberated from detergent micelles, SCOR bicelles, POPC bicelles, and POPC nanodiscs. All fingerprints shown are for the 9+ monomeric charge state. **A**). Feature detection analysis of WT_{tag} PMP22 monomers liberated from C12E8 micelles, N = 3, shows three features of 17.0 ± 0.2, 19.9 ± 0.1, and 21.7 ± 0.2 ms. CIU50 transitions fit to these features occur at 27.8 ± 1.5 and 41.2 ± 0.5 V **B)**. Feature detection analysis of WT_{tag} PMP22 monomers liberated from SCOR bicelles, N = 3, shows four features of 16.8 ± 0.2, 19.8 ± 0.3, 21.7 ± 0.2, and 26.4 ± 0.2 ms. CIU50 transitions fit to these features occur at 22.4 ± 1.3 V, 29.2 ± 2.0 V, and 62.8 ± 0.7 V.**C)** Feature detection analysis of WT_{tag} PMP22 monomers liberated from POPC-DDMB bicelles, N = 3, shows four features of 16.5 ± 0.4, 21.0 ± 0.2, 23.0 ± 0.2, and 27.0 ± 0.3 ms. CIU50 transitions fit to these features occur at 22.7 ± 0.6, 32.4 ± 1.6, and 51.9 ± 0.1 V **D)**. Feature detection analysis of WT_{tag} PMP22 monomers liberated from POPC nanodiscs, N = 3, shows three features of 20.0 ± 0.5, 22.0 ± 0.3, and 27.2 ± 0.2 ms. CIU 50 transitions fit to these features occur at 27.8 ± 1.1 and 44.7 ± 3.3 V

The features detected in the WT_{tag} PMP22 ND CIU fingerprints are significantly different than those detected for ions generated from micellar and bicellar samples, with features at 20.0 ± 0.5 ms, 22.0 ± 0.3 ms, and 27.2 ± 0.2 ms (Figure 5-3D). The differences in low-energy CCSs recorded for WT_{tag} PMP22 monomers liberated from POPC NDs adopt a more extended state following ejection from the membrane mimetic relative to those generated from micelles and SCOR bicelles. A comprehensive difference analysis for this CIU data indicates that WT_{tag} PMP22 ND fingerprints are significantly different from those generated from micellar and bicellar

samples, with RMSDs of 25.4% and 34.8% (Appendix Figure I-5), which are at least two times greater than the ND baseline for replicate analyses (RMSD of 16.0%). Next, to further probe the role that solubilization techniques play in promoting the adoption of specific MP structures, we liberated WT_{tag} PMP22 from a POPC-DDMB bicelles and compared these data directly to WT_{tag} PMP22 data produced from NDs, as they both provide a POPC bilayer environment. As above, we see marked differences in the CIU data collected. CIU feature detection analysis of WT_{tag} PMP22 monomers liberated from POPC-DDMB bicelles (N = 3), reveals four features of 16.5 ± 0.4 ms, 21.0 ± 0.2 ms, 23.0 ± 0.2 ms, and 27.0 ± 0.3 ms. CIU50 values fit to these features occur at 22.7 ± 0.6, 32.4 ± 1.6, and 51.9 ± 0.1 V. The significant differences detected in our CIU data indicate that PMP22 can adopt different conformations within these differently produced POPC bilayers. It is possible that detergents act to orient lipids to form a bilayer differently than MSP, causing PMP22 to adopt different conformations.

2.4 Conclusions

MS methods have been extended to directly analyze MPs solubilized using many techniques, and here we have demonstrated how IM-MS and CIU methods can also be broadly extended from detergent micelles to more complex membrane mimetics. We report CIU fingerprints from SCOR bicelles and NDs for multiple proteins which are readily analyzed by existing software workflows. In the case of CYP3A4, we observe excess detergent, salt, and glycerol adduction, which may cause increases in stability as observed by CIU for CYP3A4 samples analysed from of micellar samples relative to ND samples. In the case of L16P PMP22 dimers, our evidence indicates that SCOR bicelles may support more compact gas phase structures than C12E8 micelles. Similarly, we observe that GDX produces different CIU data when liberated from environments containing detergent when compared to ions liberated from a lipid-based

environment. Indeed, this data suggests not only compaction of the MP but also stabilization. Additionally, we find that for WT_{tag} PMP22, CIU fingerprints collected across four different solubilization vehicles exhibit differences which are most directly explained through differences in PMP22 conformation promoted in each of the four environments.

Overall, we find extensive CIU and IM-MS evidence suggesting that MP structure strongly depends upon the solubilization method used to house the protein prior to liberation in the gas-phase. Our data also reveals that solubilization techniques can strongly influence MP S/N and the robustness of the IM-MS data collected (Figure S2). In order to further advance the analysis of MP structure using IM-MS and CIU, studies must be conducted in an effort to parse the contributions of lipid composition, the structures of the mimetics used, and the various methods employed for their preparation on the ultimate MP structure and stability differences observed in our data. Additionally, extending the data shown here to a broader array of protein systems, such as GPCRs, could be vital for defining the role of nMS in the assessment of solubilization agents for applications such as MP cryo-EM or pharmaceutical screens.

2.5 Acknowledgments

Membrane protein research in the Ruotolo lab is supported by the National Institute of Health under Grants GM105942. The author thanks collaborators (co-first authors) Iliana Levesque and Sarah M. Fantin for their contributions to this chapter. As well as collaborators, Chuck Sanders (Vanderbilt University), Melanie Ohi (University of Michigan) and Randy Stockbridge (University of Michigan) labs for their contribution for providing protein stocks (Sanders/Ohi: PMP22 & Stockbridge: GDX)

Bibliography

(1) Deamer, D. Membranes and the Origin of Life: A Century of Conjecture. *J. Mol. Evol.* **2016**, *83* (5–6), 159–168.

(2) Newman, S. A. Cell Differentiation: What Have We Learned in 50 Years? *J. Theor. Biol.* **2020**, *485*.

(3) How Many Cells Are In Your Body? https://www.nationalgeographic.com/science/article/how-many-cells-are-in-your-body (accessed Jun 16, 2022).

(4) Thoma, J.; Burmann, B. M. Fake It 'Till You Make It-The Pursuit of Suitable Membrane Mimetics for Membrane Protein Biophysics. *Int. J. Mol. Sci.* **2020**, *22* (1), 1–22.

(5) Zimmerberg, J. Membrane Biophysics. *Curr. Biol.* **2006**, *16* (8).

(6) Cullis, P. R.; De Kruijff, B. Lipid Polymorphism and the Functional Roles of Lipids in Biological Membranes. *BBA - Rev. Biomembr.* **1979**, *559* (4), 399–420.

(7) Membrane Proteins - Molecular Biology of the Cell - NCBI Bookshelf https://www.ncbi.nlm.nih.gov/books/NBK26878/ (accessed Jun 16, 2022).

(8) Wallin, E.; Heijne, G. Von. Genome-Wide Analysis of Integral Membrane Proteins from Eubacterial, Archaean, and Eukaryotic Organisms. *Protein Sci.* **2008**, *7* (4), 1029–1038.

(9) Shimizu, K.; Cao, W.; Saad, G.; Shoji, M.; Terada, T. Comparative Analysis of Membrane Protein Structure Databases. *Biochim. Biophys. Acta - Biomembr.* **2018**, *1860* (5), 1077–1091.

(10) Moraes, I.; Evans, G.; Sanchez-Weatherby, J.; Newstead, S.; Stewart, P. D. S. Membrane Protein Structure Determination-The next Generation ☆☆. **2014**.

(11) Almén, M. S.; Nordström, K. J.; Fredriksson, R.; Schiöth, H. B. Mapping the Human Membrane Proteome: A Majority of the Human Membrane Proteins Can Be Classified According to Function and Evolutionary Origin. **2009**.

(12) Santos, R.; Ursu, O.; Gaulton, A.; Patrícia Bento, A.; Donadi, R. S.; Bologa, C. G.; Karlsson, A.; Al-Lazikani, B.; Hersey, A.; Oprea, T. I.; Overington, J. P. A Comprehensive Map of Molecular Drug Targets. **2017**.

(13) Cho, W.; Stahelin, R. V. Membrane-Protein Interactions in Cell Signaling and Membrane Trafficking. *Annu. Rev. Biophys. Biomol. Struct.* **2005**, *34*, 119–151.

(14) Phillips, R.; Ursell, T.; Wiggins, P.; Sens, P. Emerging Roles for Lipids in Shaping Membrane-Protein Function. *Nature* **2009**, *459* (7245), 379–385.

(15) Weekes, M. P.; Antrobus, R.; Lill, J. R.; Duncan, L. M.; Hör, S.; Lehner, P. J. Comparative Analysis of Techniques to Purify Plasma Membrane Proteins. *J. Biomol. Tech.* **2010**, *21* (3), 108.

(16) Haffke, M.; Duckely, M.; Bergsdorf, C.; Jaakola, V. P.; Shrestha, B. Development of a Biochemical and Biophysical Suite for Integral Membrane Protein Targets: A Review. *Protein Expr. Purif.* **2020**, *167*, 105545.

(17) Oluwole, A. O.; Danielczak, B.; Meister, A.; Babalola, J. O.; Vargas, C.; Keller, S. Solubilization of Membrane Proteins into Functional Lipid-Bilayer Nanodiscs Using a Diisobutylene/Maleic Acid Copolymer. *Angew. Chemie - Int. Ed.* **2017**, *56* (7), 1919–

1924.
(18) White, S. H.; Wimley, W. C. MEMBRANE PROTEIN FOLDING AND STABILITY: Physical Principles. *http://dx.doi.org.proxy.lib.umich.edu/10.1146/annurev.biophys.28.1.319* **2003**, *28*, 319–365.
(19) Lacapère, J.-J.; Pebay-Peyroula, E.; Neumann, J.-M.; Etchebest, C. Determining Membrane Protein Structures: Still a Challenge! *Trends Biochem. Sci.* **2007**, *32* (6), 259–270.
(20) Cross, T. A.; Sharma, M.; Yi, M.; Zhou, H.-X. Influence of Solubilizing Environments on Membrane Protein Structures. *Trends Biochem. Sci.* **2011**, *36* (2), 117.
(21) C, B.; A, R. Picturing the Membrane-Assisted Choreography of Cytochrome P450 with Lipid Nanodiscs. *Chemphyschem* **2018**, *19* (20), 2603–2613.
(22) Frey, L.; Lakomek, N. A.; Riek, R.; Bibow, S. Micelles, Bicelles, and Nanodiscs: Comparing the Impact of Membrane Mimetics on Membrane Protein Backbone Dynamics. *Angew. Chem. Int. Ed. Engl.* **2017**, *56* (1), 380–383.
(23) Zhan, L.-P.; Liu, C.-Z.; Nie, Z.-X. Mass Spectrometry of Membrane Proteins. In *Membrane Biophysics*; Springer Singapore: Singapore, 2018; pp 285–317.
(24) Sobott, F.; Konijnenberg, A.; Van Dyck, J. F.; Kailing, L. L. Extending Native Mass Spectrometry Approaches to Integral Membrane Proteins. *Biol. Chem* **2015**, *396* (910), 991–1002.
(25) Gault, J.; Donlan, J. A. C.; Liko, I.; Hopper, J. T. S.; Gupta, K.; Housden, N. G.; Struwe, W. B.; Marty, M. T.; Mize, T.; Bechara, C.; Zhu, Y.; Wu, B.; Kleanthous, C.; Belov, M.; Damoc, E.; Makarov, A.; Robinson, C. V. High-Resolution Mass Spectrometry of Small Molecules Bound to Membrane Proteins.
(26) Konijnenberg, A.; Yilmaz, D.; Ingólfsson, H. I.; Dimitrova, A.; Marrink, S. J.; Li, Z.; Vénien-Bryan, C.; Sobott, F.; Kocer, A. Global Structural Changes of an Ion Channel during Its Gating Are Followed by Ion Mobility Mass Spectrometry. *Proc. Natl. Acad. Sci. U. S. A.* **2014**, *111* (48), 17170–17175.
(27) Gupta, K.; Donlan, J. A. C.; Hopper, J. T. S.; Uzdavinys, P.; Landreh, M.; Struwe, W. B.; Drew, D.; Baldwin, A. J.; Stansfeld, P. J.; Robinson, C. V. The Role of Interfacial Lipids in Stabilizing Membrane Protein Oligomers Oligomerization of Membrane Proteins in Response to Lipid Binding Has a Critical Role in Many Cell-Signalling Pathways. **2017**.
(28) Gupta, K.; Li, J.; Liko, I.; Gault, J.; Bechara, C.; Wu, D.; S Hopper, J. T.; Giles, K.; P Benesch, J. L.; Robinson, C. V. Identifying Key Membrane Protein Lipid Interactions Using Mass Spectrometry. *Nat. Publ. Gr.* **2018**, *13*.
(29) Landreh, M.; Costeira-Paulo, J.; Gault, J.; Marklund, E. G.; Robinson, C. V. Effects of Detergent Micelles on Lipid Binding to Proteins in Electrospray Ionization Mass Spectrometry. **2017**.
(30) I, L.; MT, D.; S, L.; TD, N.; J, G.; E, R.; JTS, H.; NG, H.; P, W.; M, C.; A, S.; BA, W.; C, K.; PJ, S.; H, B.; JLP, B.; TM, A.; CV, R. Lipid Binding Attenuates Channel Closure of the Outer Membrane Protein OmpF. *Proc. Natl. Acad. Sci. U. S. A.* **2018**, *115* (26), 6691–6696.
(31) AJ, B.; DJ, H.; CV, R. Detergent Release Prolongs the Lifetime of Native-like Membrane Protein Conformations in the Gas-Phase. *J. Am. Chem. Soc.* **2013**, *135* (16), 6078–6083.
(32) Fantin, S. M.; Parson, K. F.; Niu, S.; Liu, J.; Polasky, D. A.; Dixit, S. M.; Ferguson-Miller, S. M.; Ruotolo, B. T. Collision Induced Unfolding Classifies Ligands Bound to the

Integral Membrane Translocator Protein (TSPO). *Anal. Chem.* **2019**, acs.analchem.9b03208.
(33) Gault, J.; Liko, I.; Landreh, M.; Shutin, D.; Reddy Bolla, J.; Jefferies, D.; Agasid, M.; Yen, H.-Y.; G W Ladds, M. J.; Lane, D. P.; Khalid, S.; Mullen, C.; Remes, P. M.; Huguet, R.; McAlister, G.; Goodwin, M.; Viner, R.; Syka, J. E.; Robinson, C. V. Combining Native and 'Omics' Mass Spectrometry to Identify Endogenous Ligands Bound to Membrane Proteins. *Nat. Methods*.
(34) Watkinson, T. G.; Calabrese, A. N.; Ault, J. R.; Radford, S. E.; Ashcroft, A. E. FPOP-LC-MS/MS Suggests Differences in Interaction Sites of Amphipols and Detergents with Outer Membrane Proteins. *J. Am. Soc. Mass Spectrom 28*, 50–55.
(35) Calabrese, A. N.; Watkinson, T. G.; Henderson, P. J. F.; Radford, S. E.; Ashcroft, A. E. Amphipols Outperform Dodecylmaltoside Micelles in Stabilizing Membrane Protein Structure in the Gas Phase. *Anal. Chem.* **2015**, *87* (2), 1118–1126.
(36) SM, F.; KF, P.; P, Y.; B, J.; GC, L.; CR, S.; MD, O.; BT, R. Ion Mobility-Mass Spectrometry Reveals the Role of Peripheral Myelin Protein Dimers in Peripheral Neuropathy. *Proc. Natl. Acad. Sci. U. S. A.* **2021**, *118* (17).
(37) Hutchison, J. M.; Shih, K. C.; Scheidt, H. A.; Fantin, S. M.; Parson, K. F.; Pantelopulos, G. A.; Harrington, H. R.; Mittendorf, K. F.; Qian, S.; Stein, R. A.; Collier, S. E.; Chambers, M. G.; Katsaras, J.; Voehler, M. W.; Ruotolo, B. T.; Huster, D.; McFeeters, R. L.; Straub, J. E.; Nieh, M. P.; Sanders, C. R. Bicelles Rich in Both Sphingolipids and Cholesterol and Their Use in Studies of Membrane Proteins. *J. Am. Chem. Soc.* **2020**, *142* (29), 12715–12729.
(38) Keener, J. E.; Zambrano, D. E.; Zhang, G.; Zak, C. K.; Reid, D. J.; Deodhar, B. S.; Pemberton, J. E.; Prell, J. S.; Marty, M. T. Chemical Additives Enable Native Mass Spectrometry Measurement of Membrane Protein Oligomeric State within Intact Nanodiscs. *J. Am. Chem. Soc.* **2019**, *141* (2), 1054–1061.
(39) Henrich, E.; Peetz, O.; Hein, C.; Laguerre, A.; Hoffmann, B.; Hoffmann, J.; Dötsch, V.; Bernhard, F.; Morgner, N. Analyzing Native Membrane Protein Assembly in Nanodiscs by Combined Non-Covalent Mass Spectrometry and Synthetic Biology. *Elife* **2017**, *6*.
(40) Harvey, S. R.; Vanaernum, Z. L.; Kostelic, M. M.; Marty, M. T.; Wysocki, V. H. Probing the Structure of Nanodiscs Using Surface-Induced Dissociation Mass Spectrometry †. **2020**.
(41) Marty, M. T.; Hoi, K. K.; Robinson, C. V. Interfacing Membrane Mimetics with Mass Spectrometry. *Acc. Chem. Res.* **2016**, *49* (11), 2459–2467.
(42) Marty, M. T. Nanodiscs and Mass Spectrometry: Making Membranes Fly. *Int. J. Mass Spectrom.* **2020**, 116436.
(43) Hellwig, N.; Peetz, O.; Ahdash, Z.; Tascó, I.; Booth, P. J.; Mikusevic, V.; Diskowski, M.; Politis, A.; Hellmich, Y.; Hä, I.; Reading, E.; Morgner, N. Native Mass Spectrometry Goes More Native: Investigation of Membrane Protein Complexes Directly from SMALPs †. *Chem. Commun* **2018**, *54*, 13702.
(44) Chorev, D. S.; Tang, H.; Rouse, S. L.; Reddy Bolla, J.; Von Kügelgen, A.; Baker, L. A.; Wu, D.; Gault, J.; Grünewald, K.; Bharat, T. A. M.; Matthews, S. J.; Robinson, C. V. The Use of Sonicated Lipid Vesicles for Mass Spectrometry of Membrane Protein Complexes. *Nat. Protoc.*
(45) Marty, M. T.; Hoi, K. K.; Gault, J.; Robinson, C. V. Probing the Lipid Annular Belt by Gas-Phase Dissociation of Membrane Proteins in Nanodiscs. *Angew. Chemie Int. Ed.*

2016, *55* (2), 550–554.
(46) Chorev, D. S.; Baker, L. A.; Wu, D.; Beilsten-Edmands, V.; Rouse, S. L.; Zeev-Ben-Mordehai, T.; Jiko, C.; Samsudin, F.; Gerle, C.; Khalid, S.; Stewart, A. G.; Matthews, S. J.; Grünewald, K.; Robinson, C. V. Protein Assemblies Ejected Directly from Native Membranes Yield Complexes for Mass Spectrometry. *Science* **2018**, *362* (6416), 829–834.
(47) Ruotolo, B. T.; Benesch, J. L. P.; Sandercock, A. M.; Hyung, S. J.; Robinson, C. V. Ion Mobility-Mass Spectrometry Analysis of Large Protein Complexes. *Nat. Protoc.* **2008**, *3* (7), 1139–1152.
(48) Polasky, Daniel A; Dixit, Sugyan M.; Fantin, Sarah M.; Ruotolo, B. T. "CIUSuite 2: Next-Generation Software for the Analysis of Gas-Phase Protein Unfolding Data." *Press*.
(49) Barrera, N. P.; Isaacson, S. C.; Zhou, M.; Bavro, V. N.; Welch, A.; Schaedler, T. A.; Seeger, M. A.; Miguel, R. N.; Korkhov, V. M.; van Veen, H. W.; Venter, H.; Walmsley, A. R.; Tate, C. G.; Robinson, C. V. Mass Spectrometry of Membrane Transporters Reveals Subunit Stoichiometry and Interactions. *Nat. Methods 2009 68* **2009**, *6* (8), 585–587.
(50) Landreh, M.; Liko, I.; Uzdavinys, P.; Coincon, M.; Hopper, J. T. S.; Drew, D.; Robinson, C. V. Controlling Release, Unfolding and Dissociation of Membrane Protein Complexes in the Gas Phase through Collisional Cooling. *Chem. Commun.* **2015**, *51* (85), 15582–15584.
(51) Laganowsky, A.; Reading, E.; Allison, T. M.; Ulmschneider, M. B.; Degiacomi, M. T.; Baldwin, A. J.; Robinson, C. V. Membrane Proteins Bind Lipids Selectively to Modulate Their Structure and Function. *Nature* **2014**.
(52) Allison, T. M.; Reading, E.; Liko, I.; Baldwin, A. J.; Laganowsky, A.; Robinson, C. V. Quantifying the Stabilizing Effects of Protein-Ligand Interactions in the Gas Phase. *Nat. Commun.* **2015**, *6*.
(53) Hosea, N. A.; Miller, G. P.; Guengerich, F. P. Elucidation of Distinct Ligand Binding Sites for Cytochrome P450 3A4. *Biochemistry* **2000**, *39* (20), 5929–5939.
(54) Gillam, E. M. J.; Baba, T.; Kim, B. R.; Ohmori, S.; Guengerich, F. P. Expression of Modified Human Cytochrome P450 3A4 in Escherichia Coli and Purification and Reconstitution of the Enzyme. *Arch. Biochem. Biophys.* **1993**, *305* (1), 123–131.
(55) Wade, J. H.; Jones, J. D.; Lenov, I. L.; Riordan, C. M.; Sligar, S. G.; Bailey, R. C. Microfluidic Platform for Efficient Nanodisc Assembly, Membrane Protein Incorporation, and Purification. *Lab Chip* **2017**, *17* (17), 2951–2959.
(56) Schlebach, J. P.; Peng, D.; Kroncke, B. M.; Mittendorf, K. F.; Narayan, M.; Carter, B. D.; Sanders, C. R. Reversible Folding of Human Peripheral Myelin Protein 22, a Tetraspan Membrane Protein. *Biochemistry* **2013**, *52* (19), 3229–3241.
(57) Kermani, A. A.; Macdonald, C. B.; Gundepudi, R.; Stockbridge, R. B. Guanidinium Export Is the Primal Function of SMR Family Transporters. **2018**.
(58) Zhan, L. P.; Liu, C. Z.; Nie, Z. X. Mass Spectrometry of Membrane Proteins. In *Membrane Biophysics: New Insights and Methods*; Springer Singapore, 2017; pp 285–317.
(59) Sligar, S. G.; Denisov, I. G. Nanodiscs: A Toolkit for Membrane Protein Science. *Protein Sci.* **2021**, *30* (2), 297–315.
(60) Denisov, I. G.; Sligar, S. G. Nanodiscs in Membrane Biochemistry and Biophysics. *Chem. Rev.* **2017**, *117*, 4669–4713.
(61) Li, F.; Liu, J.; Zheng, Y.; Garavito, R. M.; Ferguson-Miller, S. Crystal Structures of

Translocator Protein (TSPO) and Mutant Mimic of a Human Polymorphism. *Science (80-.).* **2015**, *347* (6221), 555–558.
(62) Mittendorf, K. F.; Kroncke, B. M.; Meiler, J.; Sanders, C. R. The Homology Model of PMP22 Suggests Mutations Resulting in Peripheral Neuropathy Disrupt Transmembrane Helix Packing. *Biochemistry* **2014**, *53* (39), 6139–6141.
(63) Ruotolo, B. T.; Benesch, J. L. P.; Sandercock, A. M.; Hyung, S. J.; Robinson, C. V. Ion Mobility-Mass Spectrometry Analysis of Large Protein Complexes. *Nat. Protoc.* **2008**, *3* (7), 1139–1152.
(64) Marklund, E. G.; Degiacomi, M. T.; Baldwin, A. J.; Benesch, J. L. P.; Marklund, E. G.; Degiacomi, M. T.; Robinson, C. V; Baldwin, A. J.; Benesch, J. L. P. Collision Cross Sections for Structural Proteomics Resource Collision Cross Sections for Structural Proteomics. *Struct. Des.* **2015**, *23* (4), 791–799.
(65) Haynes, S. E.; Polasky, D. A.; Dixit, S. M.; Majmudar, J. D.; Neeson, K.; Ruotolo, B. T.; Martin, B. R. Variable-Velocity Traveling-Wave Ion Mobility Separation Enhancing Peak Capacity for Data-Independent Acquisition Proteomics. *Anal. Chem.* **2017**, *89* (11), 5669–5672.
(66) Polasky, D. A.; Dixit, S. M.; Vallejo, D. D.; Kulju, K. D.; Ruotolo, B. T. An Algorithm for Building Multi-State Classifiers Based on Collision-Induced Unfolding Data. **2019**.
(67) Polasky, D. A.; Dixit, S. M.; Fantin, S. M.; Ruotolo, B. T. CIUSuite 2: Next-Generation Software for the Analysis of Gas-Phase Protein Unfolding Data. *Press*.
(68) Dowhan, W.; Vitrac, H.; Bogdanov, · Mikhail. Lipid-Assisted Membrane Protein Folding and Topogenesis. *Protein J.* **1234**, *38*, 274–288.
(69) Kostelic, M. M.; Ryan, A. M.; Reid, D. J.; Noun, J. M.; Marty, M. T. *Expanding the Types of Lipids Amenable to Native Mass Spectrometry of Lipoprotein Complexes Supplementary Material*.
(70) Gupta, K.; Donlan, J. A. C.; Hopper, J. T. S.; Uzdavinys, P.; Landreh, M.; Struwe, W. B.; Drew, D.; Baldwin, A. J.; Stansfeld, P. J.; Robinson, C. V. The Role of Interfacial Lipids in Stabilising Membrane Protein Oligomers Europe PMC Funders Group. *Nature* **2017**, *541* (7637), 421–424.
(71) Ilag, L. L.; Ubarretxena-Belandia, I.; Tate, C. G.; Robinson, C. V. Drug Binding Revealed by Tandem Mass Spectrometry of a Protein-Micelle Complex. *J. Am. Chem. Soc.* **2004**, *126* (44), 14362–14363.
(72) Bay, D. C.; Rommens, K. L.; Turner, R. J. Small Multidrug Resistance Proteins: A Multidrug Transporter Family That Continues to Grow. *Biochim. Biophys. Acta - Biomembr.* **2008**, *1778* (9), 1814–1838.
(73) Peetz, O.; Hellwig, N.; Henrich, E.; Mezhyrova, J.; Dötsch, V.; Bernhard, F.; Morgner, N. LILBID and NESI: Different Native Mass Spectrometry Techniques as Tools in Structural Biology. *J. Am. Soc. Mass Spectrom* **2061**, *30*, 181–191.
(74) Jamshad, M.; Lin, Y.-P.; Knowles, T. J.; Parslow, R. A.; Harris, C.; Wheatley, M.; Poyner, D. R.; Bill, R. M.; Thomas, O. R. T.; Overduin, M.; Dafforn, T. R. Surfactant-Free Purification of Membrane Proteins with Intact Native Membrane Environment. *Biochem. Soc. Annu. Symp.* No. 78.
(75) Bechara, C.; Robinson, C. V. Different Modes of Lipid Binding to Membrane Proteins Probed by Mass Spectrometry. *J. Am. Chem. Soc.* **2015**, *137* (16), 5240–5247.
(76) Kermani, A. A.; Macdonald, C. B.; Burata, O. E.; Ben Koff, B.; Koide, A.; Denbaum, E.; Koide, S.; Stockbridge, R. B. The Structural Basis of Promiscuity in Small Multidrug

Resistance Transporters. *Nat. Commun. 2020 111* **2020**, *11* (1), 1–9.
(77) Sahin, C.; Reid, D. J.; Marty, M. T.; Landreh, M. Scratching the Surface: Native Mass Spectrometry of Peripheral Membrane Protein Complexes. **2020**.
(78) Allen, K. N.; Entova, S.; Ray, L. C.; Imperiali, B. Monotopic Membrane Proteins Join the Fold. *Trends in Biochemical Sciences*. Elsevier Ltd January 1, 2019, pp 7–20.
(79) Shah, M. B.; Jang, H. H.; Wilderman, P. R.; Lee, D.; Li, S.; Zhang, Q.; Stout, C. D.; Halpert, J. R. Effect of Detergent Binding on Cytochrome P450 2B4 Structure as Analyzed by X-Ray Crystallography and Deuterium-Exchange Mass Spectrometry. *Biophys. Chem.* **2016**, *216*, 1–8.
(80) Lössl, P.; Snijder, J.; Heck, A. J. R. Boundaries of Mass Resolution in Native Mass Spectrometry. *J. Am. Soc. Mass Spectrom.* **2014**.
(81) Denisov, I. G.; Sligar, S. G. Cytochromes P450 in Nanodiscs. *Biochimica et Biophysica Acta - Proteins and Proteomics*. Elsevier January 2011, pp 223–229.
(82) Grinkova, Y. V.; Denisov, I. G.; Sligar, S. G. Functional Reconstitution of Monomeric CYP3A4 with Multiple Cytochrome P450 Reductase Molecules in Nanodiscs. *Biochem. Biophys. Res. Commun.* **2010**, *398* (2), 194–198.
(83) Barnaba, C.; Ramamoorthy, A. Picturing the Membrane-Assisted Choreography of Cytochrome P450 with Lipid Nanodiscs. *ChemPhysChem* **2018**, *19* (20), 2603–2613.
(84) Han, L.; Ruotolo, B. T. Traveling-Wave Ion Mobility-Mass Spectrometry Reveals Additional Mechanistic Details in the Stabilization of Protein Complex Ions through Tuned Salt Additives.

Chapter 3 **Local lipid environment plays a critical role in Cytochrome P450 structure and stability**

3.1 Introduction

Membrane proteins (MPs) are responsible for a variety of biological functions and critical physiological responses[1,2] and currently represent >60% of all drug targets[1,3–5]. Despite the importance of these proteins, our knowledge of MP structure and dynamics lags significantly behind that of cytosolic proteins, as evidenced by the fact that MPs currently represent less than 3% of the structures in the protein data bank[2,6]. The difficulty in characterizing MPs stems partly from their low levels of expression and insolubility in aqueous solutions[7]. Recent advancements in cyro-electron microscopy (cryoEM), X-ray crystallography, and nuclear magnetic resonance (NMR) have served to dramatically advance our understanding of MPs and their complexes, yet many challenges still remain.[8,9]

The development of novel membrane mimetics such as nanodiscs (NDs) present a promising opportunity for the analysis of MPs[10–14]. NDs are discoidal membrane bilayer mimics which encircle the MP with phospholipids and are held together by an amphipathic helical scaffold composed of protein, peptide or polymer.[15–19] They are an appealing construct for MP characterization due to their ability to stabilize native MP structure by mimicking a membrane bilayer environment. However, there are multiple variables in ND construction that have the potential to impact the structure and function of MPs, including lipid composition and scaffold material.[20–22] As such, while NDs represent a promising technology for MP solubilization, questions remain about the effects of these variables on MP dynamics and how ND composition might alter MP function, such as drug binding.

Cytochrome P450 (CYP) enzymes play key roles in the synthesis of a broad range of bio-active molecules and are primarily responsible for the metabolism of both pharmaceutical and cytotoxic compounds.[23–28] Despite the pharmacological importance of this class of enzymes, many unanswered questions persist regarding the relationship between the dynamic structure of CYP and its myriad of functions. While atomic-resolution structures of many CYP isoforms are available, all lack the hydrophobic α-helix region of the protein, which is critical for the association of CYPs with biological membranes.[29–31] Much regarding the impact of lipid binding and membrane composition on this CYP region is currently unknown, including the presence of allosteric networks that may link the local membrane environment to ultimate enzyme activity. Advancements in native mass spectrometry (nMS) present a unique opportunity to elucidate long-standing questions surrounding CYP structures when engaged with cellular membranes. Part of a broader revolution in structural MS technologies, nMS seeks to preserve protein structures and complexes for direct measurements in the gas-phase using MS and has provided valuable information regarding MP structure and function.[32–36] Recent developments in nMS allow for the study of large protein assemblies using nanomoles of sample.[32,37,38] In recent years, native ion mobility-mass spectrometry (IM-MS), has emerged as a robust structural biology tool capable of handling complex mixtures in a high-throughput manner.[39] Membrane mimetics such as NDs promote the retention of native MP conformations[10–13,40,41] thus enabling subsequent IM-MS measurements. IM separates ions based on their size, shape, and charge.[42–44] In native IM-MS experiments, different protein ion conformations can be separated and analyzed compared directly with their solution-phase counterparts.[36,45,46] Once inside the instrument, intact ND-MP complexes can be subjected to collisions with inert gas molecules which act to remove lipids and ND scaffolding material, leaving only a native-like MP for further analysis.[11] Following

liberation from the ND, MPs can be subjected to collision induced unfolding (CIU), which deploys stepwise ion heating to track detailed gas-phase unfolding pathways, revealing the starting structures and stabilities of MP complexes.[47–49]

Most of the nMS studies targeting MPs are limited to transmembrane proteins housed within detergent micelles or NDs of uniform composition.[50–56] As such, questions remain as to the biophysical consequences to MPs upon altering the ND lipid environment, and the general ability of NDs in combination with nMS to access structural data for monotopic membrane proteins. In this study we employ IM-MS and CIU in order to ascertain the details on how local lipid environments and ND design parameters influence CYP structure and stability, using two CYP isoforms, CYP2B4 and CYP3A4 liberated from various ND-lipid environments, including one designed to mimic the composition of the endoplasmic reticulum (ER).[57] Our results indicate significant shifts in MP structure and stability when CYP is liberated from differently constructed ND environments, illustrating the significant impact that the local lipid environment has on MP structure.

3.2 Methods

3.2.1 Membrane Protein Sample Preparation

Full length CYP2B4 and CYP3A4 were expressed in *E. Coli* using the pLW01-P450 and pCWori vectors respectively, using protocols adapted from established protocols for CYP2B4[58] and CYP3A4.[59] Membrane Scaffold Protein 1D1(-), Membrane Scaffold Protein 1E3D1, Amberlite XAD-2 beads, Ammonium acetate were purchased from Sigma Aldrich (St. Louis, MO). Potassium phosphate monobasic and potassium phosphate dibasic were purchased from Fisher Scientific (Hampton, NH). The 4F peptide scaffolding belt (DWFKAFYDKVAEKFKEAF N-terminal modification: acetylation, C-terminal modification:

amidation[60]) was purchased from GenScript (Piscataway, NJ). All lipids (1-palmitoyl-2-oleoyl-sn-glycero-3-phosphoethanolamine [POPE], -palmitoyl-2-oleoyl-sn-glycero-3-phospho-L-serine [POPS], 1-palmitoyl-2-oleoyl-glycero-3-phosphocholine [POPC], L-α-phosphatidylinositol (Soy) [PI], Sphingomyelin (egg, chicken) [eSM] and1,2-dimyristoyl-sn-glycero-3-phosphocholine [DMPC]) were purchased from Avanti Polar Lipids (Alabaster, AL). Cholesterol Hemisuccinate Tris Salt (CHEMS) was purchased from Anatrace (Maumee, OH).

CYP homologs were incorporated into the MSP NDs using the established Sligar protocol[16,17,61] or on a microfluidic device[62] as previously described. Briefly, for either method, the bulk Sligar method or the microfluidic method, dried lipid films were resuspended in 100 mM sodium cholate. Lipids, MSP, CYP and 20 mM sodium cholate were mixed in a standard disc buffer (SDB) buffer containing 20 mM Tris HCl pH 7.4, 100 mM sodium cholate, 0.5 mM EDTA and 0.01% NaN3. The components were incubated at appropriate phase temperatures for the lipids being used for 6 hours (bulk) or 20 minutes (microfluidics). For the bulk preparation, Amberlite XAD-2 Detergent Removal beads were added and left rotating overnight, then beads were removed using a 0.22 μm filter. For microfluidic preparation, the component mixture was flowed through the microfluidic device, a process which takes only 5 minutes, then simultaneously purified and buffer exchanged via size exclusion chromatography (SEC) using Superdex S200 increase 3.2/300 GL column. The peptide 4F NDs were pre-formed by rehydrating 11.25 mg of lipids (dry lipid films) in 40 mM potassium phosphate pH 7.4 buffer and mixing with 7.5 mg of 4F peptide suspended in 40 mM potassium phosphate pH 7.4 buffer. Depending on the phase temperature of the lipids, the mixture was allowed to shake at either 37ºC or 45ºC until the cloudy mixture turned transparent. Empty NDs were purified using SEC on a Superdex S200 increase 10/300 GL column and DLS measurements were obtained using Wyatt DynaPro

NanoStar and fractions with uniform size distribution were chosen for protein incorporation and measured for concentration using a Thermo Scientific NanoDrop 2000 spectrophotometer, using the extinction coefficient for 4F Ɛ = 6.99 mM^{-1} cm^{-1} taking into account 16 peptides per disc. CYP was incubated with empty ND at ratios of 1:1.1 and 1:3 for CYP2B4 and CYP3A4 respectively and incubated for 6-10 hours at room temperature with constant gentle shaking. The increase in empty ND ratio for CYP3A4 helped eliminate protein crash out during incubation. CYP incorporated NDs were simultaneously purified and buffer exchanged into 200 mM ammonium acetate pH 7.4 via SEC on Superdex S200 increase 10/300 or 3.2/300 GL column. CYP-ND only fractions were pooled and concentrated using 100 kDa Amicon Ultra-0.5 centrifugal filter units (MilliporeSigma, Burlington, MA).

3.2.2 Native Ion Mobility – Mass Spectrometry and CIU Experiments.

All IM-MS data was collected using a Synapt G2 HDMS IM-Q-ToF mass spectrometer (Waters, Milford, MA), with a direct infusion nano electrospray ionization (nESI) source set to positive ion mode. Instrument settings were tuned to dissociate solubilization agents with minimal perturbation to protein structure prior to the IM separator, including appropriately tuned settings for the source temperature (30° C), source gas flow (50 mL/min), and the sampling cone (10 V). Trapping cell wave velocity and height were 116 m/s and 0.1 V. IMS wave velocity and height were 250 m/s and 15 V. Transfer cell wave velocity and height were 300 m/s and 10 V, with an accelerating potential of 10 V used to dissociate empty NDs. Collision cross section analysis was performed by IMSCal-19v4, a program written in C. Theoretical collision cross sections (CCSs) of monomeric CYP3A4 were calculated using a previously published homology model and IMPACT. All CIU analyses were performed by increasing the trap collision voltage in a stepwise manner from 20 – 90 V in 5 V increments. CIU data from the 14+ and 15+ charge

states of CYP2B4 and CYP3A4, respectively, were extracted using TWIMExtract[63], then processed and analyzed using CIUSuite2.[49] Data processing included three rounds of 2D Savitzky-Golay smoothing with a window of five bins and interpolation of the collision voltage axis by a factor of four.

3.2.3 Molecular Dynamics

CYP2B4 amino acid sequence was homology modeled with alignment from a previously MD simulated CYP3A4 model[64] using I-TASSER[65–67], the resulting structure was used for subsequent MD simulations in various lipid nanodisc environments. NDs were build using CHARMM-GUI[68] Nanodisc Maker[69] and performed coarse grained MD relaxation using GROMACS.[70] The resulting structures were converted to all atom using Martini All Atom converter.[71,72] The final structures were viewed in PyMol.[73]

3.3 Results and Discussion

3.3.1 CIU of Ligand Bound States Liberated from NDs

Previous reports have detected ligand and lipid binding to MPs, including the identification of endogenous lipid biding,[32,74–78] lipid binding thermodynamics,[54,79–81] lipid binding stability based measurements,[82–84] and stability based measurements to identify regioselective bound ligands.[83] The primary foci of these prior reports are multi-pass transmembrane domain proteins, leaving much unknown regarding the structures and binding activities of monotopic, bitopic and peripherally bound MPs. Among monotopic MPs, CYP is a centrally important hemeprotein, that performs enzymatic activity on a large number of small molecules.[24,85] CYP catalytic activity is mediated by the transfer of two electrons that are donated from its redox partners, cytochrome b5 (cytb5) and cytochrome oxioreductase (POR). A heme lies at the center of the CYP active site

and is spectroscopically active, providing a methodological tool for a wide range of investigations that have revealed many aspects of CYP structure and function.[86–89] The model CYP system CYP2B4 (*Oryctolagus cuniculus*) shares 78% sequence identity with CYP2B6

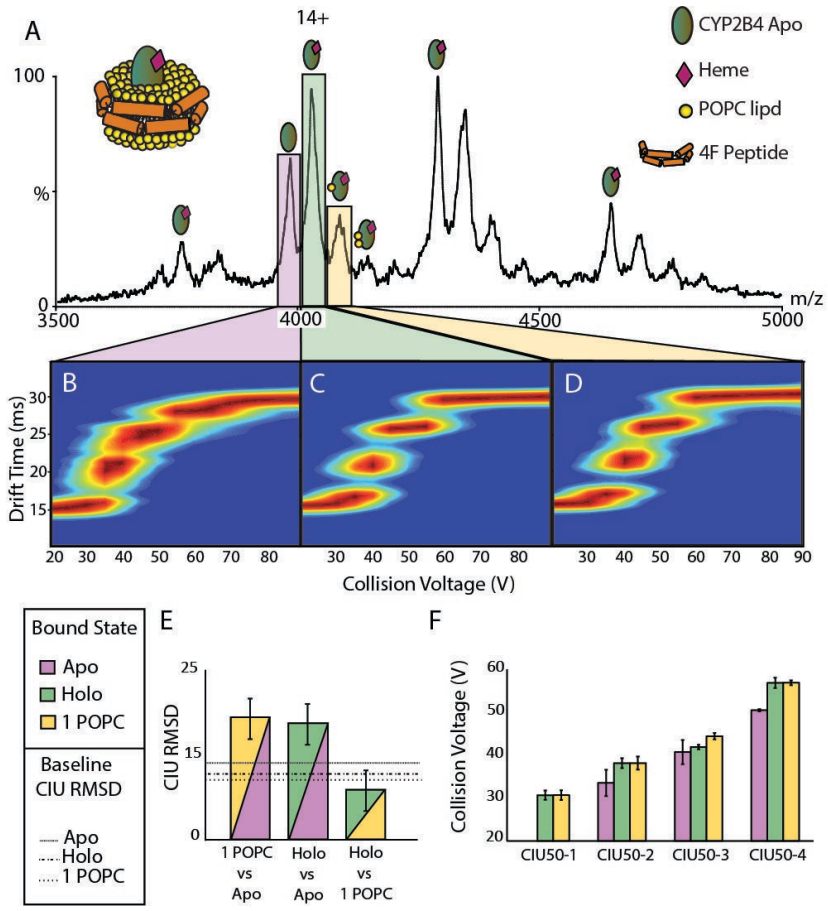

Figure 3-1 Native ion mobility mass spectrometry of CYP2B4 liberated from POPC 4F-peptide NDs **A)** Mass spectra of CYP2B4 liberated from POPC 4F-pepide ND reveals native like charge state distribution of 12-15+ at 80 V as well as various bound states including the heme cofactor and lipid binding **B)** Collision induced unfolding for the 14+ apo species **C)** Collision induced unfolding for 14+ holo (heme intact) species **D)** Collision induced unfolding fingerprint for 14+ holo + 1 POPC bound species **E**) RMSD values determined by total difference analysis of each bound state. The mixed colored bars indicate which species were compared and the baseline RMSD is indicated by the dashed line reporting the day to day error (Apo 11.4%, holo 9.8%, and 1 POPC 8.9%) **F)** CIU50 transition of each bound state N=3 indicating the loss of the heme results in destabilization and 1 POPC bound does not significantly stabilize the CYP2B4

(*homo sapiens*) which is responsible for the metabolism of approximately 3-12% of current small molecule drugs.[90,91] Due to its high homology with CY2B6, and its higher degree of solubility

and stability compared to the human isoform, it is often used as a replacement for CYP2B6 in studies aiming to evaluate CYP structure and function.[57]

We began our experiments by inserting CYP2B4 into POPC 4F NDs, which we then and liberated mimetic and released into the gas phase, yielding IM-MS spectra indicative of native-like CYP monomers (Figure 3-1A). Using IM-MS, chemical noise generated by the peptide and free lipids were separated from the CYP-related signals to aide in detection. We observe discrete ligand bound states including CYP2B4 lacking heme (apo), with heme bound (holo), and attached to both heme and 1 POPC. CIU analysis of these ions was performed to access the relative stability of each CYP state observed. Our results indicate discrete shifts in CYP stability upon both heme and lipid binding. An RMSD based analysis of the CIU data collected (Figure 3-1B-D) reveals significant global differences in the CIU fingerprints collected between apo CYP and both heme and POPC bound protein, producing RMSD values of 17.1 and 18.0 respectively, while detecting strong similarities in the fingerprint data recorded for holo and lipid-bound forms of CYP,

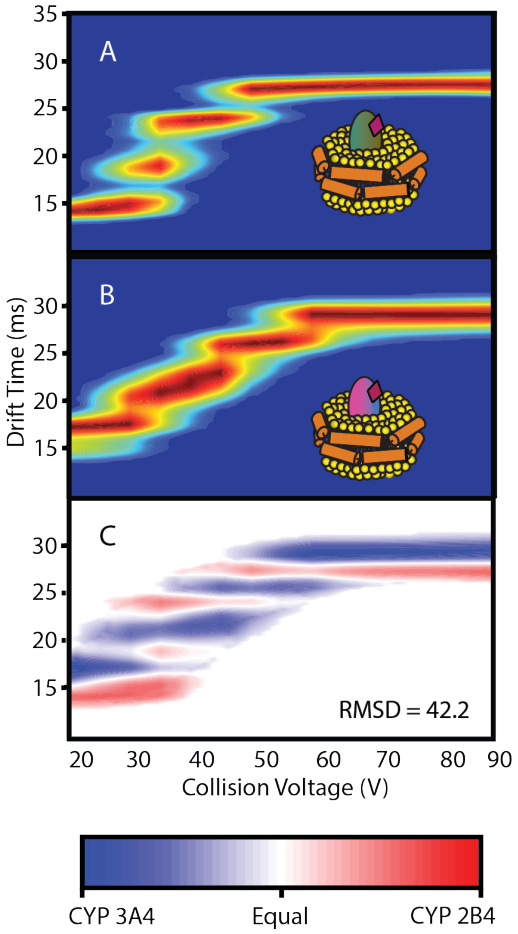

Figure 3-2 CIU comparison of CYP homologs, CYP2B4 and CYP3A4. **A)** Collision induced unfolding of 15+ CYP2B4 (rabbit homolog) liberated from POPC 4F-peptide nanodisc. **B)** Collision induced unfolding of 15+ CYP3A4 (human homolog) liberated from POPC 4F-peptide NDs. **C)** Root mean squared difference plot comparing the two CYP homologs that possess a 28.32% percent identity matrix score. Red and blue traces indicate where CIU data recorded for CYP2B4 or CYP3A4 is more intense in our difference analysis.

producing an RMSD comparison value similar to baseline (Figure 3-1E). Additionally, when comparing CIU50 values recorded for each bound species (Figure 3-1F) we observe evidence of consistent destabilization of apo CYP when compared to either holo or POPC bound CYP states. Taken together, our CYP2B4 IM-MS and CIU data reveals significant structural changes and stabilization CYP upon heme binding, but minimal impacts to protein stability and structure upon lipid attachment.

3.3.2 CIU Comparisons of CYP Homologues

One of the most important members of the human CYP3A subfamily is CYP3A4, which accounts for nearly 30-60% of the total adult population of human CYP.[90,92] In order to evaluate the ability of CIU to differentiate CYP variants, and move our analyses towards a more pharmaceutically relevant human CYP homolog, we collected CIU data for both CYP2B4 and CYP3A4 housed within identically structured ND environments. The sequence identity between CYP2B4 and CYP3A4 is 28.3% (Expasy ProtParam) and thus CIU is expected to produce unique fingerprint data that allows for their rapid differentiation.

Our IM-MS data collected for CYP3A4 liberated from POPC 4F NDs is indicative of native-like CYP monomers, and we selected the 15+ holo charge state for comparison against the same charge state observed for holo CYP2B4 ions prepared through identical means. CIU data collected for both analogues contain a similar number of features, but also display clear differences in the centroid drift times, and by extension the collision cross sections (CCSs) adopted, by the initial and unfolded states observed, the format observed for the initial CIU features detected between 30-40 V, and in the overall appearance voltages associated with all the CIU features observed. A global RMSD comparison of our CYP2B4 and CYP3A4 data produces a value of 42.2, a figure over four times the baseline RMSD value established through an

analysis of technical replicates (9.8, Figure 3-1). This data indicates significant structure and stability differences in the two CYP homologues studied here, with CYP3A4 generating a larger initial CCSs and CIU transitions characterized by both greater stabilities as well as larger CCS, when compared to CYP2B4 (Figure 3-2).

3.3.3 CIU comparisons of ND scaffolding belts

Over the past decade, the use of NDs as membrane mimetics have increased significantly in a manner strongly correlated with increases in our overall understanding of MP-driven biochemistry. NDs are embraced by a scaffolding belt, with the earliest discs constructed using ApoA1 protein.[93] Since then, ApoA1 has been modified to create the membrane scaffolding protein (MSP) belt typically used in ND construction have allowed for the size of assembled NDs to be controlled, further alterations to this belt protein construct, including the design of 4F peptides optimized to increased disc flexibility.[60,94] The process for incorporating a protein into an MSP ND typically involves a co-assembly process that occurs spontaneously upon detergent removal, while peptide NDs are assembled using a detergent free

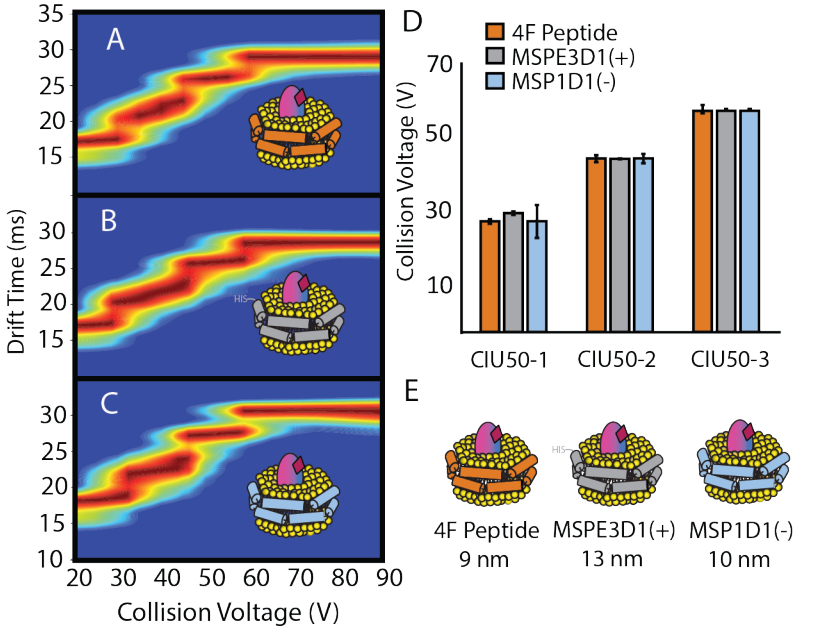

Figure 3-3 Collision induced unfolding of CYP3A4 liberated from various ND belt types **A**) CIU of holo CYP3A4 liberated from a nanodisc containing POPC lipids embraced using the 4F peptide scaffolding belt (11 nm diameter). **B**) CIU of holo 14+ CYP3A4 liberated from a nanodisc containing POPC lipids embraced using the MSPE3D1(+) scaffolding belt (12 nm diameter). **C**). CIU of holo 14+ CYP3A4 liberated from a nanodisc containing POPC lipids embraced using the MSP1D1(-) scaffolding belt (10 nm diameter) **D**). CIU50 transition of each scaffolding type N=3, illustrating the similarities in feature transitions

procedure.[17] While this process is time consuming and laborious, microfluidic approaches are capable of rapidly assembling NDs in a semi-automated fashion.[62] While NDs represent a promising technology for MP solubilization, many questions remain regarding the influence of ND design variables on MP structure and stability.

In order to evaluate the structural consequences associated with ND design elements for CYP3A4, we incorporated the protein into a variety of POPC NDs consisting of three different belt types, 4F peptide, MSPE3D1(+), and MSP1D1(-), resulting in disc diameters 9 nm, 13 nm, and 10 nm respectively. This approach allows us to simultaneously evaluate NDs in terms of their scaffolding materials and but the resulting disc diameter. CIU fingerprints recorded for CYP3A4 recorded across all three ND designs studied here (Figure 3-3A-C) indicate remarkably similar ion CCS, CIU features, and stabilities associated with the liberated CYP ions detected. A further analysis of CIU50 values extracted from our CYP3A4 data reveals quantitatively identical stabilities across all CIU transitions observed in our survey (Figure 3-3D). Overall, our data strongly indicate that the structure and stability of CYPs are not significantly influenced through ND design choices associated protein or peptide belt types (Figure 3-3E).

3.3.4 Local Lipid Environment Influences the Stability and Structure of CYP

Recent work has indicated that full-length CYP2B4 embedded within NDs demonstrates an increased capacity for drug binding and exhibits heme-related spin shift perturbations when compared truncated CYP removed from cellular membrane environments.[57,64,95,96] Such measurements remain challenging, as CYP occupies a wide range of bound states alongside the extreme polydispersity of the lipid bilayer making it difficult for most structural biology technologies to track changes in protein conformation in a manner connected to lipid interactions. IM-MS is well positioned to probe membrane-CYP interactions and their role in

protein structure, stability, and ligand binding. In general, our CIU discussed below strongly indicates that both CYP2B4 and CYP3A4 undergo profound changes in stability and structure in a manner that depends strongly upon the lipid components present within their ND environments.

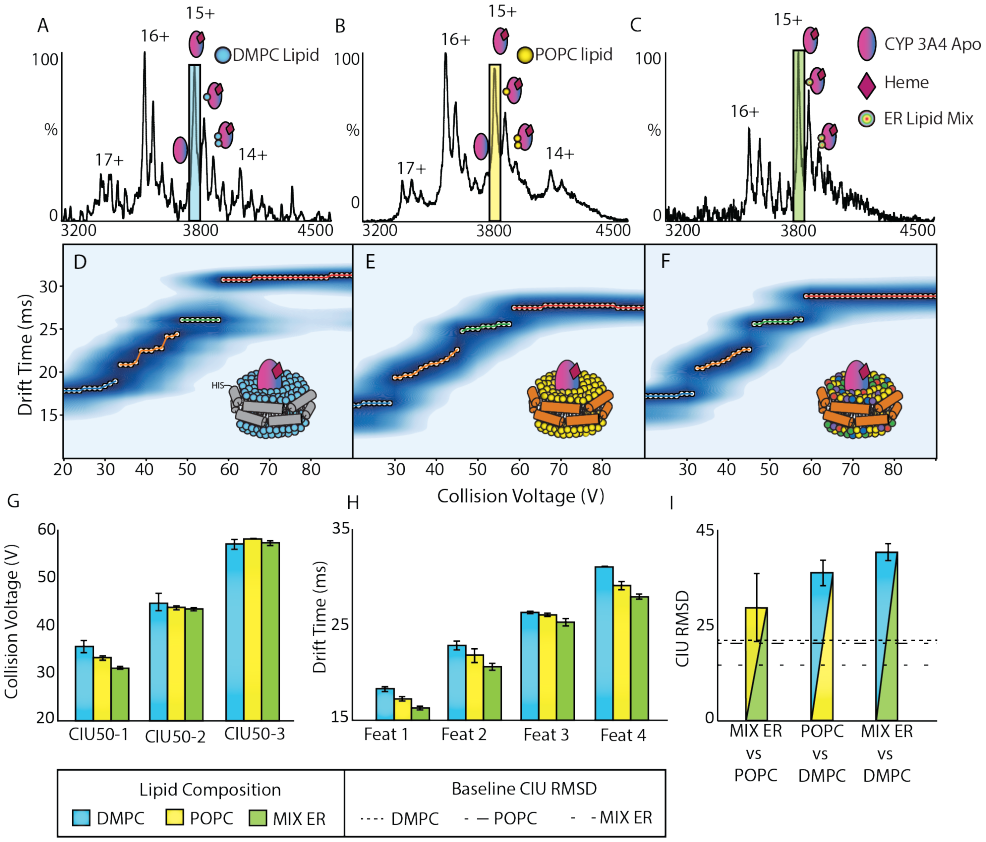

Figure 3-4 Native ion mobility-mass spectrometry of CYP3A4 liberated from various lipid compositions **A**) Mass spectra of CYP3A4 liberated from DMPC MSPE3D1(+) nanodisc revealing charge states 14-17+ and multiple bound states. **B**) Mass spectra of CYP3A4 liberated from POPC 4F-peptide nanodisc revealing charge states 14-17+ and multiple bound states. **C**) Mass spectra of CYP3A4 liberated from ER Mixture 4F-peptide nanodisc revealing charge states 16-15+ and multiple bound states. **D**) CIU of 15+ holo CYP3A4 liberated from DMPC MSPE3D1(+) nanodisc **E**) CIU of 15+ holo CYP3A4 liberated from POPC 4F-peptide nanodisc **F**) CIU of 15+ holo CYP3A4 liberated from ER Mixture 4F-peptide nanodisc **G**) CIU50 analysis comparing stabilization between lipid compositions **H**) Drift time analysis comparing collision cross section between lipid composition **I**) RMSD values determined by total difference analysis of each lipid composition. The mixed colored bars indicate which lipid type was compared and the baseline RMSD is indicated by the dashed line reporting the day to day error.

In order to evaluate the lipid environment dependency of CYP3A4 structure, we incorporated the protein into DMPC MSP1D1(-) NDs, POPC 4F NDs, and Mix ER 4F NDs, the latter of which containing 6 components (POPC, POPE, POPS, POPI, eSM, and cholesterol) and

designed to mimic the cellular ER membrane, the native CYP environment. The nMS data collected for CYP3A4 liberated from the different lipid environments described above reveals evidence of CYP-lipid complexes in both 1:1 and 1:2 stoichiometries, alongside apo and holo CYP forms (Figure 3-4 AC). Evaluated in isolation, this nMS data does not provide clear evidence of any structural differences in CYP ions liberated from the ND environments probed here; however, CIU data reveals significant differences in feature CCS and stabilities in the CYP ions detected in our experiments (Figure 3-4D-F). It is important to note that CIU data shown in Figure 3-4 are extracted from CYP species that lack any bound lipid, thus the differences observed result primarily from a memory effect associated with the differing CYP structures housed within lipid environments installed within the NDs used to prepare the samples analyzed. A quantitative analysis of the CIU501 values recorded from these samples reveals that CYP ions ejected from NDs containing lipids designed to replicate the ER membrane are the least stable of those screened in our studies, while higher-energy CIU transitions retain similar stabilities throughout all the CYP ions evaluated (Figure 3-4G). An examination of CIU feature CCS values further highlight CYPs housed within NDs mimicking the ER as being the most compact ions detected in our survey (Figure 3-4H). Finally, an RMSD analysis of the complete CIU fingerprints for CYP generated from each ND environment indicates the strongest degree of similarity for ions produced from POPC and ER NDs, while CYP ions produced from DMPC NDs produce significantly different CYP CIU data relative to our other two ND-associated conditions. Since ER NDs contain 60% POPC, the most abundant component of the six used in the construction of the ND lipid bilayer, the similarity observed between CYP ions liberated from ER and POPC NDs. Overall, our CIU data provides strong evidence that the local lipid

environment confers specific structures upon embedded CYPs, and more native lipid environments promote more compact and less stable CYP conformers.

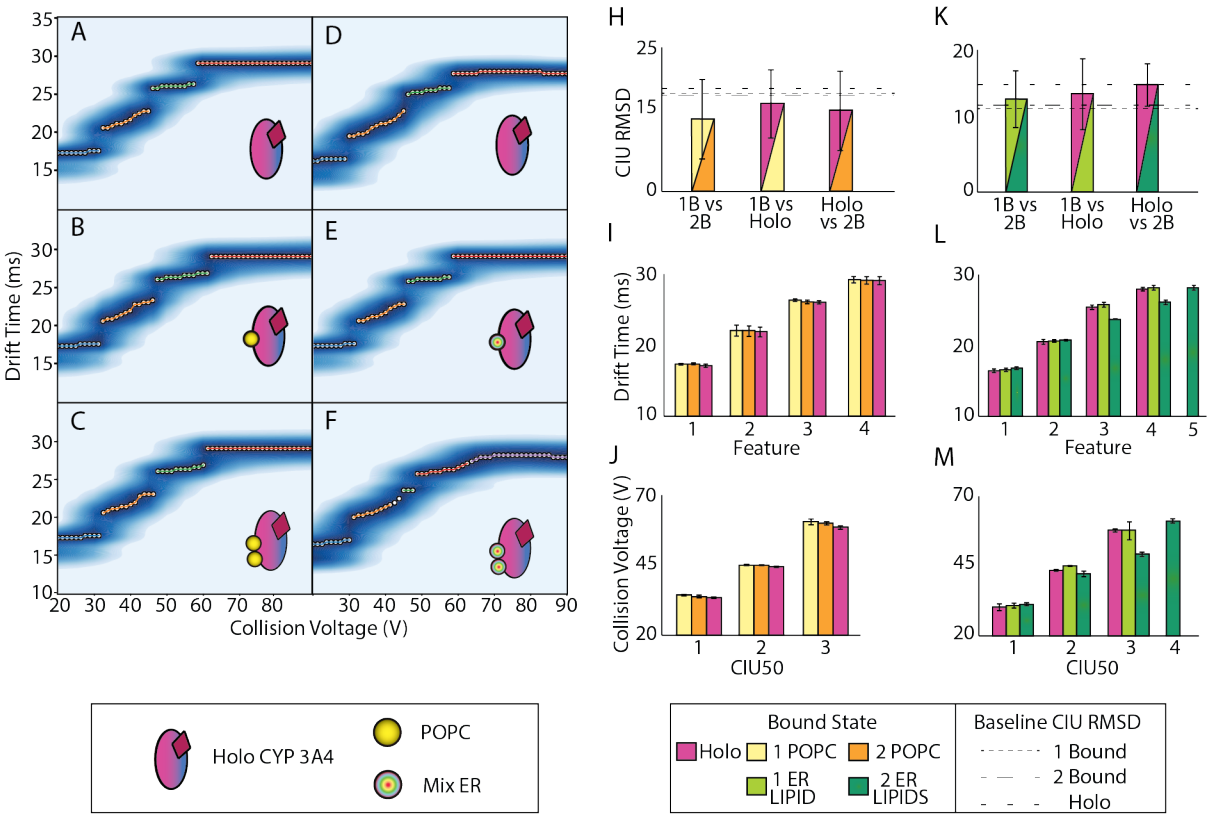

Figure 3-5 Lipid binding to CYP3A4 liberated from POPC and ER Mix 4F-peptide nanodiscs. **A)** feature detection analysis of 14+ holo CYP3A4 liberated from POPC 4F-peptide based nanodisc **B)** feature detection analysis of 14+ 1 POPC lipid bound CYP3A4 liberated from POPC 4F-peptide based nanodisc C. feature detection analysis of 14+ 2 POPC lipids bound CYP3A4 liberated from POPC 4F-peptide based nanodisc **D)** feature detection analysis of 14+ holo CYP3A4 liberated from ER lipid Mix 4F-peptide based nanodisc **E)** feature detection analysis of 14+ 1 lipid bound CYP3A4 liberated from ER lipid Mix 4F-peptide based nanodisc **F)** feature detection analysis of 14+ 2 lipids bound CYP3A4 liberated from ER lipid Mix 4F-peptide based nanodisc H & K. RMSD values determined by total difference analysis of each bound state resulting from **H)** POPC containing ND and **K)** Mix lipid ER ND. The mixed colored bars indicate which bound state was compared and the baseline RMSD is indicated by the dashed line reporting the day to day error. (holo 13.2%, 1B lipid 15.1%, and 2B lipids 11.6%) **I & L**) Drift time analysis comparing collision cross section between lipid compositions respectively for **I)** POPC ND and **L)** ER lipid Mix. **J & M)** CIU50 analysis comparing stabilization between lipid bound states for **J)** POPC ND and **K)** ER lipid Mix

3.3.5 Quantifying lipid bound stability shifts in CYP liberated from Mix ER 4F NDs

Lipid binding is known to influence the structure and function for MPs in a manner linked to stabilizing native structures or supporting native functions. Recent work has illustrated

that CYP3A4 will recruit lipids from its surroundings in a manner associated with the relative fluidity lipid bilayer environment and the noted preference of CYP for sphingomyelin.[97] Next we decided to focus on the bound lipids observed when CYP3A4 was liberated from the mix ER ND (Figure 3-4C), due to the poor resolving power on the Synapt G2, we were unable to identify lipid binding based off of mass alone. Recent work from our group has shown that lipid attachment can impact protein structure and by extensions the CIU fingerprints allowed for classification of lipid ID when screened through a CIU lipid binding experiments.[83] In Figure 1-5 we compare the binding of two lipid binding events, both from the pure POPC NDs and the mix ER NDs, since we do not have lipid IDs, they are labeled as 1 ER lipid and 2 ER Lipids. We see evidence that 1 bound ER lipid appears similar in CIU as that of the 1 POPC bound data, which likely suggests this first bound state could be POPC, the majority of the mix ER % is POPC at 54%. Next, the second bound ER lipid CIU does not seem to match that from the POPC NDs, which may indicate that this second bound lipid is one of the other lipids in the mixture. Further work on higher resolution mass spectrometer will be needed in order to confidently assign these lipid IDs. Interestingly, the second ER lipid appears to also impart structural shifts consistent with that discussed in this manuscript, with the evidence of a fourth feature and overall decreased median drift times throughout the CIU fingerprint.

3.4 Conclusions

CYP enzymes are responsible for the metabolism of a broad range of bio-active molecules, including both pharmaceutical and cytotoxic compounds. Many unanswered questions persist regarding the relationship between the dynamic structure of CYP and its myriad of functions. While atomic-resolution structures of many CYP isoforms are available, all lack the hydrophobic α-helix region of the protein, which is critically important for the association of

CYPs with biological membranes. Information regarding the impact of lipid binding and membrane composition on this CYP region is currently unknown, including the presence of allosteric networks that link the local membrane environment to ultimate enzyme activity. To extract structural information from full length CYP isoforms, in the context of chemical mixtures that include the constituents of biological membranes, in this work we developed IM-MS

Figure 3-6 CYP2B4 structure overlay. The starting structure, teal, was rendered without lipid environment, orange structure was performed with POPC MD and overlaid in PyMol with an RMSD value of 4.96

methods to study the structure and stability of full length CYPs in NDs.

Most often, when NDs are used as a mimetic they are constructed using homogeneous lipid compositions, and thus do not reflect the complexity of real cellular membranes. The goal of this work was to optimize ND compositions so that they better emulate biologically relevant lipid compositions, including efforts to add molecules that modulate bilayer structure, such as cholesterol. To fully optimize the NDs, a range of scaffolding materials, which can influence the shape, size, and dynamics of the ND was also evaluated using IM-MS and CIU measurements.

In conclusions, we used NDs of carefully designed compositions to study the role of different lipid environments and ND scaffolding proteins on CYP structure. We found that CYP CIU data, and by extension its structure, strongly depends on its local environment, and that more native membrane environments can result in more compact and more destabilized CYP forms additionally, we observed that the choice of membrane scaffolding belt does not perturb the protein structure. We observed that lipid binding from the ER mix imposes a structural shift on the CYP protein suggesting that these lipids do indeed, play a role on the protein overall topology. Figure 3-5 illustrates our efforts to gain insights on these structural shifts, MD workflows were implemented with and without a membrane environment to further test our hypothesis, with the teal structure being the CYP2B4 full length structure as determined by homology modeling and the orange structure having different overall shape when calculated out of a membrane environment consisting of POPC lipids. This work provides a framework for using IM-MS and CIU as a method to robustly view full length CYP structural changes in response to differing membrane environments, previous work has only been able to focus on spectroscopically probing the heme active site. By extension this workflow could be implemented for other membrane proteins in which gaining crystal structures for and would do so in a more native-like environment, one in which that directly reflects the complex biological bilayer

3.5 Acknowledgments

Membrane protein research in the Ruotolo lab is supported by the National Institute of Health under Grants GM105942. The author thanks collaborators Professor Ryan Bailey and Marina Sarcinella and Colleen Riordan as well as Professor Ayyalusamy Ramamoorthy and Katie Gentry and Carlo Barnaba for their contribution in this chapter

Bibliography

(1) Fagerberg, L.; Jonasson, K.; von Heijne, G.; Uhlén, M.; Berglund, L. Prediction of the Human Membrane Proteome. *Proteomics* **2010**, *10* (6), 1141–1149.

(2) Lacapère, J.-J.; Pebay-Peyroula, E.; Neumann, J.-M.; Etchebest, C. Determining Membrane Protein Structures: Still a Challenge! *Trends Biochem. Sci.* **2007**, *32* (6), 259–270.

(3) Wallin, E.; Heijne, G. Von. Genome-Wide Analysis of Integral Membrane Proteins from Eubacterial, Archaean, and Eukaryotic Organisms. *Protein Sci.* **2008**, *7* (4), 1029–1038.

(4) Overington, J. P.; Al-Lazikani, B.; Hopkins, A. L. How Many Drug Targets Are There? *Nat. Rev. Drug Discov.* **2006**, *5* (12), 993–996.

(5) Yıldırım, M. A.; Goh, K.-I.; Cusick, M. E.; Barabási, A.-L.; Vidal, M. Drug—Target Network. *Nat. Biotechnol.* **2007**, *25* (10), 1119–1126.

(6) Hendrickson, W. A. *Atomic-Level Analysis of Membrane-Protein Structure*; 2016; Vol. 23.

(7) Nicolson, G. L. The Fluid—Mosaic Model of Membrane Structure: Still Relevant to Understanding the Structure, Function and Dynamics of Biological Membranes after More than 40years. *Biochim. Biophys. Acta - Biomembr.* **2014**, *1838* (6), 1451–1466.

(8) Pyle, E.; Kalli, A. C.; Amillis, S.; Hall, Z.; Lau, A. M.; Hanyaloglu, A. C.; Diallinas, G.; Byrne, B.; Politis, A. Structural Lipids Enable the Formation of Functional Oligomers of the Eukaryotic Purine Symporter UapA. *Cell Chem. Biol.* **2018**, *25* (7), 840-848.e4.

(9) Peng, T.; Yuan, X.; Hang, H. C. Turning the Spotlight on Protein–Lipid Interactions in Cells. *Curr. Opin. Chem. Biol.* **2014**, *21*, 144–153.

(10) Abhinav Nath, ‡; William M. Atkins, *,‡ and; Stephen G. Sligar*, §. Applications of Phospholipid Bilayer Nanodiscs in the Study of Membranes and Membrane Proteins†. **2007**.

(11) Marty, M. T.; Hoi, K. K.; Gault, J.; Robinson, C. V. Probing the Lipid Annular Belt by Gas-Phase Dissociation of Membrane Proteins in Nanodiscs. *Angew. Chemie Int. Ed.* **2016**, *55* (2), 550–554.

(12) Hoi, K. K.; Robinson, C. V; Marty, M. T. Unraveling the Composition and Behavior of Heterogeneous Lipid Nanodiscs by Mass Spectrometry. *Anal. Chem* **2017**, *88* (12), 6199–6204.

(13) Li, J.; Fan, X.; Kitova, E. N.; Zou, C.; Cairo, C. W.; Eugenio, L.; Ng, K. K. S.; Xiong, Z. J.; Privé, G. G.; Klassen, J. S. Screening Glycolipids Against Proteins in Vitro Using Picodiscs and Catch-and-Release Electrospray Ionization-Mass Spectrometry. *Anal. Chem.* **2016**, *88* (9), 4742–4750.

(14) Marty, M. T.; Hoi, K. K.; Robinson, C. V. Interfacing Membrane Mimetics with Mass Spectrometry. *Acc. Chem. Res.* **2016**, *49* (11), 2459–2467.

(15) Midtgaard, S. R.; Pedersen, M. C.; Judas, J.; Kirkensgaard, K.; Sørensen, K. K.; Mortensen, K.; Jensen, K. J.; Arleth, L. Self-Assembling Peptides Form Nanodiscs That Stabilize Membrane Proteins. **2014**.

(16) Bayburt, T. H.; Sligar, S. G. Membrane Protein Assembly into Nanodiscs. *FEBS Lett.*

2010, *584* (9), 1721–1727.
(17) Schuler, M. A.; Denisov, I. G.; Sligar, S. G. Nanodiscs as a New Tool to Examine Lipid-Protein Interactions.
(18) Sligar, S. G.; Denisov, I. G. Nanodiscs: A Toolkit for Membrane Protein Science. *Protein Sci.* **2021**, *30* (2), 297–315.
(19) Lee, S. C.; Knowles, T. J.; Postis, V. L. G.; Jamshad, M.; Parslow, R. A.; Lin, Y.; Goldman, A.; Sridhar, P.; Overduin, M.; Muench, S. P.; Dafforn, T. R. A Method for Detergent-Free Isolation of Membrane Proteins in Their Local Lipid Environment. *Nat. Protoc.* **2016**, *11* (7), 1149–1162.
(20) Denisov, I. G.; Sligar, S. G. NANODISCS IN MEMBRANE BIOCHEMISTRY AND BIOPHYSICS.
(21) Rouck, J. E.; Krapf, J. E.; Roy, J.; Huff, H. C.; Das, A. Recent Advances in Nanodisc Technology for Membrane Protein Studies (2012–2017). *FEBS Lett.* **2017**, *591* (14), 2057–2088.
(22) Etzkorn, M.; Viegas, A.; Viennet, T.; Aldino Viegas, R. The Power, Pitfalls and Potential of the Nanodisc System for NMR-Based Studies. *Biol. Chem* **2016**, *397* (12).
(23) *Cytochrome P450*; Ortiz de Montellano, P. R., Ed.; Springer US: Boston, MA, 2005.
(24) Denisov, I. G.; Makris, T. M.; Sligar, S. G.; Schlichting, I. Structure and Chemistry of Cytochrome P450. **2005**.
(25) Guengerich, F. P.; Wu, Z.-L.; Bartleson, C. J. Function of Human Cytochrome P450s: Characterization of the Orphans. *Biochem. Biophys. Res. Commun.* **2005**, *338* (1), 465–469.
(26) Isin, E. M.; Guengerich, F. P. Substrate Binding to Cytochromes P450.
(27) Guengerich, F. P. Cytochrome P450s and Other Enzymes in Drug Metabolism and Toxicity. *AAPS J.* **2006**, *8* (1), E101-11.
(28) Guengerich, X. F. P.; Wilkey, C. J.; Phan, T. T. N. Human Cytochrome P450 Enzymes Bind Drugs and Other Substrates Mainly through Conformational-Selection Modes. **2019**.
(29) Prade, E.; Mahajan, M.; Im, S.-C.; Zhang, M.; Anantharamaiah, G. M.; Waskell, L.; Ramamoorthy, A.; Gentry, K. A. Angewandte International Edition Title: A Minimal Functional Complex of Cytochrome P450 and FBD of Cytochrome P450 Reductase in Nanodiscs A Minimal Functional Complex of Cytochrome P450 and FBD of Cytochrome P450 Reductase in Nanodiscs. *Angew. Chem. Int. Ed. Angew. Chem* **2018**, *10* (10).
(30) Im, S.-C.; Waskell, L. The Interaction of Microsomal Cytochrome P450 2B4 with Its Redox Partners, Cytochrome P450 Reductase and Cytochrome B5. *Arch. Biochem. Biophys.* **2011**, *507*, 144–153.
(31) Dürr, U. H. N.; Waskell, L.; Ramamoorthy, A. The Cytochromes P450 and b 5 and Their Reductases-Promising Targets for Structural Studies by Advanced Solid-State NMR Spectroscopy. **2007**.
(32) Laganowsky, A.; Reading, E.; Hopper, J. T. S.; Robinson, C. V. Mass Spectrometry of Intact Membrane Protein Complexes. *Nat. Protoc.* **2013**.
(33) Barrera, N. P.; Zhou, M.; Robinson, C. V. The Role of Lipids in Defining Membrane Protein Interactions: Insights from Mass Spectrometry.
(34) Alfonso-Garrido, J.; Garcia-Calvo, E.; Luque-Garcia, J. L. Sample Preparation Strategies for Improving the Identification of Membrane Proteins by Mass Spectrometry. *Anal. Bioanal. Chem.* **2015**, *407* (17), 4893–4905.
(35) Robinson, C. V.; V., C. From Molecular Chaperones to Membrane Motors: Through the

Lens of a Mass Spectrometrist. *Biochem. Soc. Trans.* **2017**, *45* (1), 251–260.
(36) Reading, E.; Hall, Z.; Martens, C.; Haghighi, T.; Findlay, H.; Ahdash, Z.; Politis, A.; Booth, P. J. Interrogating Membrane Protein Conformational Dynamics within Native Lipid Compositions. *Angew. Chemie Int. Ed.* **2017**, *56* (49), 15654–15657.
(37) Zhan, L.-P.; Liu, C.-Z.; Nie, Z.-X. Mass Spectrometry of Membrane Proteins. In *Membrane Biophysics*; Springer Singapore: Singapore, 2018; pp 285–317.
(38) Schmidt, C.; Robinson, C. V. Dynamic Protein Ligand Interactions - Insights from MS. *FEBS J.* **2014**, *281* (8), 1950–1964.
(39) Ben-Nissan, G.; Sharon, M. The Application of Ion-Mobility Mass Spectrometry for Structure/Function Investigation of Protein Complexes. *Curr. Opin. Chem. Biol.* **2018**, *42*, 25.
(40) Han, L.; Kitova, E. N.; Li, J.; Nikjah, S.; Lin, H.; Pluvinage, B.; Boraston, A. B.; Klassen, J. S. Protein–Glycolipid Interactions Studied in Vitro Using ESI-MS and Nanodiscs: Insights into the Mechanisms and Energetics of Binding. *Anal. Chem.* **2015**, *87* (9), 4888–4896.
(41) Marty, M. T.; Hoi, K. K.; Robinson, C. V. Interfacing Membrane Mimetics with Mass Spectrometry. *Acc. Chem. Res.* **2016**, *49* (11), 2459–2467.
(42) Graves, D. B. Transport Properties of Ions in Gases by Edward A. Mason and Earl W. McDaniel, John Wiley and Sons, New York, 1988, 560+ Xvi Pp. *AIChE J.* **1989**, *35* (4), 701–701.
(43) Revercomb, E.; Mason, E. A. *Theory of Plasma Chromatography/Gaseous Electrophoresis-A Review*.
(44) Dwivedi, P.; Wu, C.; Hill, H. H. Gas Phase Chiral Separations By Ion Mobility Spectrometry. *Anal. Chem* **2006**, *78* (24), 8200–8206.
(45) Allison, T. M.; Landreh, M.; Benesch, J. L. P.; Robinson, C. V. Low Charge and Reduced Mobility of Membrane Protein Complexes Has Implications for Calibration of Collision Cross Section Measurements. *Anal. Chem* **2016**, *88*, 5879–5884.
(46) Baldwin, A. J.; Lioe, H.; Hilton, G. R.; Baker, L. A.; Rubinstein, J. L.; Kay, L. E.; Benesch, J. L. P. The Polydispersity of AB-Crystallin Is Rationalized by an Interconverting Polyhedral Architecture. *Structure* **2011**, *19* (12), 1855–1863.
(47) Eschweiler, J. D.; Rabuck-Gibbons, J. N.; Tian, Y.; Ruotolo, B. T. CIUSuite: A Quantitative Analysis Package for Collision Induced Unfolding Measurements of Gas-Phase Protein Ions. *Anal. Chem* **2015**, *87*, 11516–11522.
(48) Dixit, S. M.; Polasky, D. A.; Ruotolo, B. T. Collision Induced Unfolding of Isolated Proteins in the Gas Phase: Past, Present, and Future. *Curr. Opin. Chem. Biol.* **2018**, *42*, 93–100.
(49) Polasky, Daniel A; Dixit, Sugyan M.; Fantin, Sarah M.; Ruotolo, B. T. "CIUSuite 2: Next-Generation Software for the Analysis of Gas-Phase Protein Unfolding Data." *Press*.
(50) AN, C.; SE, R. Mass Spectrometry-Enabled Structural Biology of Membrane Proteins. *Methods* **2018**, *147*, 187–205.
(51) Souda, P.; Ryan, C. M.; Cramer, W. A.; Whitelegge, J. Profiling of Integral Membrane Proteins and Their Post Translational Modifications Using High-Resolution Mass Spectrometry. *Methods* **2011**, *55* (4), 330.
(52) Morgan, C. R.; Hebling, C. M.; Rand, K. D.; Stafford, D. W.; Jorgenson, J. W.; Engen, J. R. Conformational Transitions in the Membrane Scaffold Protein of Phospholipid Bilayer Nanodiscs* □ S. *Mol. Cell. Proteomics* **2011**, *10*, 1–11.

(53) Campuzano, I. D. G.; Li, H.; Bagal, D.; Lippens, J. L.; Svitel, J.; Kurzeja, R. J. M.; Xu, H.; Schnier, P. D.; Loo, J. A. Native MS Analysis of Bacteriorhodopsin and an Empty Nanodisc by Orthogonal Acceleration Time-of-Flight, Orbitrap and Ion Cyclotron Resonance. *Anal. Chem* **2016**, *88*.
(54) Cong, X.; Liu, Y.; Liu, W.; Liang, X.; Russell, D. H.; Laganowsky, A. Determining Membrane Protein-Lipid Binding Thermodynamics Using Native Mass Spectrometry. *J. Am. Chem. Soc.* **2016**.
(55) Harvey, S. R.; Vanaernum, Z. L.; Kostelic, M. M.; Marty, M. T.; Wysocki, V. H. *Probing the Structure of Nanodiscs Using Surface Induced Dissociation*; 2020.
(56) Roy, J.; Pondenis, H.; Fan, T. M.; Das, A. Direct Capture of Functional Proteins from Mammalian Plasma Membranes into Nanodiscs. **2015**.
(57) Barnaba, C.; Sahoo, R.; Ravula, T.; Medina-Meza, I. G.; Im, S.-C.; Anantharamaiah, G. M.; Waskell, L.; Ramamoorthy, A. Biophysics Cytochrome-P450-Induced Ordering of Microsomal Membranes Modulates Affinity for Drugs. *Angew. Chemie Int. Ed.* **2018**, *47*, 1–6.
(58) Saribas, A. S.; Gruenke, L.; Waskell, L. Overexpression and Purification of the Membrane-Bound Cytochrome P450 2B4. *Protein Expr. Purif.* **2001**, *21* (2), 303–309.
(59) Gillam, E. M. J.; Baba, T.; Kim, B. R.; Ohmori, S.; Guengerich, F. P. Expression of Modified Human Cytochrome P450 3A4 in Escherichia Coli and Purification and Reconstitution of the Enzyme. *Arch. Biochem. Biophys.* **1993**, *305* (1), 123–131.
(60) Mishra, V. K.; Palgunachari, M. N.; Krishna, R.; Glushka, J.; Segrest, J. P.; Anantharamaiah, G. M. Effect of Leucine to Phenylalanine Substitution on the Nonpolar Face of a Class A Amphipathic Helical Peptide on Its Interaction with Lipid: High Resolution Solution NMR Studies of 4F-Dimyristoylphosphatidylcholine Discoidal Complex. *J. Biol. Chem.* **2008**, *283* (49), 34393–34402.
(61) Luthra, A.; Gregory, M.; Grinkova, Y. V; Denisov, I. G.; Sligar, S. G. Nanodiscs in the Studies of Membrane-Bound Cytochrome P450 Enzymes. *Methods Mol Biol* **2013**, *987*, 115–127.
(62) Wade, J. H.; Jones, J. D.; Lenov, I. L.; Riordan, C. M.; Sligar, S. G.; Bailey, R. C. Microfluidic Platform for Efficient Nanodisc Assembly, Membrane Protein Incorporation, and Purification. *Lab Chip* **2017**, *17* (17), 2951–2959.
(63) Haynes, S. E.; Polasky, D. A.; Dixit, S. M.; Majmudar, J. D.; Neeson, K.; Ruotolo, B. T.; Martin, B. R. Variable-Velocity Traveling-Wave Ion Mobility Separation Enhancing Peak Capacity for Data-Independent Acquisition Proteomics. *Anal. Chem.* **2017**, *89* (11), 5669–5672.
(64) Šrejber, M.; Navrátilová, V.; Paloncýová, M.; Bazgier, V.; Berka, K.; Anzenbacher, P.; Otyepka, M. Membrane-Attached Mammalian Cytochromes P450: An Overview of the Membrane's Effects on Structure, Drug Binding, and Interactions with Redox Partners. *J. Inorg. Biochem.* **2018**, *183*, 117–136.
(65) Yang, J.; Yan, R.; Roy, A.; Xu, D.; Poisson, J.; Zhang, Y. The I-TASSER Suite: Protein Structure and Function Prediction. *Nat. Methods* **2015**, *12* (1), 7–8.
(66) Roy, A.; Kucukural, A.; Zhang, Y. I-TASSER: A Unified Platform for Automated Protein Structure and Function Prediction. *Nat. Protoc. 2010 54* **2010**, *5* (4), 725–738.
(67) Zhang, Y. I-TASSER Server for Protein 3D Structure Prediction. **2008**.
(68) Jo, S.; Kim, T.; Iyer, V. G.; Im, W. CHARMM-GUI: A Web-Based Graphical User Interface for CHARMM. *J. Comput. Chem.* **2008**, *29* (11), 1859–1865.

(69) Qi, Y.; Lee, J.; Klauda, J. B.; Im, W. CHARMM-GUI Nanodisc Builder for Modeling and Simulation of Various Nanodisc Systems. *J. Comput. Chem.* **2019**, *40* (7), 893–899.
(70) Lee, J.; Cheng, X.; Swails, J. M.; Yeom, M. S.; Eastman, P. K.; Lemkul, J. A.; Wei, S.; Buckner, J.; Jeong, J. C.; Qi, Y.; Jo, S.; Pande, V. S.; Case, D. A.; Brooks, C. L.; MacKerell, A. D.; Klauda, J. B.; Im, W. CHARMM-GUI Input Generator for NAMD, GROMACS, AMBER, OpenMM, and CHARMM/OpenMM Simulations Using the CHARMM36 Additive Force Field. *J. Chem. Theory Comput.* **2016**, *12* (1), 405–413.
(71) Monticelli, L.; Kandasamy, S. K.; Periole, X.; Larson, R. G.; Peter, D.; Marrink, S.-J. The MARTINI Coarse-Grained Force Field: Extension to Proteins.
(72) Hsu, P. C.; Bruininks, B. M. H.; Jefferies, D.; Cesar Telles de Souza, P.; Lee, J.; Patel, D. S.; Marrink, S. J.; Qi, Y.; Khalid, S.; Im, W. CHARMM-GUI Martini Maker for Modeling and Simulation of Complex Bacterial Membranes with Lipopolysaccharides. *J. Comput. Chem.* **2017**, *38* (27), 2354–2363.
(73) The PyMOL Molecular Graphics System, Version 1.2r3pre, Schrödinger, LLC.
(74) Yen, H.-Y.; Hopper, J. T. S.; Liko, I.; Allison, T. M.; Zhu, Y.; Wang, D.; Stegmann, M.; Mohammed, S.; Wu, B.; Robinson, C. V. *Ligand Binding to a G Protein-Coupled Receptor Captured in a Mass Spectrometer*; 2017.
(75) Mehmood, S.; Marcoux, J.; Hopper, J. T. S.; Allison, T. M.; Liko, I.; Borysik, A. J.; Robinson, C. V. Charge Reduction Stabilizes Intact Membrane Protein Complexes for Mass Spectrometry. *J. Am. Chem. Soc.* **2014**, *136* (49), 17010–17012.
(76) Kliman, M.; May, J. C.; McLean, J. A. Lipid Analysis and Lipidomics by Structurally Selective Ion Mobility-Mass Spectrometry. *Biochim. Biophys. Acta - Mol. Cell Biol. Lipids* **2011**, *1811* (11), 935–945.
(77) Gault, J.; Liko, I.; Landreh, M.; Shutin, D.; Reddy Bolla, J.; Jefferies, D.; Agasid, M.; Yen, H.-Y.; G W Ladds, M. J.; Lane, D. P.; Khalid, S.; Mullen, C.; Remes, P. M.; Huguet, R.; McAlister, G.; Goodwin, M.; Viner, R.; Syka, J. E.; Robinson, C. V. Combining Native and 'Omics' Mass Spectrometry to Identify Endogenous Ligands Bound to Membrane Proteins. *Nat. Methods*.
(78) Bolla, J. R.; Agasid, M. T.; Mehmood, S.; Robinson, C. V. Membrane Protein–Lipid Interactions Probed Using Mass Spectrometry. *https://doi.org/10.1146/annurev-biochem-013118-111508* **2019**, *88*, 85–111.
(79) Bechara, C. C.; Robinson, C. V. Different Modes of Lipid Binding to Membrane Proteins Probed by Mass Spectrometry. *J. Am. Chem. Soc* **2015**, *137*, 44.
(80) X, C.; Y, L.; W, L.; X, L.; A, L. Allosteric Modulation of Protein-Protein Interactions by Individual Lipid Binding Events. *Nat. Commun.* **2017**, *8* (1).
(81) ZM, M.; JD, Z.; WA, D.; JS, P. Gas-Phase Protonation Thermodynamics of Biological Lipids: Experiment, Theory, and Implications. *Anal. Chem.* **2020**, *92* (15), 10365–10374.
(82) Bechara, C. C.; Robinson, C. V. Different Modes of Lipid Binding to Membrane Proteins Probed by Mass Spectrometry. *J. Am. Chem. Soc* **2015**, *137*, 33.
(83) Fantin, S. M.; Parson, K. F.; Niu, S.; Liu, J.; Polasky, D. A.; Dixit, S. M.; Ferguson-Miller, S. M.; Ruotolo, B. T. Collision Induced Unfolding Classifies Ligands Bound to the Integral Membrane Translocator Protein (TSPO). *Anal. Chem.* **2019**, acs.analchem.9b03208.
(84) Landreh, M.; Marty, M. T.; Gault, J.; Robinson, C. V. A Sliding Selectivity Scale for Lipid Binding to Membrane Proteins. *Curr. Opin. Struct. Biol.* **2016**, *39*, 54–60.
(85) Yang, Y.; Zhang, H.; Usharani, D.; Bu, W.; Im, S.; Tarasev, M.; Rwere, F.; Pearl, N. M.;

Meagher, J.; Sun, C.; Stuckey, J.; Shaik, S.; Waskell, L. Structural and Functional Characterization of a Cytochrome P450 2B4 F429H Mutant with an Axial Thiolate−Histidine Hydrogen Bond. **2014**.

(86) Zhang, M.; Le Clair, S. V; Huang, R.; Ahuja, S.; Im, S.-C.; Waskell, L.; Ramamoorthy, A. Insights into the Role of Substrates on the Interaction between Cytochrome b 5 and Cytochrome P450 2B4 by NMR. **2015**.

(87) Huang, R.; Zhang, M.; Rwere, F.; Waskell, L.; Ramamoorthy, A. Kinetic and Structural Characterization of the Interaction between the FMN Binding Domain of Cytochrome P450 Reductase and Cytochrome c *. **2014**.

(88) Barnaba, C.; Gentry, K.; Sumangala, N.; Ramamoorthy, A.; Denisov, I.; Melacini, G. Open Peer Review The Catalytic Function of Cytochrome P450 Is Entwined with Its Membrane-Bound Nature [Version 1; Referees: 4 Approved]. **2017**.

(89) Kandel, S. E.; Lampe, J. N. Role of Protein−Protein Interactions in Cytochrome P450-Mediated Drug Metabolism and Toxicity. *Chem. Res. Toxicol.* **2014**, *27*, 1474–1486.

(90) Zanger, U. M.; Schwab, M. Cytochrome P450 Enzymes in Drug Metabolism: Regulation of Gene Expression, Enzyme Activities, and Impact of Genetic Variation. *Pharmacol. Ther.* **2013**, *138* (1), 103–141.

(91) Scott, E. E.; White, M. A.; He, Y. A.; Johnson, E. F.; Stout, C. D.; Halpert, J. R. Structure of Mammalian Cytochrome P450 2B4 Complexed with 4-(4-Chlorophenyl)Imidazole at 1.9-Å Resolution: Insight into the Range of P450 Conformations and the Coordination of Redox Partner Binding. *J. Biol. Chem.* **2004**, *279* (26), 27294–27301.

(92) Natilie A. Hosea, ‡; Grover P. Miller, and; Guengerich*, F. P. Elucidation of Distinct Ligand Binding Sites for Cytochrome P450 3A4†. **2000**.

(93) Oda, M. N. Lipid-Free ApoA-I Structure - Origins of Model Diversity. *Biochim. Biophys. Acta - Mol. Cell Biol. Lipids* **2017**, *1862* (2), 221–233.

(94) Bayburt, T. H.; Sligar, S. G. Membrane Protein Assembly into Nanodiscs. **2009**.

(95) Liu, K.-C.; Hughes, J. M. X.; Hay, S.; Scrutton, N. S. Liver Microsomal Lipid Enhances the Activity and Redox Coupling of Colocalized Cytochrome P450 Reductase-Cytochrome P450 3A4 in Nanodiscs. *FEBS J.* **2017**, *284*, 2302.

(96) Ortiz de Montellano, P. R. Mechanism and Role of Covalent Heme Binding in the CYP4 Family of P450 Enzymes and the Mammalian Peroxidases. *Drug Metab. Rev.* **2008**, *40* (3), 405–426.

(97) Barnaba, C.; Sahoo, B. R.; Ravula, T.; Medina-Meza, I. G.; Im, S.-C.; Anantharamaiah, G. M.; Waskell, L.; Ramamoorthy, A. Cytochrome-P450-Induced Ordering of Microsomal Membranes Modulates Affinity for Drugs. *Angew. Chemie Int. Ed.* **2018**, *57* (13), 3391–3395

Chapter 4 **Collision Induced Unfolding Identifies Ligand Binding Modes within Membrane-associated Cytochrome P450 Complexes**

4.1 Introduction

Cytochrome P450s (CYPs) represent an important class of monotopic membrane protein (MP) monooxygenases involved in drug metabolism, including >70% of commercially available drugs.[1,2] CYPs are most often studied in a truncated form, resulting in a CYP version separated from critical interactions with its native membrane environment. The first CYP structures solved were all bacterial origin, [3–6] with the first mammalian CYPs solved only after major modifications including removal of the transmembrane (TM) domain, many decades after the initial CYP structures were revealed.[7] The level of structural alignment between the CYP families is high. For example, the CYP2 subfamily share 73% structural identity amongst all available structures, a value which is higher (85%) when only those structures captured in the closed state are considered.[8] Another characteristic of CYP is the heme coordinating cysteine, which acts as a thiolate ligand that is buried deeply inside the globular domain of the protein. The proximal side of CYP, which acts as a binding surface for protein redox partners, is also highly conserved.[9–12]

The distal CYP surface, where the enzyme active site is located, is more dynamic and exhibits less sequence homology amongst different CYP isoforms, providing a structural basis for ligand specificity.[3] Binding specificity in CYP has also been linked to the proximity of its active site to the biological membrane. The structural elements of CYP that have been implicated in binding to the membrane are the F', G', and A helices, as well as other features

close to these helices like the BC loop and the β1 strand.[13–15] While the F/G-loop has been identified as potentially inserting into the membrane, the B/C-loop and several β-strands also make extensive contacts with the membrane.[16–19] Recent work has observed evidence of increased membrane engagement when CYP3A4 was incorporated in lipid nanodiscs (NDs) containing larger amounts of anionic phospholipids, which the authors of that work attributed to changes in the redox potential of both CYP3A4 and cytochrome P450 oxioreductase (POR).[20] It is also believed that the TM domain of CYPs serves as an "anchor" to the membrane, playing a pivotal role in establishing overall protein orientation within the lipid bilayer.[21–23]

After the discovery that CYP interacts with the membrane beyond just being anchored to the bilayer, efforts have been made to reconstitute CYP catalytic activity in membrane mimetics, from using simple binary[24] or ternary[25] lipid mixtures, to employing more sophisticated NDs,[26,27] which consist of a lipid bilayer embraced by a protein, peptide, or polymer scaffold. More recently, CYP activity has been reconstituted in a biomimetic with a lipid composition that closely matches that of the endoplasmic reticulum (ER) to study protein-lipid interactions at a single-molecule level.[28]

Through previous molecular dynamics (MD) studies, the membrane has been highlighted as the main access pathway to CYP for hydrophobic substrates, which amplifies the need to study full length CYP in a lipid environment. Indeed, it has been shown that the membrane can impede the access of water, as well substrate, to the active site.[29] Also, lipophilic compounds that are poorly soluble are predominantly partitioned in the membrane, allowing for CYP to directly recruit hydrophobic substrates directly from the lipid phase.[30–32] Differences in the binding affinities and spin equilibrium in soluble vs. membrane-anchored CYP have already been reported,[19,30,33,34] and their significance is relevant if considering how crucial such affinity

parameters are for pharmacokinetic models.[35] In this regard, recent work has demonstrated the presence of an allosteric site at the membrane interface of CYP3A4, emphasizing of the critical role of the membrane in evaluating drug-drug interactions in pharmacological studies.[30] MD simulations and H/D exchange studies on CYP3A4 have shown that the interaction with the membrane occurs through specific lipid interactions,[15,19] and is able to affect the opening/closing of the access tunnel,[32] confirming experimental evidence obtained two decades before.[36] MD studies have also elucidated how phospholipids can induce an opening of the membrane-facing tunnels within CYPs.[37] The proposed mechanism relies on the ability of the upper part of the TM helix to interact with a proline rich segment of the catalytic domain that, along with the FG loop, are immersed in the membrane.[37] This gave rise to several access channels from both the solvent and membrane facing channels. Similar studies conducted on CYPs have revealed that additional CYP access tunnels can be opened in the presence of cellular membrane.[9,38]

Here, we use lipid nanodiscs (ND) to mimic the native membrane CYP environment. Our ion mobility-mass spectrometry (IM-MS) and collision induced unfolding (CIU) data, reveals that the lipid compositions of NDs can dramatically influence the stabilities of CYP-drug complexes. We tested four drug ligands to CYP2B4 and 11 drug ligands to CYP3A4 differing in their binding types and hydrophobicity, in all scenarios CIU and CIUSuite2 classification algorithm classified each binding according to the mode of binding as well as based on hydrophobic interactions.

4.2 Methods

4.2.1 Membrane Protein Preparation

Full length CYP2B4 and CYP3A4 were expressed in E. Coli using the pLW01-P450 and pCWori vectors respectively, using protocols adapted from established protocols for CYP2B41

and CYP3A42. Membrane Scaffold Protein 1D1(-), Membrane Scaffold Protein 1E3D1, Amberlite XAD-2 beads, Ammonium acetate were purchased from Sigma Aldrich (St. Louis, MO). Potassium phosphate monobasic and potassium phosphate dibasic were purchased from Fisher Scientific (Hampton, NH). The 4F peptide scaffolding belt (DWFKAFYDKVAEKFKEAF N-terminal modification: acetylation, C-terminal modification: amidation3) was purchased from GenScript (Piscataway, NJ). All lipids (1-palmitoyl-2-oleoyl-sn-glycero-3-phosphoethanolamine [POPE], -palmitoyl-2-oleoyl-sn-glycero-3-phospho-L-serine [POPS], 1-palmitoyl-2-oleoyl-glycero-3-phosphocholine [POPC], L-α-phosphatidylinositol (Soy) [PI], Sphingomyelin (egg, chicken) [eSM] and1,2-dimyristoyl-sn-glycero-3-phosphocholine [DMPC]) were purchased from Avanti Polar Lipids (Alabaster, AL). Cholesterol Hemisuccinate Tris Salt (CHEMS) was purchased from Anatrace (Maumee, OH). The peptide 4F NDs were pre-formed by rehydrating 11.25 mg of lipids (dry lipid films) in 40 mM potassium phosphate pH 7.4 buffer and mixing with 7.5 mg of 4F peptide suspended in 40 mM potassium phosphate pH 7.4 buffer. Depending on the phase temperature of the lipids, the mixture was allowed to shake at either 37oC (POPC) or 45oC (Mix ER) until the cloudy mixture turned transparent. Empty NDs were purified using SEC on a Superdex S200 increase 10/300 GL column and DLS measurements were obtained using Wyatt DynaPro NanoStar and fractions with uniform size distribution were chosen for protein incorporation and measured for concentration using a Thermo Scientific NanoDrop 2000 spectrophotometer, using the extinction coefficient for 4F Ɛ = 6.99 mM-1 cm-1 taking into account 16 peptides per disc. CYP was incubated with empty ND at ratios of 1:1.1 and 1:3 for CYP2B4 and CYP3A4 respectively and incubated for 6-10 hours at room temperature with constant gentle shaking. The increase in empty ND ratio for CYP3A4 helped eliminate protein crash out during incubation. CYP

incorporated NDs were simultaneously purified and buffer exchanged into 200 mM ammonium acetate pH 7.4 via SEC on Superdex S200 increase 10/300 or 3.2/300 GL column. CYP-ND only fractions were pooled and concentrated using 100 kDa Amicon Ultra-0.5 centrifugal filter units (MilliporeSigma, Burlington, MA).

4.2.2 Drug Binding

All drugs: 7-ethoxycoumarin, butylated hydroxytoluene (BHT), 1-(p,α-Diphenylbenzyl)imidazole (bifonazole), 4-(4-chlorophenyl) imidazole (4-CPI), α-[4-(1,1-Dimethylethyl)phenyl]-4-(hydroxydiphenylmethyl)-1-piperidinebutanol (terfenadine), 2-butan-2-yl-4-[4-[4-[4-[4-[[(2R,4S)-2-(2,4-dichlorophenyl)-2-(1,2,4-triazol-1-ylmethyl)-1,3-dioxolan-4-yl]methoxy]phenyl]piperazin-1-yl]phenyl]-1,2,4-triazol-3-one (itraconazole), (1S,3R,7S,8S,8aR)-8-[2-[(2R,4R)-4-hydroxy-6-oxooxan-2-yl]ethyl]-3,7-dimethyl-1,2,3,7,8,8a-hexahydronaphthalen-1-yl] (2S)-2-methylbutanoate (lovastatin), 1,4-Dihydro-2,6-dimethyl-4-(2-nitrophenyl)-3,5-pyridinedicarboxylic acid dimethyl ester,(nifedipine), 2-[(2,6-Dichlorophenyl)amino]benzeneacetic acid sodium salt (diclofenac), (±)-cis-1-Acetyl-4-(4-[(2-[2,4-dichlorophenyl]-2-[1H-imidazol-1-ylmethyl]-1,3-dioxolan-4-yl)-methoxy]phenyl)piperazine (ketoconazole), 11β,17α,21-Trihydroxypregn-4-ene-3,20-dione (hydrocortisone), and, 3-(4-Methylpiperazinyliminomethyl)rifamycin (Rifampin), and amlodipine were purchased from MilliporeSigma (Burlington, MA), imatinib and dasatinib were purchased from LC Laboratories (Woburn, MA) and were prepared at a 100 mM concentration in DMSO then diluted to 10 mM into ammonium acetate pH 7.4 buffer, these working stocks were used to add 1 mM of drug per 10 μM CYP protein incorporated into ND. These serial dilutions allowed for the solubility of hydrophobic compounds in DMSO and then subsequently keeping the final DMSO

concentration less than 1% (0.7%) in solution with protein. All samples were left to incubate for at least 30 minutes on ice prior to analysis.

4.2.3 Native Ion Mobility – Mass Spectrometry and CIU Experiments.

All IM-MS data was collected using a Synapt G2 HDMS IM-Q-ToF mass spectrometer (Waters, Milford, MA), with a direct infusion nESI source set to positive ion mode. Instrument settings were tuned to dissociate solubilization agents with minimal perturbation to protein structure prior to the IM separator, including appropriately tuned settings for the source temperature (30° C), source gas flow (50 mL/min), and the sampling cone (10 V). Trapping cell wave velocity and height were 116 m/s and 0.1 V. IMS wave velocity and height were 250 m/s and 15 V. Transfer cell wave velocity and height were 300 m/s and 10 V, with an accelerating potential of 10 V used to dissociate empty NDs. All CIU analyses were performed by increasing the trap collision voltage in a stepwise manner from 20 – 90 V in 5 V increments. CIU data from the 13+ charge states of CYP2B4 and CYP3A4 drug bound peaks were extracted using TWIMExtract[39], then processed and analyzed using CIUSuite2[40]. Data processing included three rounds of 2D Savitzky-Golay smoothing with a window of five bins and interpolation of the collision voltage axis by a factor of four. CIU fingerprints were cropped: 10-40 ms. Classification was performed using CIUSuite2. For CYP2B4 ligand classification, first performing Gaussian fittings then building an appropriate classifier using Gaussian Feature mode, for the CYP3A4 data, classifiers were built in All Data mode

4.3 Results and Discussion

4.3.1 Classification of CIU fingerprints based on lipid environment effects on CYP2B4

Previously, we have discussed the influence of the lipid environment and the way it can impact MP structure, as observed through CIU data. Here, we expand these observations and use

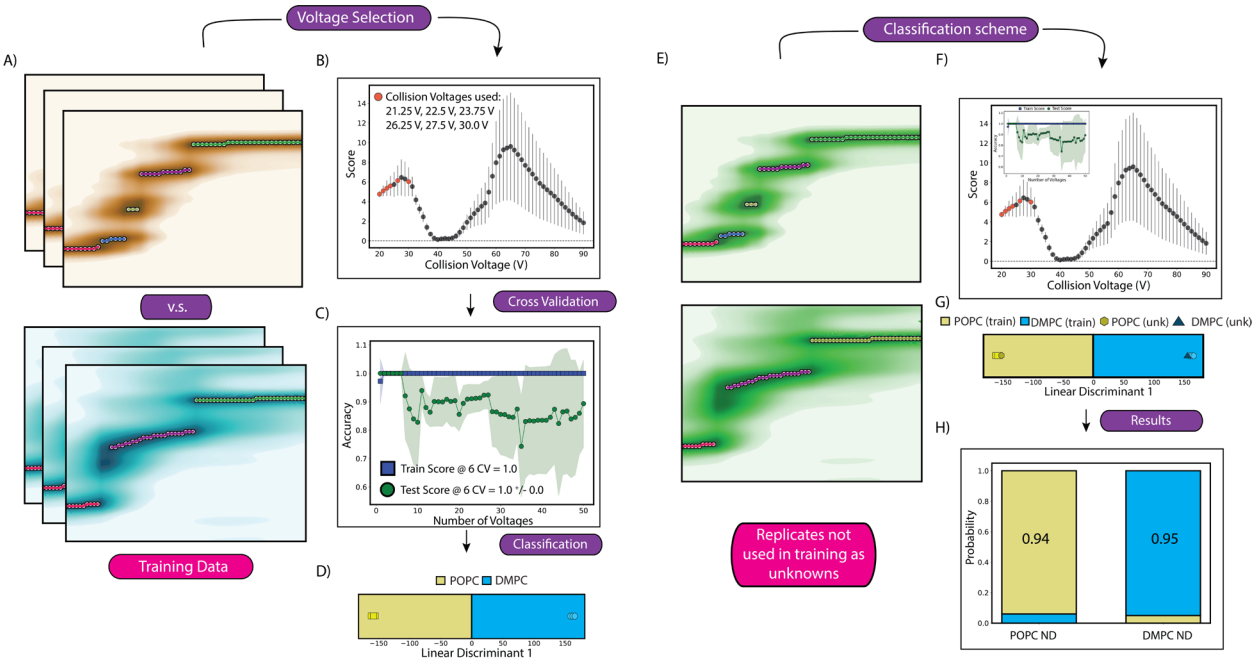

Figure 4-1 CIUSuite2 Classification workflow for CYP CIUs. **A)** training CIU data CYP2B4 liberated from POPC 4F NDs (orange) and CYP2B4 liberated from DMPC NDs (teal) **B**) univariant feature selection plot **C**) leave one out cross validation analysis **D**) training data results plotted in linear discriminant space **E**) unknown CIUs not used in training (CYP2B4 liberated from POPC 4F ND on top and DMPC on bottom) **F**) UFS plot **G**) linear discriminate plot with unknowns plotted **H**) probability scores for each unknown

an automated classification algorithm to detect differences in CYP CIU in an effort to evaluate CYP ligand binding modes in a manner that includes the role of an ND membrane mimetic in the assay performed.

Our classification algorithm approach uses a set of training data to build classifiers capable of confidently assigning unknown data into the classes previously defined during the above-referenced training period. We began (Figure 4-1) generating a deep training data set (Figure 4-1a) to build a two-state classifier system that tracks the impact of POPC (orange) and DMPC (teal) NDs on CYP2B4 CIU data and, by extension, its structure. Voltage steps where CIU fingerprints exhibit the most distinct differences between classes, are identified by the machine learning classification algorithm within CIUSuite2, as illustrated in the univariate

feature selection (UFS) plots shown in Figure 4-1B. A “leave-one-out” cross validation analysis, where each of the replicates is individually held out of the training data and used as an unknown to quantify the ability of the classification scheme to assign the target replicate as an unknown (Figure 4-1C), is then used to evaluate the accuracy of the classification scheme created. For our CYP2B4 classifier for differentiating ions ejected from POPC and DMPC NDs, we compute a cross-validation accuracy of 1.0 using 6 collision voltages, the highest achievable score for such an analysis. Finally, when plotted in linear discriminant space, the separation achieved between CYP2B4 CIU data acquired from POPC and DMPC samples can be visualized (Figure 4-1D). Mock unknowns (Figure 4-1E), corresponding to POPC and DMPC CYP2B4 CIU data (green) that were not used in classifier training, resulted in correct exhibiting a high probability score of 0.95 (Figure 4-1G and Figure 4-1H).

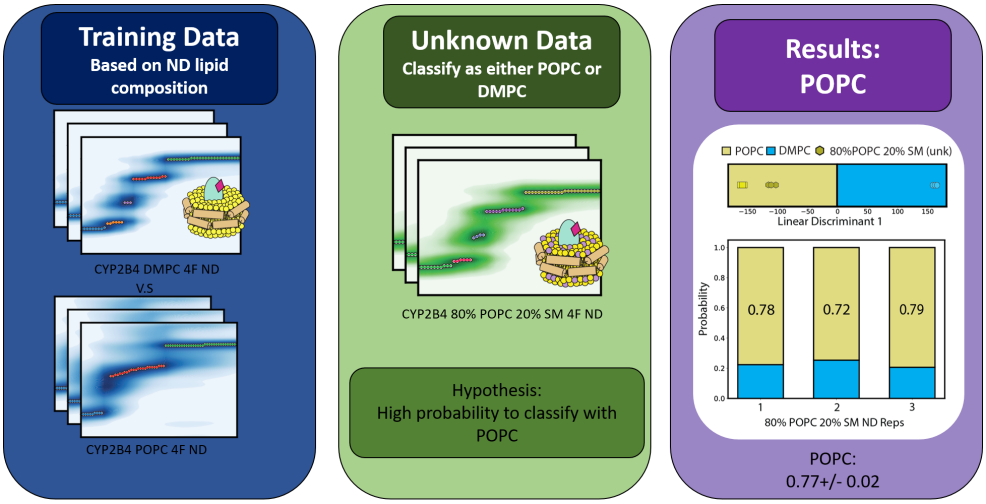

Figure 4-2 Classification of CYP2B4 liberated from POPC/SM mixed NDs. Training data used for classification scheme was CYP2B4 liberated from POPC or DMPC 4F ND, unknown to be classified was CYP2B4 liberated from a ND containing 20% SM and 80% POPC, the hypothesis that the classification outcome would align with POPC ND CIU, and results with high probability classifying with the POPC ND CIU.

Once verifying the strength of our CYP2B4 classification scheme, we moved to use it to analyze true unknowns, specifically CIU fingerprint data acquired from CYP2B4 liberated from a NDs containing 80% POPC and 20% SM. These data can be confidently assigned to the

CYP2B4 POPC ND class with a probability score of 0.77 +/- 0.02, a result which aligns with the fact that these unknowns are generated from ions liberated from NDs primarily comprised of POPC lipids (Figure 4-2).

4.3.2 Classification of CIU fingerprints based on drug binding modes to CYP2B4

Cytochrome P450s bind to various ligand classes. Type I CYP substates displace heme-bound water and bind to the substrate binding site, leaving a heme coordination position free (Figure 4-3). In contrast, type II inhibitors contain imidazole, acting to also displace water and binding directly to the sixth heme coordination position, blocking other molecules from entering the active site. Current assays capable of differentiating these CYP binding modes involve spectroscopically probing spin-shift perturbations in the CYP heme[41], but typically require large amounts of purified protein and lack the ability to study the full length CYP associated with a lipid bilayer. The membrane mimetic chosen to study CYP ligand binding also is known to play a significant role in functional states accessed by the protein during experiments, as prior reports have indicated that including CYP within a lipid bilayer enables its metabolism of hydrophobic compounds and avoids known detergent interactions with the CYP active site.[21]

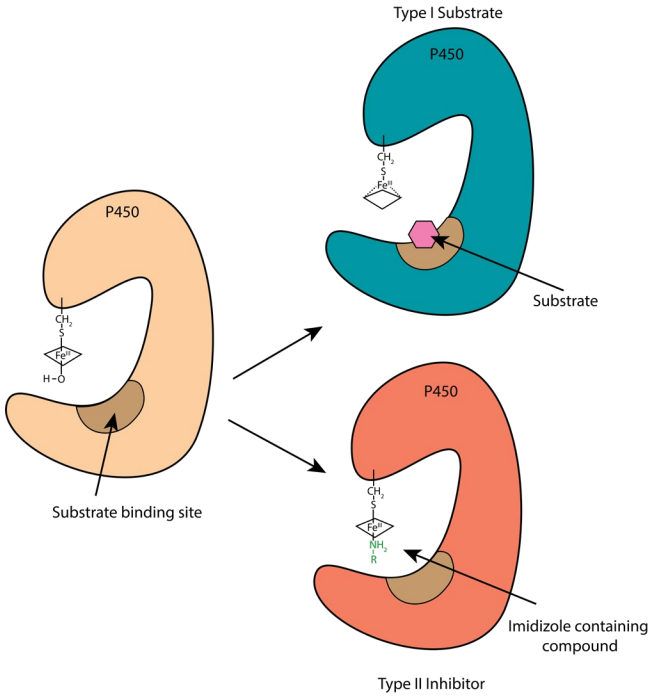

Figure 4-3 P450 active site and binding modes. CYP P450 can bind to various ligand types and has two binding modes open free conformation (tan) can bind to substrates (type I teal) or imidazole containing compounds (type II orange)

To build a CIU based assay that overcomes many of the limitations described above for standard spectroscopic CYP ligand binding assays, we began by analyzing CIU collected for 13+ ions detected for drug bound CYP2B4 liberated from POPC 4F peptide NDs. In order to build a CYP2B4- ligand classification scheme, we included the known type I molecules 7-ethoxycoumarin (ethoxy) and butylated hydroxytoluene (BHT) and the known type II inhibitors are bifonazole (BFZ) and 4-4-chlorophenyl imidazole (4-CPI) individually bound to CYP in our CIU analysis. For example, a two-way classification scheme was constructed using CYP-ethoxy and CYP-4CPI complexes and used to evaluate the CYP binding mode accessed by BHT. A UFS analysis of this classifier indicates a cross-validation accuracy of 0.94 utilizing 1 voltage slice (Appendix Figure III-1). As expected, we can correctly assign BHT as a type I CYP binder, producing a confidence score of 0.80, a value indicative of a high-confidence assignment. This approach can be expanded to confidently assign type II CYP inhibitors (Appendix Figure III-2) and our approach appears to be insensitive to the various permutations of training data and unknowns tested in our studies (Appendix Figure III-3).

Full length CYP binds hydrophobic ligands through access tunnels positioned such that the substrate enters through the cellular membrane and the product is then released through a separate egress. MD simulations have predicted a variety of such tunneling pathways based primarily upon the ligand hydrophobicity. To evaluate the ability of CIU to differentiate CYP-ligand complexes based on ligand hydrophobicity, we constructed a classifier where the binding types discussed above are kept constant, and only the hydrophobicity of the ligands probed vary. Specifically, our training data consisted of CIU data collected for BFZ and 4CPI CYP complexes where the former compound is hydrophobic, and the latter is hydrophilic but both act as type II binders. The UFS plot obtained for this classifier indicates a cross validation score of 0.91

(Appendix Figure III-4). When CIU data collected for CYP complexes with the hydrophobic type I substrate BHT are evaluated using this classifier, the result is clustered in linear discriminant space with the data CYP complexes bound to the hydrophobic training compound BFZ, exhibiting a probability score of 0.86.

To illustrate the robustness of CYP CIU classification workflow, Figure 4-4 contains results for all possible classifier/unknown combinations. The outcomes shown align with

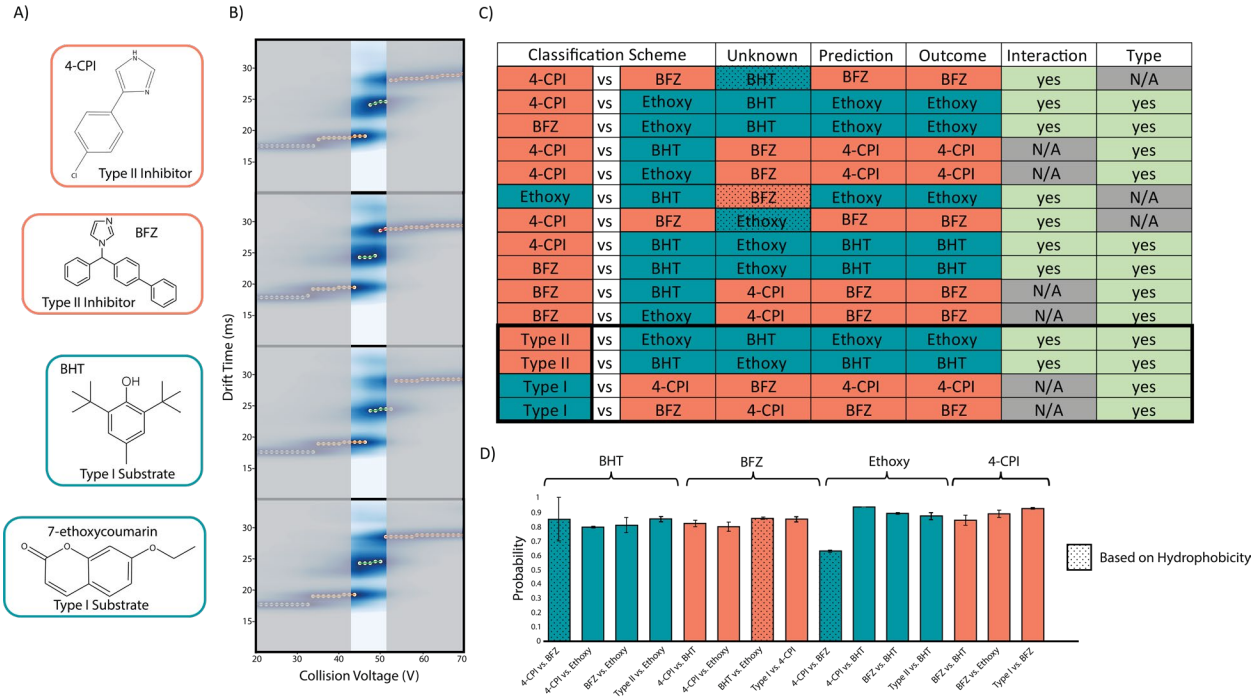

Classification Scheme			Unknown	Prediction	Outcome	Interaction	Type
4-CPI	vs	BFZ	BHT	BFZ	BFZ	yes	N/A
4-CPI	vs	Ethoxy	BHT	Ethoxy	Ethoxy	yes	yes
BFZ	vs	Ethoxy	BHT	Ethoxy	Ethoxy	yes	yes
4-CPI	vs	BHT	BFZ	4-CPI	4-CPI	N/A	yes
4-CPI	vs	Ethoxy	BFZ	4-CPI	4-CPI	N/A	yes
Ethoxy	vs	BHT	BFZ	Ethoxy	Ethoxy	yes	N/A
4-CPI	vs	BFZ	Ethoxy	BFZ	BFZ	yes	N/A
4-CPI	vs	BHT	Ethoxy	BHT	BHT	yes	yes
BFZ	vs	BHT	Ethoxy	BHT	BHT	yes	yes
BFZ	vs	BHT	4-CPI	BFZ	BFZ	N/A	yes
BFZ	vs	Ethoxy	4-CPI	BFZ	BFZ	N/A	yes
Type II	vs	Ethoxy	BHT	Ethoxy	Ethoxy	yes	yes
Type II	vs	BHT	Ethoxy	BHT	BHT	yes	yes
Type I	vs	4-CPI	BFZ	4-CPI	4-CPI	N/A	yes
Type I	vs	BFZ	4-CPI	BFZ	BFZ	N/A	yes

Figure 4-4 CYP2B4 classification Summary.**A**) structures for all molecules used: orange – type II inhibitors, 4-CPI and BFZ and teal type I substrates BHT and 7-ethoxy **B**) CIU fingerprints for respective CYP2B4 13+ ligand bound species – grey boxes illustrating that 45-50V were used in all classification outcomes **C**) summary of all possible classifiers built with unknown and prediction indicated as well as outcome and whether the outcome was based on interaction (hydrophobicity) or type (I or II) **D**) probability score summary with hydrophobic molecules indicated with shaded bars

expectations with high probabilities. In all cases, our CYP CIU classification method appears to be most sensitive to CYP binding type. When type is not a factor in the comparison made, CIU classification detects differences in compound hydrophobicity. For all the CYP2B4-ligand bound CIU results shown, collision voltages 45-50 V are used to construct the classifiers. Classification of CIU fingerprints based on drug binding modes to CYP3A4

Recently discussed was CYP2B4, originating from Oryctolagus cuniculus (rabbit), in order to move towards a more clinical relevant CYP homolog, we turn our attention to CYP3A4, which is involved in the metabolism of more drugs in clinical use than any other foreign compound-metabolizing enzyme in humans. CYP3A4 is responsible for the metabolism of ~30% of all drugs[1,2], making it a very attractive target to study.

While rabbit CYP2B4 is a widely utilized model system to study the structure and function of CYP enzymes in general, the human CYP3A4 variant is a centrally important enzyme associated with drug metabolism. Similar to CYP2B4, CYP3A4 possesses a similar range of binding modes in the context of inhibitors, substrates and inducers. To evaluate the ability of our CYP CIU ligand classification assays to extend to CYP3A4, we comprehensively studied a range of ligand types bound to CYP3A4 including, type I substrates, type II substrates,

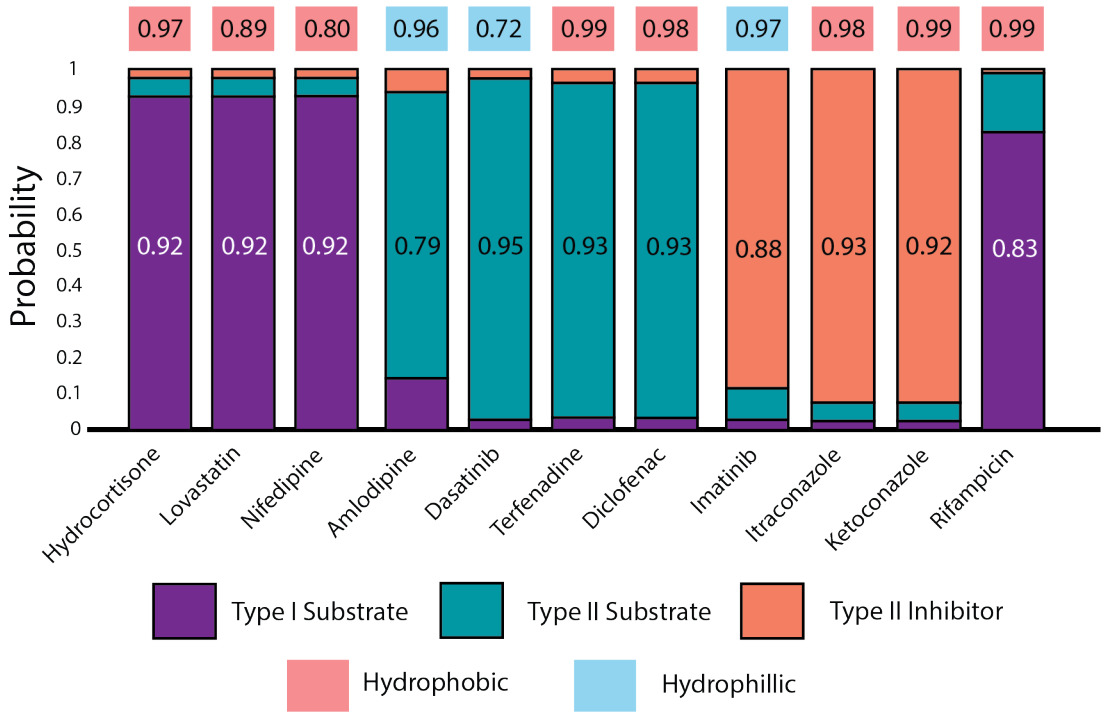

Figure 4-5 Classification summary for CYP3A4 ligand binding out of POPC 4F NDs.Above scores in red and blue indicates scores based on hydrophobicity (red = hydrophobic and blue = hydrophilic) as well as the probability scores for all molecules classification within a three part classifier classifying as either a type I substrate (purple), type II substrate (teal) or type II inhibitor (orange)

type II inhibitors, inducers as well as hydrophobic and hydrophilic compounds. As above,

CYP3A4 13+ ligand bound species were chosen for CIU analysis (Appendix Figure III-5) for the following ligands: (type I substrates) hydrocortisone, nifedipine, lovastatin, (type II substrates) amlodipine, dasatinib, diclofenac, terfenadine, (type II inhibitors) imatinib, ketoconazole, itraconazole, and (inducer) rifampin. Of these molecules, amlodipine, dasatinib, and imatinib were more polar and the rest hydrophobic.

Two separate classification schemes were built, one for determining compound hydrophobicity (Appendix Figure III-6) and a second for determining CYP binding type (Appendix Figure III-7). In addition, the classification scheme built for the determination of CYP binding type was a three-part classifier, able to identify type 1 substates, type II substrates, and type II inhibitors. The output of this analysis is shown in Figure 4-5 where hydrocortisone, lovastatin and nifedipine are all correctly classified as type I CYP substrates (purple) with high probability scores of 0.92 ± 0.01, 0.92 ± 0.03, and 0.92 ± 0.05 respectively. Above each bar is the score describing the confidence with which these same compounds were classified as hydrophobic CYP binders (red) resulting in values of 0.97 ± 0.02, 0.89 ± 0.13 and 0.80 ± 0.14 respectively. For the type II CYP substrates: amlodipine, dasatinib, terfenadine, and diclofenac we observe correct classification with high probability scores of 0.79 ± 0.11. 0.95 ± 0.03, 0.93 ± 0.09, and 0.93 ± 0.11respectively. Correct hydrophobicity scores were obtained for amlodipine and dasatinib, producing scores of 0.96 ± 0.5 and 0.72 ± 0.15 respectively as hydrophilic interactors (blue) and terfenadine and diclofenac with 0.99 ±0.1 and 0.98 ± 0.11 were scored respectively as hydrophobic interactors (red). The type II CYP inhibitors imatinib, itraconazole, and ketoconazole were classified with high probability scores of 0.88 ± 0.06, 0.93 ± 0.07, 0.92 ± 0.5 respectively (orange). These same compounds classified correctly according to their expected hydrophobicity, with imatinib scoring 0.97 ± 0.02 as a hydrophilic (blue) binder and

itraconazole and ketoconazole scoring 0.99 ± 0.02 and 0.99 ± 0.05 respectively as hydrophobic binders. Finally, the inducer molecule scored with high confidence as a hydrophobic (0.99 ± 0.7) type I substrate (0.83 ± 0.16).

4.4 Conclusions

In this report, we successfully constructed CIU based assays capable of differentiating CYP binders based on their mode of attachment to the protein and their hydrophilicities. The ability of our CIU assays to sort CYP-ligand complexes according to hydrophilicities relates directly to the proximity of the CYP active site to the biological membrane and supports the conclusion that lipids are significantly involved in structure of the CYP active site, as indicated in prior MD simulation results.[9,10] Prior to the CIU measurements discussed here, CYP-ligand binding studies were limited to spectroscopic spin shift perturbations targeting the CYP heme, and typically involved removal of the TM alpha helix. As such, our work provides an exciting framework for further advance our knowledge of drug metabolism, protein engineering, CYP biochemistry, and MP-associated drug discovery in general. This assay can be extended towards other MPs such as GPCRs extracted from cells using sonicated lipid vesicles or over expressed, purified proteins incorporated into NDs of various lipid compositions.

More generally, our CIU results for CYP-ligand complexes highlight the ability of gas-phase ions to retain a memory of their native structures when housed within ND-based membrane mimetics. The technology described in this report is amenable to high-throughput data acquisition modes, as the classifier-based data analysis strategy deployed can be automated after the construction of appropriate classifiers. In addition, since our approach is constructed around IM-MS technology, such assays can be performed without the need for large amounts of purified protein and in the context of mixtures. Future work in our laboratory will include

expanding the assays described in this report to include larger libraries of potential CYP binders in a high-throughput mode.

4.5 Acknowledgments

Membrane protein research in the Ruotolo lab is supported by the National Institute of Health under Grants GM105942. The author thanks collaborators Professor Ayyalusamy Ramamoorthy and Katie Gentry and Carlo Barnaba for their contribution in this chapter

Bibliography

Werk, A. N.; Cascorbi, I. Functional Gene Variants of CYP3A4. *Clin. Pharmacol. Ther.* **2014**, *96* (3), 340–348.

(2) Zanger, U. M.; Schwab, M. Cytochrome P450 Enzymes in Drug Metabolism: Regulation of Gene Expression, Enzyme Activities, and Impact of Genetic Variation. *Pharmacol. Ther.* **2013**, *138* (1), 103–141.

(3) Lewis, D. F. V. Guide to Cytochromes P450 : Structure and Function. *Guid. to Cytochromes P450* **1996**.

(4) Poulos, T. L. The Crystal Structure of Cytochrome P-450. *Cytochrome P-450* **1986**, 505–523.

(5) Ravichandran, K. G.; Boddupalli, S. S.; Hasemann, C. A.; Peterson, J. A.; Deisenhofer, J. Crystal Structure of Hemoprotein Domain of P450BM-3, a Prototype for Microsomal P450's. *Science* **1993**, *261* (5122), 731–736.

(6) Hasemann, C. A.; Ravichandran, K. G.; Peterson, J. A.; Deisenhofer, J. Crystal Structure and Refinement of Cytochrome P450terp at 2·3 Å Resolution. *J. Mol. Biol.* **1994**, *236* (4), 1169–1185.

(7) Williams, P. A.; Cosme, J.; Sridhar, V.; Johnson, E. F.; McRee, D. E. Mammalian Microsomal Cytochrome P450 Monooxygenase: Structural Adaptations for Membrane Binding and Functional Diversity. *Mol. Cell* **2000**, *5* (1), 121–131.

(8) Mestres, J. Structure Conservation in Cytochromes P450. *Proteins* **2005**, *58* (3), 596–609.

(9) Cojocaru, V.; Balali-Mood, K.; Sansom, M.; Wade, R. C. Structure and Dynamics of the Membrane-Bound Cytochrome P450 2C9. *PLoS Comput Biol* **2011**, *7* (8), 1002152.

(10) Šrejber, M.; Navrátilová, V.; Paloncýová, M.; Bazgier, V.; Berka, K.; Anzenbacher, P.; Otyepka, M. Membrane-Attached Mammalian Cytochromes P450: An Overview of the Membrane's Effects on Structure, Drug Binding, and Interactions with Redox Partners. *J. Inorg. Biochem.* **2018**, *183*, 117–136.

(11) Jang, H.-H.; Liu, J.; Lee, G.-Y.; Halpert, J. R.; Wilderman, P. R. Functional Importance of a Peripheral Pocket in Mammalian Cytochrome P450 2B Enzymes * HHS Public Access. *Arch Biochem Biophys* **2015**, *584*, 61–69.

(12) Treuheit, N. A.; Redhair, M.; Kwon, H.; Mcclary, W. D.; Guttman, M.; Sumida, J. P.; Atkins, W. M. *Membrane Interactions, Ligand-Dependent Dynamics, and Stability of Cytochrome P4503A4 in Lipid Nanodiscs*.

(13) Headlam, M. J.; Wilce, M. C. J.; Tuckey, R. C. The F-G Loop Region of Cytochrome P450scc (CYP11A1) Interacts with the Phospholipid Membrane. *Biochim. Biophys. Acta* **2003**, *1617* (1–2), 96–108.

(14) Monk, B. C.; Tomasiak, T. M.; Keniya, M. V.; Huschmann, F. U.; Tyndall, J. D. A.; O'Connell, J. D.; Cannon, R. D.; McDonald, J. G.; Rodriguez, A.; Finer-Moore, J. S.; Stroud, R. M. Architecture of a Single Membrane Spanning Cytochrome P450 Suggests Constraints That Orient the Catalytic Domain Relative to a Bilayer. *Proc. Natl. Acad. Sci. U. S. A.* **2014**, *111* (10), 3865–3870.

(15) McDougle, D. R.; Baylon, J. L.; Meling, D. D.; Kambalyal, A.; Grinkova, Y. V.;

Hammernik, J.; Tajkhorshid, E.; Das, A. Incorporation of Charged Residues in the CYP2J2 F-G Loop Disrupts CYP2J2-Lipid Bilayer Interactions. *Biochim. Biophys. Acta* **2015**, *1848* (10 Pt A), 2460–2470.
(16) Gay, S. C.; Sun, L.; Maekawa, K.; Halpert, J. R.; Stout, D. Crystal Structures of Cytochrome P450 2B4 in Complex with the Inhibitor 1-Biphenyl-4-Methyl-1H-Imidazole: Ligand-Induced Structural Response through R-Helical Repositioning †, ‡. *Biochemistry* **2009**, *48*, 4762–4771.
(17) Cojocaru, V.; Winn, P. J.; Wade, R. C. The Ins and Outs of Cytochrome P450s. *Biochim. Biophys. Acta* **2007**, *1770* (3), 390–401.
(18) Yoshimoto, F. K.; Auchus, R. J. The Diverse Chemistry of Cytochrome P450 17A1 (P450c17, CYP17A1). **2014**.
(19) Treuheit, N. A.; Redhair, M.; Kwon, H.; Mcclary, W. D.; Guttman, M.; Sumida, J. P.; Atkins, W. M. Membrane Interactions, Ligand-Dependent Dynamics, and Stability of Cytochrome P4503A4 in Lipid Nanodiscs. **2016**.
(20) Grinkova, Y. V.; Denisov, I. G.; McLean, M. A.; Sligar, S. G. Oxidase Uncoupling in Heme Monooxygenases: Human Cytochrome P450 CYP3A4 in Nanodiscs. *Biochem. Biophys. Res. Commun.* **2013**, *430* (4), 1223–1227.
(21) Liu, K.-C.; Hughes, J. M. X.; Hay, S.; Scrutton, N. S. Liver Microsomal Lipid Enhances the Activity and Redox Coupling of Colocalized Cytochrome P450 Reductase-Cytochrome P450 3A4 in Nanodiscs. *FEBS J.* **2017**, *284*, 2302.
(22) Duggal, R.; Liu, Y.; Gregory, M. C.; Denisov, I. G.; Kincaid, J. R.; Sligar, S. G. Evidence That Cytochrome B5 Acts as a Redox Donor in CYP17A1 Mediated Androgen Synthesis. *Biochem. Biophys. Res. Commun.* **2016**, *477* (2), 202–208.
(23) Nath, A.; Grinkova, Y. V; Sligar, S. G.; Atkins, W. M. Ligand Binding to Cytochrome P450 3A4 in Phospholipid Bilayer Nanodiscs THE EFFECT OF MODEL MEMBRANES * Downloaded From. *J. Biol. Chem.* **2007**, *282* (39), 28309–28320.
(24) Ingelman-sundberg, M.; Glaumann, H. Reconstitution of the Liver Microsomal Hydroxylase System into Liposomes. *FEBS Lett.* **1977**, *78* (1), 72–76.
(25) Shaw, P. M.; Hosea, N. A.; Thompson, D. V.; Lenius, J. M.; Guengerich, F. P. Reconstitution Premixes for Assays Using Purified Recombinant Human Cytochrome P450, NADPH-Cytochrome P450 Reductase, and Cytochrome B5. *Arch. Biochem. Biophys.* **1997**, *348* (1), 107–115.
(26) Denisov, I. G.; Sligar, S. G. Cytochromes P450 in Nanodiscs. *Biochimica et Biophysica Acta - Proteins and Proteomics*. Elsevier January 2011, pp 223–229.
(27) Denisov, I. G.; Sligar, S. G. NANODISCS IN MEMBRANE BIOCHEMISTRY AND BIOPHYSICS.
(28) Barnaba, C.; Martinez, M. J.; Taylor, E.; Barden, A. O.; Brozik, J. A. Single-Protein Tracking Reveals That NADPH Mediates the Insertion of Cytochrome P450 Reductase into a Biomimetic of the Endoplasmic Reticulum. *J. Am. Chem. Soc.* **2017**, *139* (15), 5420–5430.
(29) Cojocaru, V.; Winn, P. J.; Wade, R. C. The Ins and Outs of Cytochrome P450s. *Biochimica et Biophysica Acta - General Subjects*. March 2007, pp 390–401.
(30) Denisov, I. G.; Grinkova, Y. V.; Baylon, J. L.; Tajkhorshid, E.; Sligar, S. G. Mechanism of Drug-Drug Interactions Mediated by Human Cytochrome P450 CYP3A4 Monomer. *Biochemistry* **2015**, *54* (13), 2227–2239.
(31) Das, A.; Sligar, S. G. Modulation of the Cytochrome P450 Reductase Redox Potential by

the Phospholipid Bilayer. *Biochemistry* **2009**, *48* (51), 12104.
(32) Denisov, I. G.; Shih, A. Y.; Sligar, S. G. Structural Differences between Soluble and Membrane Bound Cytochrome P450s. *J. Inorg. Biochem.* **2012**, *108*, 150–158.
(33) Barnaba, C.; Humphreys, S. C.; Barden, A. O.; Jones, J. P.; Brozik, J. A. Substrate Dependent Native Luminescence from Cytochromes P450 3A4, 2C9, and P450cam. *J. Phys. Chem. B* **2016**, *120* (12), 3038–3047.
(34) Mcclary, W. D.; Sumida, J. P.; Scian, M.; Paç, L.; Atkins, W. M. Membrane Fluidity Modulates Thermal Stability and Ligand Binding of Cytochrome P4503A4 in Lipid Nanodiscs. **2016**.
(35) Nagar, S.; Korzekwa, K. Commentary: Nonspecific Protein Binding versus Membrane Partitioning: It Is Not Just Semantics. *Drug Metab. Dispos.* **2012**, *40* (9), 1649–1652.
(36) Ingelman-Sundberg, M.; Hagbjörk, A. L.; Ueng, Y. F.; Yamazaki, H.; Guengerich, F. P. High Rates of Substrate Hydroxylation by Human Cytochrome P450 3A4 in Reconstituted Membranous Vesicles: Influence of Membrane Charge. *Biochem. Biophys. Res. Commun.* **1996**, *221* (2), 318–322.
(37) Jeřábek, P.; Florián, J.; Martínek, V. Lipid Molecules Can Induce an Opening of Membrane-Facing Tunnels in Cytochrome P450 1A2 HHS Public Access. *Phys Chem Chem Phys* **2016**, *18* (44), 30344–30356.
(38) Berka, K.; Hendrychová, T.; Anzenbacher, P.; Otyepka, M. Membrane Position of Ibuprofen Agrees with Suggested Access Path Entrance to Cytochrome P450 2C9 Active Site. *J. Phys. Chem. A* **2011**, *115* (41), 11248–11255.
(39) Haynes, S. E.; Polasky, D. A.; Dixit, S. M.; Majmudar, J. D.; Neeson, K.; Ruotolo, B. T.; Martin, B. R. Variable-Velocity Traveling-Wave Ion Mobility Separation Enhancing Peak Capacity for Data-Independent Acquisition Proteomics. *Anal. Chem.* **2017**, *89* (11), 5669–5672.
(40) Polasky, Daniel A; Dixit, Sugyan M.; Fantin, Sarah M.; Ruotolo, B. T. "CIUSuite 2: Next-Generation Software for the Analysis of Gas-Phase Protein Unfolding Data." *Press*.
(41) Das, A.; Zhao, J.; Schatz, G. C.; Sligar, S. G.; Van Duyne, R. P. Screening of Type I and II Drug Binding to Human Cytochrome P450-3A4 in Nanodiscs by Localized Surface Plasmon Resonance Spectroscopy.

Chapter 5 **Co-factor Binding and Protein-Protein Interactions Drive Structural Transitions in Cytochrome P450 and its Redox Partners**

5.1 Introduction

Fifty-seven genes have been identified in humans as coding for various cytochrome P450 (CYP) enzymes. Of these, approximately 13 CYP isoforms are responsible for the metabolism of more than 80% of clinically used drugs.[1] Human CYPs that typically mediate the metabolic clearance of drugs are targeted to the smooth endoplasmic reticulum (ER) by an N-terminal transmembrane domain with the catalytic domain residing in the cytosol.[2,3] The key CYP isoforms that are involved in drug metabolism are primarily located in the liver whereas the other CYP isoforms, which are primarily involved in steroid metabolism, are localized mainly to the adrenal glands and gonads with smaller amounts expressed in the brain, placenta, and heart.[4,5]

CYPs carry out the first metabolic step for an exceptional variety of compounds. The most common reaction CYP catalyzes is the insertion of a hydroxyl group into a hydrophobic substrate, breaking a C-C or C-H bond in the process. Two reducing equivalents are required for this catalytic cycle which originates from electrons donated from protein redox partners. These redox partners are Cytochrome P450 oxidoreductase (POR) or cytochrome b5 (cytb5), and CYP reduction is carried out either entirely by POR, where both electrons originate from its bound NADPH cofactor, or by both cytb5 and POR, where both proteins act to donate electrons to CYP, the first of which always originating from POR[6] (Figure 5-1).

The inability of cytb5 to donate the first CYP reducing electron relates to the large potential difference between oxidized CYP and reduced cytb5 (-245 mV vs +20 mV) which is substantially lessened after CYP undergoes a one electron reduction .[7] A better understanding of how CYP interacts with the redox partners in a native membrane environment, and specifically how such interactions can influence the CYP enzyme activity, multi-compound metabolism, and inform predictions of potentially dangerous drug-drug interactions.[8–10] In addition, CYPs are also key targets associated with the treatment of several health conditions including breast cancer, prostate cancer and heart disease, and as such, evaluating structures and protein-protein interactions in the context of native membrane environments is of great importance.[11–15]

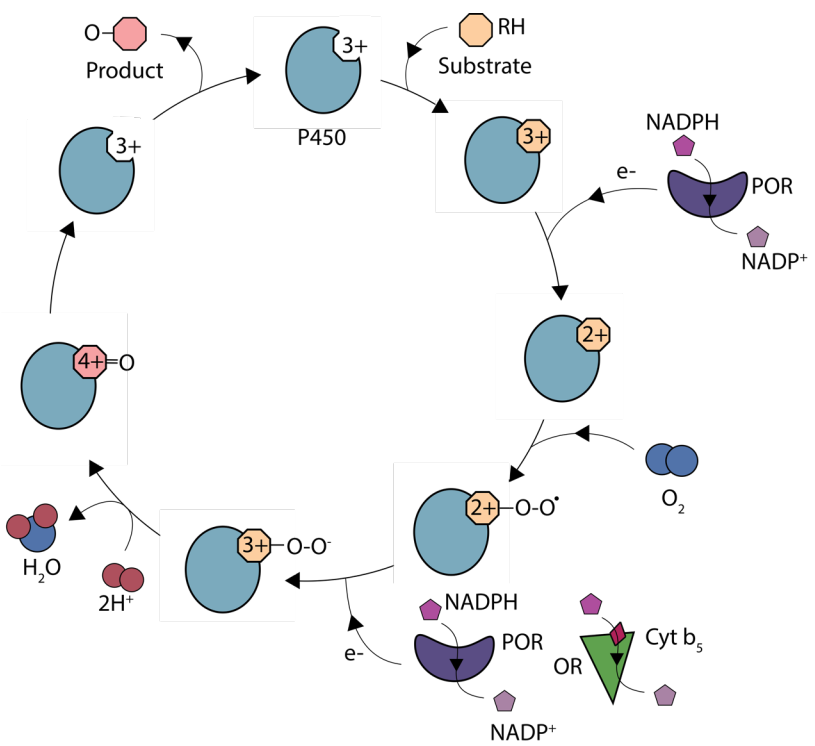

Figure 5-1 Cytochrome P450 catalytic cycle. Blue circles represent the P450 as well as the charge state of the iron centered in the active site, redox partners POR shown in purple and cytochrome b5 as a green triangle are responsible for the donation of electrons from NADPH

POR acts as the obligate redox partner of CYP, and many studies have characterize the binding of POR to CYP, interacting through the POR flavin mononucleotide binding domain (FBD) domain.[16] Details surrounding potential competition between cytb5 over POR for electron donation to CYP remains unclear and is a current area of active research. Additionally, the influences of the

lipid bilayer in combination with protein redox partner proximity and binding on full-length CYP structure are currently unknown.

In recent years, native ion mobility-mass spectrometry (IM-MS), has emerged as a robust structural biology tool capable of handling complex mixtures in a high-throughput manner. With the use of membrane mimetics such as nanodiscs the native conformation of membrane proteins is retained and allowed to be studied using a gas phase technique such as IM-MS.[17–21]22–27 IM separates the ions based on their size, shape, and charge. In native IM-MS experiments, we can observe different conformations of protein ions and perform experiments like collision induced unfolding (CIU) to get a global picture of protein conformation when exposed to various variables.[22] In this work we use full length CYP3A4, POR, and cytb5 constructs in the presence of a lipid bilayer using nanodiscs and employ IM-MS and CIU to get insights on protein: protein interactions as well as how POR structure responds to reduction of NADPH. In doing so, our results indicated that when redox partners are co-incubated in NDs we observe no direct evidence of stable protein:protein complexes, but do observe significant alterations in each of the three protein structure, suggesting protein:protein interactions are inducing conformational shifts. Additionally, we observe evidence of increased lipid binding for POR when reduced by NADPH, which suggests a deeper membrane engagement as well as stabilization and retention of the FMN and FAD cofactors.

5.2 Methods

5.2.1 Membrane protein sample preparation

Full length CYP3A4 were expressed in *E. coli* using the pCWori vectors using protocols adapted from established protocols for CYP3A4[23]. Full length wild-type rabbit cytb5 was expressed and purified as described previously,[24–26] briefly, *E. coli* C41 cells were transformed with a pLW01 plasmid containing the cytb5 gene. Full length POR cDNA in pSC-POR plasmids

were expressed in *E. coli* C41 cells and purified as described previously.[25,26] Ammonium acetate and dihydronicotinamide adenine dinucleotide phosphate tetrasodium salt (NADPH) were purchased from Sigma Aldrich (St. Louis, MO). Potassium phosphate monobasic and potassium phosphate dibasic were purchased from Fisher Scientific (Hampton, NH). The 4F peptide scaffolding belt (DWFKAFYDKVAEKFKEAF N-terminal modification: acetylation, C-terminal modification: amidation[27]) was purchased from GenScript (Piscataway, NJ). All lipids (1-palmitoyl-2-oleoyl-sn-glycero-3-phosphoethanolamine [POPE], -palmitoyl-2-oleoyl-sn-glycero-3-phospho-L-serine [POPS], 1-palmitoyl-2-oleoyl-glycero-3-phosphocholine [POPC], L-α-phosphatidylinositol (Soy) [PI], and Sphingomyelin (egg, chicken) [eSM] were purchased from Avanti Polar Lipids (Alabaster, AL). Cholesterol Hemisuccinate Tris Salt (CHEMS) was purchased from Anatrace (Maumee, OH). CYP, POR and cytb5 were incorporated into the peptide 4F NDs which were pre-formed by rehydrating 11.25 mg of lipids (dry lipid films) in 40 mM potassium phosphate pH 7.4 buffer and mixing with 7.5 mg of 4F peptide suspended in 40 mM potassium phosphate pH 7.4 buffer. Depending on the phase temperature of the lipids, the mixture was allowed to shake at either 37ºC or 45ºC until the cloudy mixture turned transparent. Mix ER lipid mixture: 54% POPC, 6% POPS, 8% POPE, 8% PI, 17% eSM, and 7% CHEMS.[28] Empty NDs were purified using SEC on a Superdex S200 increase 10/300 GL column and DLS measurements were obtained using Wyatt DynaPro NanoStar and fractions with uniform size distribution were chosen for protein incorporation and measured for concentration using a Thermo Scientific NanoDrop 2000 spectrophotometer, using the extinction coefficient for 4F ε = 6.99 mM^{-1} cm^{-1} taking into account 16 peptides per disc. POR and cytb5 were incubated with empty ND at ratios of 1:1.1 and 1:3 for CYP3A4 and incubated for 6-10 hours at room temperature with constant gentle shaking. The increase in empty ND ratio for CYP3A4 helped

eliminate protein crash out during incubation. Co-incubation NDs were prepared by first incorporating and purifying CYP3A4 NDs then incubating 1:1.1 of CYP:redox partner for 6 hours. For the POR NADPH NDs, NADPH was added to the mixture to incubate. CYP and CYP-POR, CYP-cytb5 incorporated NDs were simultaneously purified and buffer exchanged into 200 mM ammonium acetate pH 7.4 via SEC on Superdex S200 increase 10/300 or 3.2/300 GL column, any POR NDs were purified with 1 mM NADPH in the running buffer, since the NADPH is a tetrasodium salt and not compatible with MS, the added NADPH was first prepared as a 100 mM stock and then buffer exchanged using Micro Bio-Spin P-6 gel resin columns (Bio-Rad, Hercules, CA) into water pH adjusted to 8.0, all buffers containing NADPH were kept refrigerated and made fresh every 6 hours. Protein incorporated into ND only fractions were pooled and concentrated using 100 kDa Amicon Ultra-0.5 centrifugal filter units (MilliporeSigma, Burlington, MA).

5.2.2 Native Ion-Mobility-Mass Spectrometry and CIU Experiments

All IM-MS data was collected using a Synapt G2 HDMS IM-Q-ToF mass spectrometer (Waters, Milford, MA), with a direct infusion nano electrospray ionization (nESI) source set to positive ion mode. Instrument settings were tuned to dissociate solubilization agents with minimal perturbation to protein structure prior to the IM separator, including appropriately tuned settings for the source temperature (30° C), source gas flow (50 mL/min), and the sampling cone (10 V). Trapping cell wave velocity and height were 116 m/s and 0.1 V. IMS wave velocity and height were 250 m/s and 15 V. Transfer cell wave velocity and height were 300 m/s and 10 V, with an accelerating potential of 10 V used to dissociate empty NDs. Collision cross section analysis was performed by IMSCal-19v4, a program written in C. Theoretical collision cross sections (CCSs) of monomeric CYP3A4 were calculated using a previously published homology model and IMPACT.

All CIU analyses were performed by increasing the trap collision voltage in a stepwise manner from 20 – 90 V in 5 V increments. CIU data from the 14+ and 15+ charge states of CYP2B4 and CYP3A4, respectively, were extracted using TWIMExtract63, then processed and analyzed using CIUSuite2. Data processing included three rounds of 2D Savitzky-Golay smoothing with a window of five bins and interpolation of the collision voltage axis by a factor of four.

5.2.3 High Resolution Mass Spectrometry Experiment QE UHMR

All high-resolution MS data was collected on a Thermo Fisher Q-Exactive Ultra High Mass Range (UHMR) Oribtrap platform using the nano ESI source. instrumental parameters include capillary temperature of 250 C, resolution of 6,250, capillary voltage 0.9 kV, C-trap pressure of 10, C-trap RF voltage of 1,800 , ion transfer m/z optimization set to high m/z, in-source trapping set to on, desolvation voltage of −150 V, detector m/z optimization set to low m/z, extended trapping of 50 eV, and, in-source CID of 10 eV and averaging of 200. Data were collected over a broad m/z range (500–8,000 m/z). Data was deconvoluted using UniDec.[29]

5.3 Results and Discussion

5.3.1 CIU of full length cytb5 liberated from NDs

The cytb5 sequence contains three domains: a heme containing globular domain, a 15-amino acid flexible linker crucial to activity, and a C-terminal transmembrane domain.[25] The globular domain consists of 5 α-helices, five β-strands, and one 3-10 helix that is bound to a heme B that is coordinated through two histidines: His 44 and His68.[25,30] The 15 amino acid random coil domain is crucial for complex formation.[31] Shortening of the linker to less than seven residues abolishes CYP binding whereas an increase in the linker length has minimal effects on CYP binding. Studying full-

length cytb5 is critical due to reports that truncated cytb5 is incapable of donating electrons to mammalian membrane-bound CYPs.[32–34]

Cytb5 has unique properties which influence CYP metabolism in a manner depending upon the CYP isoform, its concentration, or the substrate involved .[31] In all cases, the second electron delivered to CYP from either POR or cytb5 is the rate limiting step of the CYP reaction.

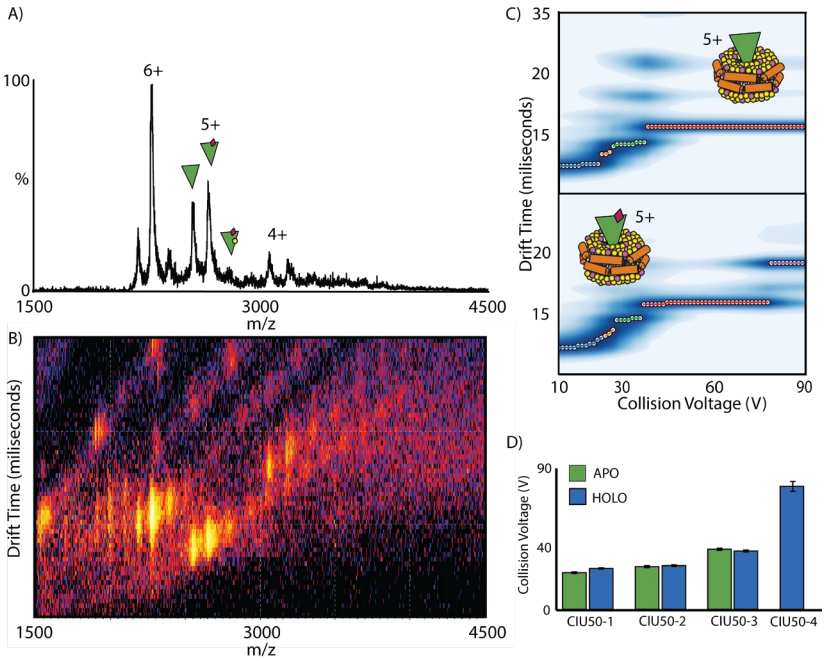

Figure 5-2 full length cytochrome b5 liberated from PC:PS 4F Nanodiscs. **A**) native MS data with native like charge states ranging from 4+ to 6+ **B**) driftscope snapshot of cytb5 and various bound states, apo, holo, and lipid binding **C**) CIU fingerprints for 5+ apo (top) and holo (bottom) **D**) CIU50 analysis comparing apo to holo

We have successfully incorporated and analyzed full length cytb5 into a 80:20 POPC:POPE 4F peptide ND and collected both IM-MS and CIU data (Figure 5-2). Our IM-MS data contains signals for 4+-6+ native-like cytb5 ions, including signals for apo, holo, and lipid bound states. An analysis of CIU data reveals evidence of cytb5 destabilization when attached to the heme, as well as global changes to the CIU features observed indicating significant heme-dependent structure changes within the protein.

5.3.2 POR and NADPH liberated from mixed lipid NDs

POR is an essential redox partner for CYP metabolic activity, as it is capable of donating both electrons to CYP during its catalytic cycle. Indeed, much CYP activity can be reconstituted just

through the addition of POR. [16] [35,36] [37] Ultimately, electrons from NADPH are transferred from the flavin adenine dinucleotide (FAD) domain, to the Flavin mononucleotide (FMN) domain on POR then finally to CYP.[37] Overall, POR contains four distinct domains that make up the roughly 80 kDa protein: a FAD binding domain where NADPH reduces the protein, a linker domain, an FMN binding domain (FBD) that interacts with and reduces CYP, as well as a N-terminal transmembrane domain.

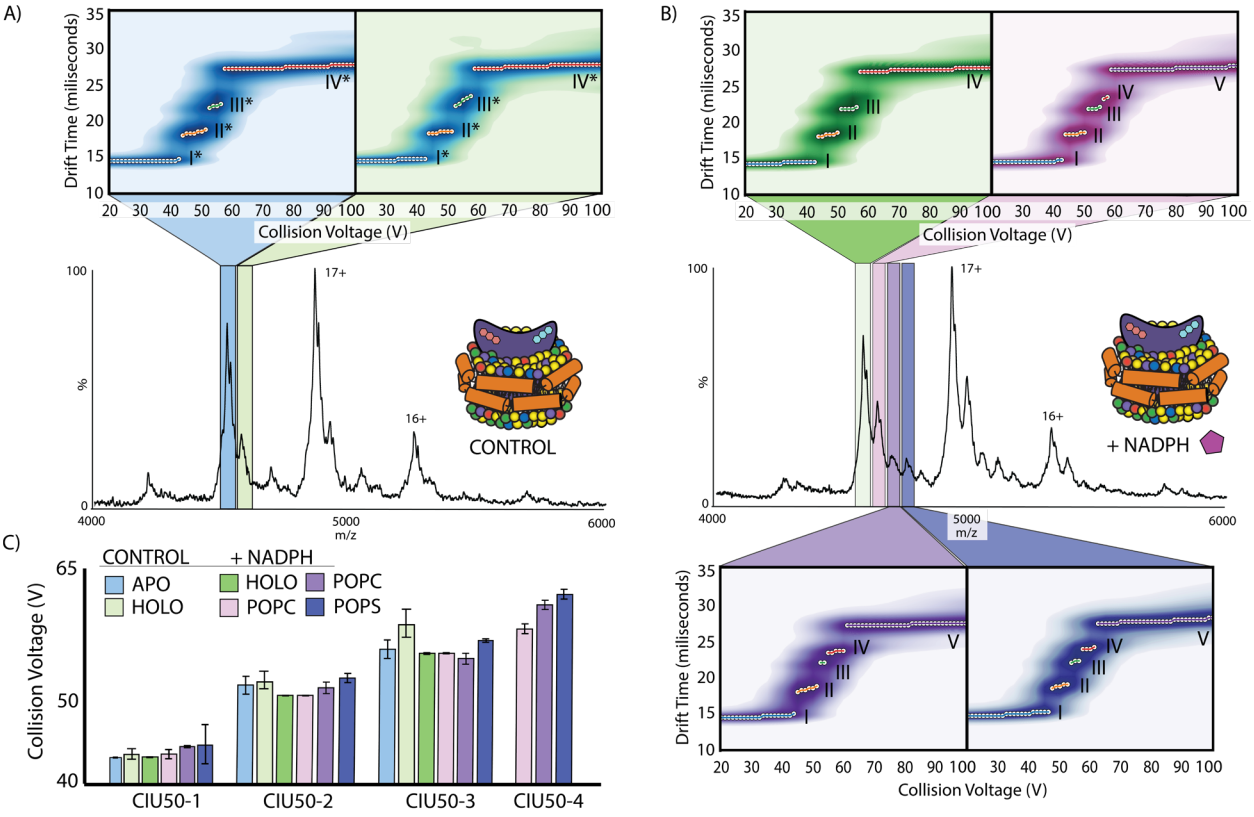

Figure 5-3 Effects of NADPH on POR. **A**) mass spectrum for POR liberated from mix ER 4F ND with charge states ranging 16+ to 19+ and the CIU fingerprints for the two main peaks observed. Features 1-4 are labeled I-IV (*denotes control no NADPH **B**) mass spectrum for POR liberated from mix ER 4F ND with NADPH with charge states ranging 16+ to 19+ and the CIU fingerprints for the four main peaks observed (holo (green, features 1-4 are labeled I-IV) including the three new lipid binding peaks (purple, features 1-5 are labeled I-V) **C**) CIU50 stability shift values for all bound states, control and with NADPH

Here, we explore the full length POR structures when housed within NDs constructed from 5 different lipids and cholesterol mixture, designed to reflect the ER,[38] both with and without NADPH. Using native IM-MS, we observe a native like charge state distribution (19+-

15+) for the ~80 kDa POR protein with and without NADPH (Figure 5-3). Interestingly, when POR-NDs are incubated with NADPH we observe significant mass shifts (Figure 5-3AB) corresponding to additional NADPH-dependent bound states (Appendix Figure IV-1). In our control data (without NADPH) we observe two main peaks which correspond to masses of 78,510 Da and 79,750 Da respectively (Appendix Figure IV-2B). High resolution native MS data was obtained in order to assign the features observed in our IM-MS data with confidence. When NAPDH is added, we observe a shift in POR bound populations with masses of 79,790 Da, 80,550 Da, 81,315 Da, and 82,095 Da respectively (Appendix Figure IV-2 D, Figure 5-3, Figure 5-4) We detect a mass difference between the two main signals found in our control data of 1240 Da, which we assign to the loss of both the FAD and FMN cofactors which have masses of 785.5 Da (FAD) and 456.3 Da (FMN) which sums to a total mass of 1,241.8 Da.

Critically, we observed the appearance of three additional POR bound states when the protein is also attached to NADPH (purple Figure 5-3B), and CIU fingerprint data suggests that these POR bound states occupy conformationally-distinct states, as indicated by the additional CIU features (III & IV) detected between 20 and 25 ms in the bound state fingerprints. Using high resolution nMS, we measured the mass shifts associated with these bound features to 760 Da, 760 Da, and 780 Da for the first, second and third additional POR bound state respectively. Based on our high-resolution nMS data, we assign the first two additional POR bound compounds to POPC lipids and the third to a POPS lipid (nominal masses of POPC and POPS are 760 Da 783 Da respectively, Appendix Figure IV-2). We note that the ER mimic ND composition used in these studies includes 54% POPC and 6% POPS, strongly indicating that the protein preferentially recruits POPS during its apparently deeper mode of membrane engagement promoted by NADPH.[28] In addition to the POPS/POPC bound states observed above, we also

detect CIU evidence of POR structural shifts in the presence of NADPH (light green, dark green Figure 5-3A,B) (For example, when comparing the CIU50 values extracted form POR ions liberated from NDs under these conditions (Figure 5-3C) it is clear NADPH binding results in a destabilized POR state. Previous work has indicated that POR adopts a peripheral membrane protein architecture when oxidized, and when reduced with NADPH the POR penetrates the bilayer and is converted to a fully transmembrane protein[39]. Taken together, in the shifts in CIU fingerprints in the POR holo state, the observed retention of FAD and FMN within the POR architecture, as well as the POPC/POPS lipid binding observed, all point towards evidence of POR more deeply interacting within the cellular membrane when bound to NADPH.

5.3.3 Redox partner interactions when housed in the same nanodisc

Next, we inserted CYP redox partners housed CYP-containing NDs in order to capture the structural consequences of the protein interactions produced under such conditions. Important residues on CYP for POR binding have been identified through site-directed mutagenesis, stopped-flow spectrometry, and other methods.[40] Both electrostatic and hydrophobic interactions have been identified as contributing to complex formation in between CYP and the FBD domain within POR. Cationic localized charge on the proximal surface of CYP, and anionic residues surrounding the FMN of FBD domains of POR, initially drive the protein-protein interaction.[31,40] Several cationic and neutral residues on CYP have been identified as being critical for binding to POR which are on the C or C' helix: R122, R126, R133, F135, M137, K139, K433, R422, R443.[26] CYP has been shown to have a greater binding affinity for POR over cytb5.[26,31]

Similarly, the interactions between CYP and cytb5 have been extensively investigated in past reports.[31,41–43] Through site directed mutagenesis, important residues within the CYP binding surface were located in the C-helix on the proximal side of the protein (R122, R126, R133, F135, M137,

K139) with K433 on the β-bulge above the axial cysteine.[26,44] Within cytb5, D65 and V66 have been identified as key residues for CYP binding.[25] Based on NMR data and prior site directed mutagenesis work, a model for the complex formed between full length cytb5 and CYP 2B4 has been predicted.[25]

Our data does not include direct evidence of CYP-redox partner complex formation. This result is not surprising given the reality weak binding constants associated with CYP complexes.[45–48] Despite this, we observe evidence of shifts in CYP structure when housed within NDs with redox partner proteins. Since POR and cytb5 have overlapping but unique binding sites on the surface of CYP, the two proteins sterically compete for CYP access. As such, we

focused our experiments on inserting CYP in NDs with each of the redox binding protein separately, specifically creating NDs containing CYP3A4 with POR and CYP3A4 with cytb5.

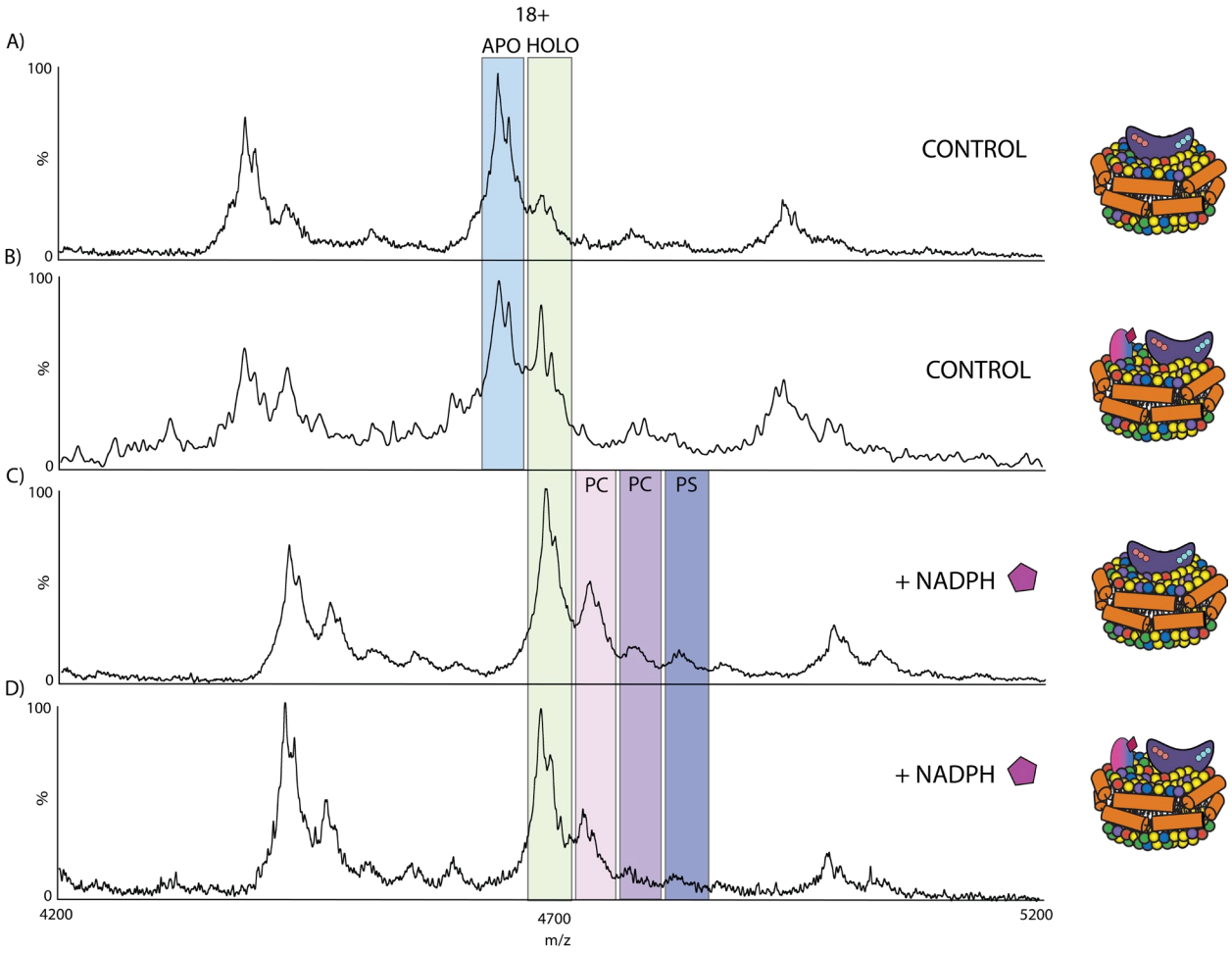

Figure 5-4 NAPDH increases lipid binding to POR. **A**) MS of POR liberated from mix ER 4F ND without any NADPH added, two peaks observed **B**) MS of POR liberated from mix ER 4F ND containing CYP3A4 without any NADPH added, two peaks observed **C**) POR liberated from mix ER 4F ND with NADPH added, four main peaks observed, three of them not observed in control **D**) MS of POR liberated from mix ER 4F ND containing CYP3A4 with NADPH added, four main peaks observed, three of them not observed in control

When CYP3A4 and POR are housed in the same mix ER peptide ND, we observe the same trends discussed previously regarding the deeper insertion of POR into the lipid bilayer, as evident through the detected stabilization of POR through attachment of FAD and FMN cofactors, as well as POPC/POPS binding (Figure 5-4). As discussed above, these shifts in POR structure and lipid engagement are detected in the presence of NADPH, and the data shown in

Figure 5-4 indicates that the presence of CYP within the ND does not significantly influence these changes in POR.

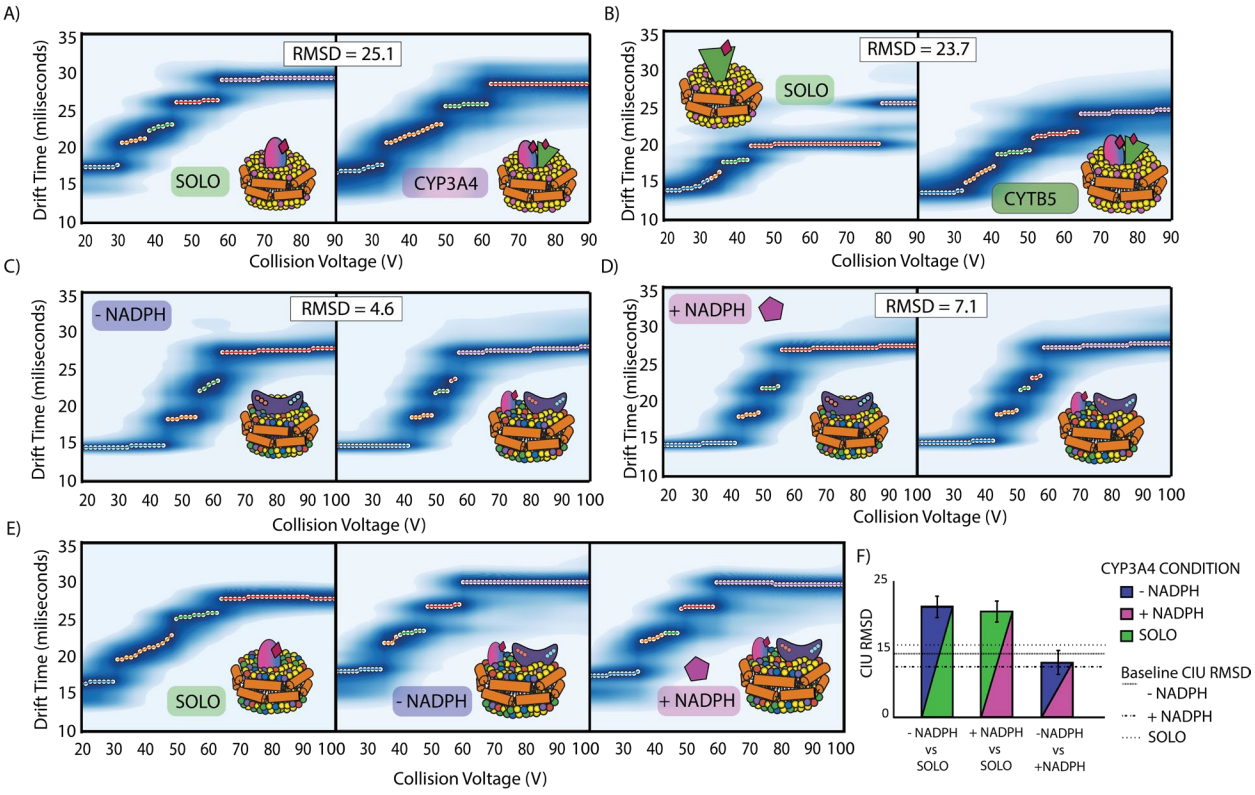

Figure 5-5 CIU fingerprints for all species housed in co-incubated redox partner ND. **A**) CYP3A4 solo vs CYP3A4 liberated co-incubated with cytb5 **B**) cytb5 solo vs cytb5 co-incubated with CYP3A4 **C**) POR solo vs POR co-incubated with CYP3A4 no NADPH added **D**) POR solo vs POR co-incubated with CYP3A4 with NADPH added **E**) CYP3A4 solo vs co-incubated with POR with and without NADPH **F**) RMSD comparison for CYP3A4 and POR conditions, all other RMSD indicated on CIUs

In Figure 5-5, CIU fingerprints collected across all CYP, cytb5, and POR species are comprehensively compared. These results illustrate how housing POR or cytb5 housed within NDs with CYP3A4 can affect the structure of both the proteins contained in the ND. RMSD values were computed for each cross comparison shown, and baseline RMSD values were computed for replicate CIU data, in order evaluate only the significant global differences detected in the CYP, cytb5, and POR fingerprint data.

Our analysis reveals that CYP3A4 undergoes the most significant changes in structure of the three proteins probed here when housed in NDs containing either cytb5 or POR. This

observation holds for NADPHPOR complexes that promote its membrane-engaged form (Figure 5-5F). In addition, cytb5 exhibits significant changes in structure as revealed through CIU data analysis. In contrast, POR seems somewhat structurally invariant in the presence of CYP, and primarily responds to the addition of NADPH, as discussed above. Taken together, our CIU data suggest that CYP, and to a lesser extent cytb5, is exquisitely sensitive to the local ND environment, including the presence of local redox proteins present locally within the cellular membrane.

5.4 Conclusions

For the first time, IM-MS and CIU has revealed that the structures of full length CYP3A4, cytb5, and POR change substantially upon co-factor binding and when housed together within the same lipid bilayer mimetic. We able to detect the structural impact of heme loss in cytb5. CIU data indicates that NADPH can dramatically change the structure of POR, inducing increased lipid binding a deeper level of engagement in the lipid bilayer. Prior reports have noted that P450 system components are not present in equimolar concentrations,[49–51] and while the reason for this remains unknown, our data may pose one explanation by invoking the possibility of POR dynamically switching between a peripheral and transmembrane mode in order service several CYPs through membrane hopping.

In addition to our POR results, our CIU data collected for NDs containing CYP and redox binding partner proteins provides evidence of the extreme environmental sensitivity of CYP structure. The smaller co-factor protein, cytb5, also responds to the presence of CYP within NDs. In contrast, POR does not respond structurally to the presence of CYP but does respond significantly to the presence of NADPH. Future work in this area will focus on probing the role of redox protein proximity in CYP small drug compound binding. IM-MS and CIU will take a

leading role in these experiments, as they are uniquely positioned to separate and individually probe the structures, stabilities, and bound states accessed within such complex ND-protein systems.

5.5 Acknowledgments

Membrane protein research in the Ruotolo lab is supported by the National Institute of Health under Grants GM105942. The author thanks collaborators Professor Richard Auchus and Neikelyn Burgos-Tirado and Sang-Choul Im for their contributions in providing full length cytb5 and POR

Bibliography

(1) De Montellano, P. R. O. Cytochrome P450: Structure, Mechanism, and Biochemistry: Third Edition. *Cytochrome P450 Struct. Mech. Biochem. Third Ed.* **2005**, 1–689.

(2) Zanger, U. M.; Schwab, M. Cytochrome P450 Enzymes in Drug Metabolism: Regulation of Gene Expression, Enzyme Activities, and Impact of Genetic Variation. *Pharmacol. Ther.* **2013**, *138* (1), 103–141.

(3) Woggon, W.-D. Cytochrome P450: Significance, Reaction Mechanisms and Active Site Analogues.

(4) Yoshimoto, F. K.; Auchus, R. J. The Diverse Chemistry of Cytochrome P450 17A1 (P450c17, CYP17A1). *J. Steroid Biochem. Mol. Biol.* **2015**, *151*, 52–65.

(5) Scott, E. E.; White, M. A.; He, Y. A.; Johnson, E. F.; Stout, C. D.; Halpert, J. R. Structure of Mammalian Cytochrome P450 2B4 Complexed with 4-(4-Chlorophenyl)Imidazole at 1.9-Å Resolution: Insight into the Range of P450 Conformations and the Coordination of Redox Partner Binding. *J. Biol. Chem.* **2004**, *279* (26), 27294–27301.

(6) Ogliaro, F.; De Visser, S. P.; Cohen, S.; Sharma, P. K.; Shaik, S. Searching for the Second Oxidant in the Catalytic Cycle of Cytochrome P450: A Theoretical Investigation of the Iron(III)-Hydroperoxo Species and Its Epoxidation Pathways. *J. Am. Chem. Soc.* **2002**, *124* (11), 2806–2817.

(7) Lewis, D. F. V. Guide to Cytochromes P450 : Structure and Function. *Guid. to Cytochromes P450* **1996**.

(8) Ogu, C. C.; Maxa, J. L. Drug Interactions Due to Cytochrome P450. *Proc. (Bayl. Univ. Med. Cent).* **2000**, *13* (4), 421–423.

(9) Denisov, I. G.; Grinkova, Y. V.; Baylon, J. L.; Tajkhorshid, E.; Sligar, S. G. Mechanism of Drug-Drug Interactions Mediated by Human Cytochrome P450 CYP3A4 Monomer. *Biochemistry* **2015**, *54* (13), 2227–2239.

(10) Ramamoorthy, A.; Barnaba, C.; Gentry, K.; Sumangala, N. The Catalytic Function of Cytochrome P450 Is Entwined with Its Membrane-Bound Nature. *F1000Research* **2017**, *6*.

(11) Nebert, D. W.; Russell, D. W. Clinical Importance of the Cytochromes P450. *Lancet (London, England)* **2002**, *360* (9340), 1155–1162.

(12) Fleming, I. Cytochrome P450-Dependent Eicosanoid Production and Crosstalk. *Curr. Opin. Lipidol.* **2011**, *22* (5), 403–409.

(13) El-Sherbeni, A. A.; El-Kadi, A. O. S. Microsomal Cytochrome P450 as a Target for Drug Discovery and Repurposing. *Drug Metab. Rev.* **2017**, *49* (1), 1–17.

(14) Kumarakulasingham, M.; Rooney, P. H.; Dundas, S. R.; Melvin, W. T.; Curran, S.; Murray, G. I. *Cytochrome P450 Profile of Colorectal Cancer: Identification of Markers of Prognosis*.

(15) Murray, G. I.; Taylor, M. C.; McFadyen, M. C. E.; McKay, J. A.; Greenlee, W. F.; Burke, M. D.; Melvin, W. T. Tumor-Specific Expression of Cytochrome P450 CYP1B1. *Cancer Res.* **1997**, *57* (14), 3026–3031.

(16) Wang, M.; Roberts, D. L.; Paschke, R.; Shea, T. M.; Masters, B. S. S.; Kim, J. J. P. Three-

Dimensional Structure of NADPH-Cytochrome P450 Reductase: Prototype for FMN- and FAD-Containing Enzymes. *Proc. Natl. Acad. Sci. U. S. A.* **1997**, *94* (16), 8411–8416.
(17) Abhinav Nath, ‡; William M. Atkins, *,‡ and; Stephen G. Sligar*, §. Applications of Phospholipid Bilayer Nanodiscs in the Study of Membranes and Membrane Proteins†. **2007**.
(18) Marty, M. T.; Hoi, K. K.; Gault, J.; Robinson, C. V. Probing the Lipid Annular Belt by Gas-Phase Dissociation of Membrane Proteins in Nanodiscs. *Angew. Chemie Int. Ed.* **2016**, *55* (2), 550–554.
(19) Hoi, K. K.; Robinson, C. V; Marty, M. T. Unraveling the Composition and Behavior of Heterogeneous Lipid Nanodiscs by Mass Spectrometry. *Anal. Chem* **2017**, *88* (12), 6199–6204.
(20) Li, J.; Fan, X.; Kitova, E. N.; Zou, C.; Cairo, C. W.; Eugenio, L.; Ng, K. K. S.; Xiong, Z. J.; Privé, G. G.; Klassen, J. S. Screening Glycolipids Against Proteins in Vitro Using Picodiscs and Catch-and-Release Electrospray Ionization-Mass Spectrometry. *Anal. Chem.* **2016**, *88* (9), 4742–4750.
(21) Han, L.; Kitova, E. N.; Li, J.; Nikjah, S.; Lin, H.; Pluvinage, B.; Boraston, A. B.; Klassen, J. S. Protein−Glycolipid Interactions Studied in Vitro Using ESI-MS and Nanodiscs: Insights into the Mechanisms and Energetics of Binding. **2015**.
(22) Dixit, S. M.; Polasky, D. A.; Ruotolo, B. T. Collision Induced Unfolding of Isolated Proteins in the Gas Phase: Past, Present, and Future. *Curr. Opin. Chem. Biol.* **2018**, *42*, 93–100.
(23) Gillam, E. M. J.; Baba, T.; Kim, B. R.; Ohmori, S.; Guengerich, F. P. Expression of Modified Human Cytochrome P450 3A4 in Escherichia Coli and Purification and Reconstitution of the Enzyme. *Arch. Biochem. Biophys.* **1993**, *305* (1), 123–131.
(24) Dürr, U. H. N.; Waskell, L.; Ramamoorthy, A. The Cytochromes P450 and B5 and Their Reductases—Promising Targets for Structural Studies by Advanced Solid-State NMR Spectroscopy. *Biochim. Biophys. Acta - Biomembr.* **2007**, *1768* (12), 3235–3259.
(25) Ahuja, S.; Jahr, N.; Im, S.-C.; Vivekanandan, S.; Popovych, N.; Le Clair, S. V; Huang, R.; Soong, R.; Xu, J.; Yamamoto, K.; Nanga, R. P.; Bridges, A.; Waskell, L.; Ramamoorthy, A. A Model of the Membrane-Bound Cytochrome b 5 -Cytochrome P450 Complex from NMR and Mutagenesis Data * □ S. **2013**.
(26) Bridges, A.; Gruenke, L.; Chang, Y. T.; Vakser, I. A.; Loew, G.; Waskell, L. Identification of the Binding Site on Cytochrome P450 2B4 for Cytochrome B5 and Cytochrome P450 Reductase. *J. Biol. Chem.* **1998**, *273* (27), 17036–17049.
(27) Mishra, V. K.; Palgunachari, M. N.; Krishna, R.; Glushka, J.; Segrest, J. P.; Anantharamaiah, G. M. Effect of Leucine to Phenylalanine Substitution on the Nonpolar Face of a Class A Amphipathic Helical Peptide on Its Interaction with Lipid: High Resolution Solution NMR Studies of 4F-Dimyristoylphosphatidylcholine Discoidal Complex. *J. Biol. Chem.* **2008**, *283* (49), 34393–34402.
(28) Barnaba, C.; Sahoo, B. R.; Ravula, T.; Medina-Meza, I. G.; Im, S.-C.; Anantharamaiah, G. M.; Waskell, L.; Ramamoorthy, A. Cytochrome-P450-Induced Ordering of Microsomal Membranes Modulates Affinity for Drugs. *Angew. Chemie Int. Ed.* **2018**, *57* (13), 3391–3395.
(29) Polasky, Daniel A; Dixit, Sugyan M.; Fantin, Sarah M.; Ruotolo, B. T. “CIUSuite 2: Next-Generation Software for the Analysis of Gas-Phase Protein Unfolding Data.” *Press*.
(30) Marty, M. T.; Baldwin, A. J.; Marklund, E. G.; Hochberg, G. K. A.; Benesch, J. L. P.;

Robinson, C. V. Bayesian Deconvolution of Mass and Ion Mobility Spectra: From Binary Interactions to Polydisperse Ensembles. *Anal. Chem.* **2015**, *87* (8), 4370–4376.
(31) Schenkman, J. B.; Jansson, I. The Many Roles of Cytochrome b 5.
(32) Im, S.-C.; Waskell, L. The Interaction of Microsomal Cytochrome P450 2B4 with Its Redox Partners, Cytochrome P450 Reductase and Cytochrome B5. *Arch. Biochem. Biophys.* **2011**, *507*, 144–153.
(33) Bonfils, C.; Balny, C.; Maurel, P. Direct Evidence for Electron Transfer from Ferrous Cytochrome B5 to the Oxyferrous Intermediate of Liver Microsomal Cytochrome P-450 LM2. *J. Biol. Chem.* **1981**, *256* (18), 9457–9465.
(34) Stayton, P. S.; Fisher, M. T.; Sligar, S. G. Determination of Cytochrome B5 Association Reactions. Characterization of Metmyoglobin and Cytochrome P-450cam Binding to Genetically Engineered Cytochromeb5. *J. Biol. Chem.* **1988**, *263* (27), 13544–13548.
(35) Chiang, J. Y. L. Interaction of Purified Microsomal Cytochrome P-450 with Cytochrome B5. *Arch. Biochem. Biophys.* **1981**, *211* (2), 662–673.
(36) Simtchouk, S.; Eng, J. L.; Meints, C. E.; Makins, C.; Wolthers, K. R. Kinetic Analysis of Cytochrome P450 Reductase from Artemisia Annua Reveals Accelerated Rates of NADH-Dependent Flavin Reduction. *FEBS J.* **2013**, *280* (24), 6627–6642.
(37) Stiborová, M.; Indra, R.; Frei, E.; Kopečková, K.; Schmeiser, H. H.; Eckschlager, T.; Adam, V.; Heger, Z.; Arlt, V. M.; Martínek, V. Cytochrome B5 Plays a Dual Role in the Reaction Cycle of Cytochrome P450 3A4 during Oxidation of the Anticancer Drug Ellipticine. *Monatshefte fur chemie* **2017**, *148* (11), 1983–1991.
(38) Hamdane, D.; Xia, C.; Im, S. C.; Zhang, H.; Kim, J. J. P.; Waskell, L. Structure and Function of an NADPH-Cytochrome P450 Oxidoreductase in an Open Conformation Capable of Reducing Cytochrome P450. *J. Biol. Chem.* **2009**, *284* (17), 11374–11384.
(39) Barnaba, C.; Sahoo, R.; Ravula, T.; Medina-Meza, I. G.; Im, S.-C.; Anantharamaiah, G. M.; Waskell, L.; Ramamoorthy, A. Biophysics Cytochrome-P450-Induced Ordering of Microsomal Membranes Modulates Affinity for Drugs.
(40) Barnaba, C.; Martinez, M. J.; Taylor, E.; Barden, A. O.; Brozik, J. A. Single-Protein Tracking Reveals That NADPH Mediates the Insertion of Cytochrome P450 Reductase into a Biomimetic of the Endoplasmic Reticulum. **2017**.
(41) Estabrook, R. W.; Shet, M. S.; Fisher, C. W.; Jenkins, C. M.; Waterman, M. R. The Interaction of NADPH-P450 Reductase with P450: An Electrochemical Study of the Role of the Flavin Mononucleotide-Binding Domain. *Arch. Biochem. Biophys.* **1996**, *333* (1), 308–315.
(42) Kandel, S. E.; Lampe, J. N. Role of Protein−Protein Interactions in Cytochrome P450-Mediated Drug Metabolism and Toxicity. *Chem. Res. Toxicol.* **2014**, *27*, 1474–1486.
(43) Duggal, R.; Liu, Y.; Gregory, M. C.; Denisov, I. G.; Kincaid, J. R.; Sligar, S. G. Evidence That Cytochrome B5 Acts as a Redox Donor in CYP17A1 Mediated Androgen Synthesis. *Biochem. Biophys. Res. Commun.* **2016**, *477* (2), 202–208.
(44) NOSHIRO, M.; ULLRICH, V.; OMURA, T. Cytochrome B5 as Electron Donor for Oxy-cytochrome P-450. *Eur. J. Biochem.* **1981**, *116* (3), 521–526.
(45) Zhang, M.; Le Clair, S. V; Huang, R.; Ahuja, S.; Im, S.-C.; Waskell, L.; Ramamoorthy, A. Insights into the Role of Substrates on the Interaction between Cytochrome b 5 and Cytochrome P450 2B4 by NMR. **2015**.
(46) Bren, U.; Oostenbrink, C. Cytochrome P450 3A4 Inhibition by Ketoconazole: Tackling the Problem of Ligand Cooperativity Using Molecular Dynamics Simulations and Free-

Energy Calculations. **2012**.
(47) Šrejber, M.; Navrátilová, V.; Paloncýová, M.; Bazgier, V.; Berka, K.; Anzenbacher, P.; Otyepka, M. Membrane-Attached Mammalian Cytochromes P450: An Overview of the Membrane's Effects on Structure, Drug Binding, and Interactions with Redox Partners. *J. Inorg. Biochem.* **2018**, *183*, 117–136.
(48) Kelley, R. W.; Reed, J. R.; Backes, W. L. *Effects of Ionic Strength on the Functional Interactions between CYP2B4 and CYP1A2*; 2005; Vol. 44.
(49) Esteves, F.; Campelo, D.; Gomes, B. C.; Urban, P.; Bozonnet, S.; Lautier, T.; Rueff, J.; Truan, G.; Kranendonk, M. The Role of the FMN-Domain of Human Cytochrome P450 Oxidoreductase in Its Promiscuous Interactions With Structurally Diverse Redox Partners. *Front. Pharmacol.* **2020**, *0*, 299.
(50) Franklin, M. R.; Estabrook, R. W. On the Inhibitory Action of Mersalyl on Microsomal Drug Oxidation: A Rigid Organization of the Electron Transport Chain. *Arch. Biochem. Biophys.* **1971**, *143* (1), 318–329.
(51) Reed, J. R.; Backes, W. L. Formation of P450 · P450 Complexes and Their Effect on P450 Function. *Pharmacol. Ther.* **2012**, *133* (3), 299–310.
(52) Reed, J. R.; Backes, W. L. Formation of P450 · P450 Complexes and Their Effect on P450 Function. *Pharmacol. Ther.* **2012**, *133* (3), 299–310.

Chapter 6 **Conclusions and Future Directions**

6.1 Conclusions

As the gate keepers of the cell, membrane proteins (MPs) represent prime targets for drug discovery due to their vital roles in a multitude of cellular functions.[1–3] Anfinsen's thermodynamic hypothesis[4] states 'that the native conformation [of a protein] is determined by the totality of inter-atomic interactions and hence by the amino acid sequence, in a given environment.' Too often, the last four words are overlooked. The influence of the environment on the structures of membrane proteins is especially noteworthy. MPs interact intimately with the cellular membranes in which they are embedded.[5] Interactions between such proteins and ligands such as membranous lipids and other small molecules can affect MP structure and function.[6] Despite their functional importance, the structural biology of membrane proteins has been particularly challenging, as evidenced by the small number of membrane protein structures that have been determined.[7–9] Ion mobility-mass spectrometry (IM-MS) has recently emerged as a valuable tool for interrogating the interactions between protein and individual ligands, offering direct measurements of protein complex stoichiometry, ligand binding strengths, and stabilities.[10–18]

In this thesis we extended IM-MS technologies to study the relationships between MPs and their lipid environment, probing directly some long-standing questions surrounding the functional role of local lipid environments on MP structure and function. We introduced the instrumentation and methods, as well as provided a background on MP types, membrane mimetics with an emphasis on nanodiscs (NDs) in the first chapter. In chapter 2 we developed a

workflow for studying different MP classes using various solubilization techniques and discussed the implications such membrane mimetics carry in the context of the embedded protein structures they stabilized. We utilized four different MPs that vary in both the way that they span the membrane and in terms of their native oligomeric states. Specifically, we utilized a small multidrug resistance transporter (GDX), a transmembrane protein that has a unique antiparallel orientation, WT and the L16P disease-associated mutant form of peripheral myelin protein (PMP22), a transmembrane protein which occupies both a monomeric and dimeric state, and Cytochrome P450 (CYP), a monotopic membrane-bound enzyme. Each MP system was studied within at least two different mimetics, including: detergent based micelles, lipid bicelles, or NDs. In general, we discovered substantial evidence of differences in MP structure, oligomeric state, and ligand binding that appeared to depend strongly on the membrane mimetic used.

In chapters 3, 4 and 5 we focused on CYP and the deployment of IM-MS and collision induced unfolding (CIU) to study how this centrally important enzyme interacts with binding partners, ligand and its membrane environment in order to carry out essential functions. In chapter 3, we used NDs of carefully designed compositions to study the role of different lipid environments and ND scaffolding proteins on CYP structure. We discovered that CYP CIU data, and by extension its structure, strongly depends on its local environment, and that more native membrane environments can result in more compact and more destabilized CYP forms. In chapter 4 we focused on CYP ligand binding and developed CIU classifiers capable of differentiating CYP binders based on their binding types to the protein and their hydrophilicities. The ability of our CIU assays to differentiate CYP-ligand complexes to differentiate hydrophobic from hydrophilic binders relates directly to the proximity of the CYP active site to the biological membrane and supports the conclusion that lipids are significantly involved in structure of the

CYP active site. Finally, in chapter 5 we studied the interactions between full length CYP, cytochrome b5 (cytb5), and P450 oxioreductase (POR) within NDs. When we co-incubated these proteins with NDs we observed no direct evidence of stable complexes, but significant alterations in protein CIU data, suggesting alterations in CYP, cytb5 and POR structure when present within the same local membrane environment to the other redox partner. We also observed evidence of additional lipid binding events within POR when reduced by NADPH, suggesting deeper membrane engagement when the protein bound to its essential cofactor. We now conclude in Chapter 6 by discussing the future of membrane protein structural biology.

6.2 Future Directions

6.2.1 Application of native IM-MS to other membrane protein systems and amyloids

There is no denying that MPs structure is dependent on the environment in which surrounds it. These high risk, high reward protein class presents many challenges in determining protein structure especially in response to a ligand, whether that be an endogenous lipid modulator or an exogenous compound use for a therapeutic purpose. The simple reality is that our knowledge basis of MPs is far lacking than that of soluble proteins, despite the majority of drugs on the market targeting MPs. In order to safely improve and create new therapeutics we must put forth efforts into understanding these complicated proteins in a membrane environment as well as how they respond to their various ligand targets. These efforts are the future of groundbreaking medical therapies.

More than 10 million people worldwide are living with Parkinson's disease (PD). Synaptic protein Alpha-synuclein (α-syn), the main component of Lewy Bodies (LB), has been identified as a hallmark of PD.[19,20] In solution, α-syn exists in an intrinsically disordered state,

and adopts a more ordered conformation upon membrane association. Misfolded oligomers that interact with the lipid membranes are proposed to be the toxic species in synucleinopathies. However, the details of membrane: α-syn interactions remain unclear and synuclein-drug interactions are rarely investigated within membrane environments.[21] Preliminary work with Yilin Han in the Ruotolo lab, we used IM-MS to investigate the structures of α-syn-drug complexes housed NDs.

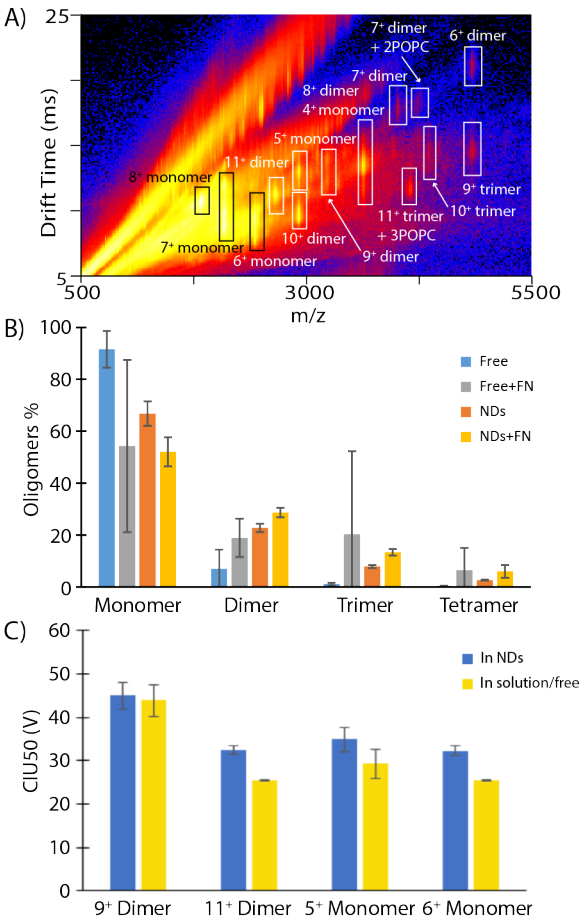

Figure 6-1 preliminary α-syn-ND work **A**) IM-MS data of α-syn incorporated with POPC 4F nanodiscs. **B**) percent oligomer of α-syn under four conditions as calculated through intensity values. **C**) CIU50 values of monomers and dimers of α-syn either free in solution or in a membrane environment.

Figure 6-1 explores our preliminary findings, as α-syn:ND samples are subjected to nESI-IM-MS analysis, we observed a range of signals corresponding to the 6^{+}-15^{+} charge states of native-like α-syn, as well as a number of peaks that relate to ND composition (*e.g.* signals associated with 4F peptides and lipids). The signals associated with α-syn reveal evidence of oligomeric states, including dimers and trimers. The relative amounts of these states are quantitatively enhanced relative to control data collected for α-syn in aqueous solution, indicating that membrane association facilitates the formation of such oligomeric states. Furthermore, the observations of α-syn signals that correspond to lipid bound states, strongly suggests successful incorporation of α-syn into NDs. Previous work by Yilin has investigated the

effect of peptidomimetic compounds on α-syn in aqueous solution, and reported they were able to promote α-syn aggregation through non-covalent binding. IM-MS analysis revealed α-syn-peptidomimetic complexes to be conformationally extended, indicating a unique mode of action for this class of compounds with respect to amyloidogenic targets. Interestingly, when α-syn was incorporated with NDs, we observed lessen small molecule binding and compaction. This mode of action is significantly different from our previous observations of free α-syn bound to this compound class, as it suggests a different conformational response for ND-associated α-syn in the context of NDs. Additional efforts are underway to further characterize peptidomimetic binding affinities, α-syn oligomer state distribution, and conformational preferences associated with ligand-attached states. System such as amyloids and other intrinsically disordered proteins, which are challenging to study with conventional methods show great promise for IM-MS workflows.

In order to make this amendable to high resolution techniques such as NMR, crystallography and cryo-EM we need ways to do this in a higher throughput manner. These high-resolution techniques are very expensive in terms of equipment and methodology. It can take multiple years just to get a structure for some proteins, and bottleneck is optimizing sample conditions. With native MS, the opportunities to screen sample conditions ensuring that the protein is compacted can provide a large advantage as the sample conditions that disrupt the protein structure can be eliminated, thus saving time and resources on these high-resolution instrumentations. Native MS can illuminate insights on a protein and its native conformation by looking at charge state distribution,[22,23] oligomeric state,[24] as well as binding events.[25] Incorporating IM-MS into these workflows will provide CCS information which will provide a more direct insight on protein compactness and thus its overall native-like conformations.[26–28]

Work with the Baily lab and their microfluidic device[29] will further increase high throughput endeavors as this device has the capabilities of adding additional lipid mixing channels allowing for fine tuning of complex lipid compositions. This device also dramatically reduces the time and materials needed to create ND incorporated into ND. One could also envision this device with modifications in order to screen other mimetics such as micelles or bicelles. Coupling this device with buffer exchange and direct infusion onto a mass spectrometer could be the future for screen MP in complicated membrane mimetics.

New improvements for high resolution protein determination is ongoing, of interest is the soft landing concept that couples electron microscopy (EM) with MS.[30–32] Currently the use of the mass spectrometer is being used to first ionize a protein then deposit them onto a grid and then imaged with either negative stain or other high power electron microscopes. The utility of this technology is further being developed into creating a single instrument that is able to ionize, land, and image. This technology is very exciting for the structural biology community as the utility of the mass spectrometry adds a very powerful tool to cryoEM. Future outlook for the technology includes quadrupole selection of discrete ion populations and imaging, for example: one could select a specific charge state and compare it to a different charge state giving us information on how charge deposited on the protein structure affect protein topology, as well as being able to select only ligand bound populations. Being able to select out specific populations of ions deposited would increase class averaging and allow for higher resolved structures.

Current efforts are being implemented into discovering appropriate landing materials for proteins as well as making this amendable to being under vacuum. Additionally, work is being conducted to create a vitreous ice like setup to allow for successful cryo-EM imaging as apart of the soft landing workflow. This technology will no doubt be of high value for soluble proteins,

but one can image this workflow being extended to MPs in the future. As a MP can be encapsulated into a mimetic then ionized and liberated from the mimetic in the gas phase then deposited. Many challenges present itself here, briefly, the landing conditions would need to optimize for MPs that may not survive the soluble protein protocol and an instrument that has a quadrupole or mass selection tool after protein liberation would also provide mass selection and eliminate background noise associated from the membrane mimetic.

Finally, the implantation of IM-MS to a soft-landing workflow would further enhance the utility of this technique. IM-MS has the capabilities of measuring size, shape and charge, so this can further increase the ability of depositing of a uniform species onto grids as well as comparing gas phase CCS values directly those imaged on the grid.[33,34] Both of these experimental values can be compared to PBD CCS values and the possibilities for increasing MD workflows can also greatly be enhanced by these technologies.

6.3 Applications of native IM-MS for drug screening

In chapter 4 we illustrated a robust way of classifying ligands bound to CYP which is a monotopic enzyme capable of interacting with over 80% of the pharmaceutical drug targets on the market.[35–40] Recent work from the Ruotolo lab has also implemented this workflow into looking kinase binders and classifying ligand binding based on how they interact with the active site.[41,42] This workflow presents for a very exciting opportunity for expansion in the drug discovery realm. If a protein target has multiple binding modes, this workflow could allow for screening of new ligands binding in the same modes that mimetic the binding types sought after. One could also envision new types of binders being discovered in the manner as well.

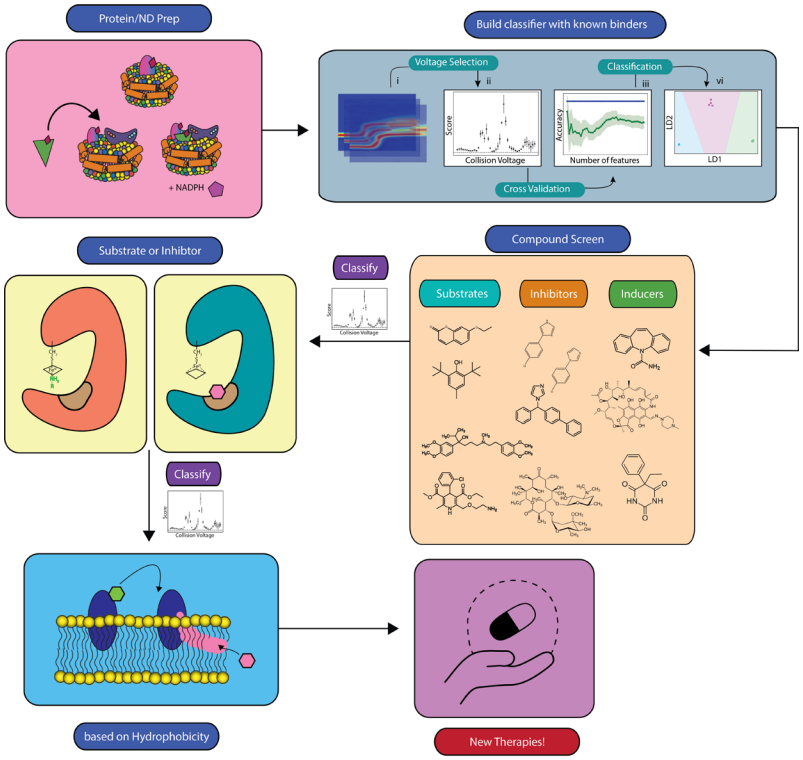

Figure 6-2. Classification drug discovery workflow. Possible expansion and future outlooks for utilizing CIU and CIUSuite2 Classification algorithm to discover new therapeutics, membrane targeted or otherwise

Using the classification algorithm on CIUSuite2 coupled with native IM-MS and CIU also has the possibilities of being another upstream process for the high-resolution techniques discussed earlier. The possibilities to get atomic resolution snap shots of how these molecules alter the protein conformation can first be screened using CIU-classification then later imaged. The ability to not only verify drug binging and buffer conditions, but also the enhanced ability to

discover new drug targets prior to time consuming and expensive atomic resolution imaging could allow for CIU and IM-MS as routine analysis in both research and industrial settings.

6.3.1 Applications of native IM-MS for studying full length CYP redox trio

Overall, the work in this dissertation has emphasized the that a membrane environment has on the membrane protein structure and in chapter 5 we extended this to looking at protein-protein interactions. In addition to add redox partners to CYP, this work further illustrated the utility of using NDs to study MP complexes as these biological membrane bilayers are very intricate and exist in a dynamic environment of not only lipids, but also other proteins.

Many questions remain regarding how cytb5 and POR compete for the second electron donation to CYP. In addition, there are many outstanding questions surrounding how cytb5 interacts with CYP, as it can increase, decrease, inhibit or do at all to the metabolism of a compound. Our work illustrated that POR undergoes a structural shift when reduced with NADPH, future work could include looking at the reduction of cytb5 with NADP. Depending on the concentration of cytb5 vs POR in the presences of CYP can stimulate or decrease activity of catalytic turnover at low ligand concentrations.[43] Future work would include keeping CYP concentration static and altering the POR and cytb5 concentrations in the presence with and without ligand and being able to look at conformation dynamics occurring in these scenarios.

Other CYP homologs have been implicated in various disease states, of these CYPs, CYP17A1 is implicated in prostate cancer, and current therapies inhibit full function of the enzyme rather than selectively inhibiting the specific activity responsible for cell proliferation. CYP17A1 support two distinct steroidogenic reactions, hydroxylation of pregnenolone or progesterone at the carbon 17 position and a 17,20-lyase reaction in which 17-hydroxypregnenolone is converted into dehydroepiandrosterone.[44] Since CYP17A1 is

responsible for all androgen production, it is a main target for the treatment of castration-resistant prostate cancer. Compounds are being tested to inhibit the 17,20-lyase reaction which ultimately reduces the circulated testosterone and prolongs survival in relapsed patients in conjunction with androgen deprivation therapy. Blocking all CYP17A1 activity causes hypertension and potassium loss due to upstream processes, so current efforts are being set forth for selective 17,20-lyase activity inhibition to improve the safety profile for new therapeutics. Cytb5 is known to selectively stimulate the 17,20-lyase activity.[45] Recent work has shown that cytb5 interaction with CYP17A1 alters the dynamics of residues distant from those residues near the active site.[44] Obtaining more information on how cytb5 is interacting with CYP17A1 could lead to groundbreaking medical discoveries to improve prostate cancer patient survival rates.

Bibliography

(1) Osadchy, M.; Kolodny, R. Maps of Protein Structure Space Reveal a Fundamental Relationship between Protein Structure and Function. *Proc. Natl. Acad. Sci. U. S. A.* **2011**, *108* (30), 12301–12306.

(2) Fagerberg, L.; Jonasson, K.; von Heijne, G.; Uhlén, M.; Berglund, L. Prediction of the Human Membrane Proteome. *Proteomics* **2010**, *10* (6), 1141–1149.

(3) Lacapère, J.-J.; Pebay-Peyroula, E.; Neumann, J.-M.; Etchebest, C. Determining Membrane Protein Structures: Still a Challenge! *Trends Biochem. Sci.* **2007**, *32* (6), 259–270.

(4) Anfinsen, C. B. Principles That Govern the Folding of Protein Chains. *Science* **1973**, *181* (4096), 223–230.

(5) Nicolson, G. L. The Fluid—Mosaic Model of Membrane Structure: Still Relevant to Understanding the Structure, Function and Dynamics of Biological Membranes after More than 40years. *Biochim. Biophys. Acta - Biomembr.* **2014**, *1838* (6), 1451–1466.

(6) Cross, T. A.; Sharma, M.; Yi, M.; Zhou, H.-X. Influence of Solubilizing Environments on Membrane Protein Structures. *Trends Biochem. Sci.* **2011**, *36* (2), 117.

(7) Wallin, E.; Heijne, G. Von. Genome-Wide Analysis of Integral Membrane Proteins from Eubacterial, Archaean, and Eukaryotic Organisms. *Protein Sci.* **2008**, *7* (4), 1029–1038.

(8) Shimizu, K.; Cao, W.; Saad, G.; Shoji, M.; Terada, T. Comparative Analysis of Membrane Protein Structure Databases. *Biochim. Biophys. Acta - Biomembr.* **2018**, *1860* (5), 1077–1091.

(9) Moraes, I.; Evans, G.; Sanchez-Weatherby, J.; Newstead, S.; Stewart, P. D. S. Membrane Protein Structure Determination-The next Generation ☆☆. **2014**.

(10) Bender, J.; Schmidt, C. Mass Spectrometry of Membrane Protein Complexes. *Biol. Chem.* **2019**, *400* (7), 813–829.

(11) Barrera, N. P.; Robinson, C. V. Advances in the Mass Spectrometry of Membrane Proteins: From Individual Proteins to Intact Complexes. *Annu. Rev. Biochem.* **2011**, *80* (1), 247–271.

(12) Barrera, N. P.; Isaacson, S. C.; Zhou, M.; Bavro, V. N.; Welch, A.; Schaedler, T. A.; Seeger, M. A.; Miguel, R. N.; Korkhov, V. M.; van Veen, H. W.; Venter, H.; Walmsley, A. R.; Tate, C. G.; Robinson, C. V. Mass Spectrometry of Membrane Transporters Reveals Subunit Stoichiometry and Interactions. *Nat. Methods 2009 68* **2009**, *6* (8), 585–587.

(13) AJ, B.; DJ, H.; CV, R. Detergent Release Prolongs the Lifetime of Native-like Membrane Protein Conformations in the Gas-Phase. *J. Am. Chem. Soc.* **2013**, *135* (16), 6078–6083.

(14) Barrera, N. P.; Zhou, M.; Robinson, C. V. The Role of Lipids in Defining Membrane Protein Interactions: Insights from Mass Spectrometry. *Trends Cell Biol.* **2013**, *23* (1), 1–8.

(15) Hellwig, N.; Peetz, O.; Ahdash, Z.; Tascó, I.; Booth, P. J.; Mikusevic, V.; Diskowski, M.; Politis, A.; Hellmich, Y.; Hä, I.; Reading, E.; Morgner, N. Native Mass Spectrometry Goes More Native: Investigation of Membrane Protein Complexes Directly from

SMALPs †. *Chem. Commun* **2018**, *54*, 13702.
(16) Laganowsky, A.; Reading, E.; Hopper, J. T. S.; Robinson, C. V. Mass Spectrometry of Intact Membrane Protein Complexes. *Nat. Protoc.* **2013**.
(17) Robinson, C. V.; V., C. From Molecular Chaperones to Membrane Motors: Through the Lens of a Mass Spectrometrist. *Biochem. Soc. Trans.* **2017**, *45* (1), 251–260.
(18) AN, C.; SE, R. Mass Spectrometry-Enabled Structural Biology of Membrane Proteins. *Methods* **2018**, *147*, 187–205.
(19) Feigin, V. L.; Nichols, E.; Alam, T.; Bannick, M. S.; Beghi, E.; Blake, N.; Culpepper, W. J.; Dorsey, E. R.; Elbaz, A.; Ellenbogen, R. G.; Fisher, J. L.; Fitzmaurice, C.; Giussani, G.; Glennie, L.; James, S. L.; Johnson, C. O.; Kassebaum, N. J.; Logroscino, G.; Marin, B.; Mountjoy-Venning, W. C.; Nguyen, M.; Ofori-Asenso, R.; Patel, A. P.; Piccininni, M.; Roth, G. A.; Steiner, T. J.; Stovner, L. J.; Szoeke, C. E. I.; Theadom, A.; Vollset, S. E.; Wallin, M. T.; Wright, C.; Zunt, J. R.; Abbasi, N.; Abd-Allah, F.; Abdelalim, A.; Abdollahpour, I.; Aboyans, V.; Abraha, H. N.; Acharya, D.; Adamu, A. A.; Adebayo, O. M.; Adeoye, A. M.; Adsuar, J. C.; Afarideh, M.; Agrawal, S.; Ahmadi, A.; Ahmed, M. B.; Aichour, A. N.; Aichour, I.; Aichour, M. T. E.; Akinyemi, R. O.; Akseer, N.; Al-Eyadhy, A.; Al-Shahi Salman, R.; Alahdab, F.; Alene, K. A.; Aljunid, S. M.; Altirkawi, K.; Alvis-Guzman, N.; Anber, N. H.; Antonio, C. A. T.; Arabloo, J.; Aremu, O.; Ärnlöv, J.; Asayesh, H.; Asghar, R. J.; Atalay, H. T.; Awasthi, A.; Ayala Quintanilla, B. P.; Ayuk, T. B.; Badawi, A.; Banach, M.; Banoub, J. A. M.; Barboza, M. A.; Barker-Collo, S. L.; Bärnighausen, T. W.; Baune, B. T.; Bedi, N.; Behzadifar, M.; Behzadifar, M.; Béjot, Y.; Bekele, B. B.; Belachew, A. B.; Bennett, D. A.; Bensenor, I. M.; Berhane, A.; Beuran, M.; Bhattacharyya, K.; Bhutta, Z. A.; Biadgo, B.; Bijani, A.; Bililign, N.; Bin Sayeed, M. S.; Blazes, C. K.; Brayne, C.; Butt, Z. A.; Campos-Nonato, I. R.; Cantu-Brito, C.; Car, M.; Cárdenas, R.; Carrero, J. J.; Carvalho, F.; Castañeda-Orjuela, C. A.; Castro, F.; Catalá-López, F.; Cerin, E.; Chaiah, Y.; Chang, J. C.; Chatziralli, I.; Chiang, P. P. C.; Christensen, H.; Christopher, D. J.; Cooper, C.; Cortesi, P. A.; Costa, V. M.; Criqui, M. H.; Crowe, C. S.; Damasceno, A. A. M.; Daryani, A.; De la Cruz-Góngora, V.; De La Hoz, F. P.; De Leo, D.; Degefa, M. G.; Demoz, G. T.; Deribe, K.; Dharmaratne, S. D.; Diaz, D.; Dinberu, M. T.; Djalalinia, S.; Doku, D. T.; Dubey, M.; Dubljanin, E.; Duken, E. E.; Edvardsson, D.; El-Khatib, Z.; Endres, M.; Endries, A. Y.; Eskandarieh, S.; Esteghamati, A.; Esteghamati, S.; Farhadi, F.; Faro, A.; Farzadfar, F.; Farzaei, M. H.; Fatima, B.; Fereshtehnejad, S. M.; Fernandes, E.; Feyissa, G. T.; Filip, I.; Fischer, F.; Fukumoto, T.; Ganji, M.; Gankpe, F. G.; Garcia-Gordillo, M. A.; Gebre, A. K.; Gebremichael, T. G.; Gelaw, B. K.; Geleijnse, J. M.; Geremew, D.; Gezae, K. E.; Ghasemi-Kasman, M.; Gidey, M. Y.; Gill, P. S.; Gill, T. K.; Gnedovskaya, E. V.; Goulart, A. C.; Grada, A.; Grosso, G.; Guo, Y.; Gupta, R.; Gupta, R.; Haagsma, J. A.; Hagos, T. B.; Haj-Mirzaian, A.; Haj-Mirzaian, A.; Hamadeh, R. R.; Hamidi, S.; Hankey, G. J.; Hao, Y.; Haro, J. M.; Hassankhani, H.; Hassen, H. Y.; Havmoeller, R.; Hay, S. I.; Hegazy, M. I.; Heidari, B.; Henok, A.; Heydarpour, F.; Hoang, C. L.; Hole, M. K.; Homaie Rad, E.; Hosseini, S. M.; Hu, G.; Igumbor, E. U.; Ilesanmi, O. S.; Irvani, S. S. N.; Islam, S. M. S.; Jakovljevic, M.; Javanbakht, M.; Jha, R. P.; Jobanputra, Y. B.; Jonas, J. B.; Józwiak, J. J.; Jürisson, M.; Kahsay, A.; Kalani, R.; Kalkonde, Y.; Kamil, T. A.; Kanchan, T.; Karami, M.; Karch, A.; Karimi, N.; Kasaeian, A.; Kassa, T. D.; Kassa, Z. Y.; Kaul, A.; Kefale, A. T.; Keiyoro, P. N.; Khader, Y. S.; Khafaie, M. A.; Khalil, I. A.; Khan, E. A.; Khang, Y. H.; Khazaie, H.; Kiadaliri, A. A.; Kiirithio, D. N.; Kim, A. S.; Kim, D.; Kim, Y. E.; Kim,

Y. J.; Kisa, A.; Kokubo, Y.; Koyanagi, A.; Krishnamurthi, R. V.; Kuate Defo, B.; Kucuk Bicer, B.; Kumar, M.; Lacey, B.; Lafranconi, A.; Lansingh, V. C.; Latifi, A.; Leshargie, C. T.; Li, S.; Liao, Y.; Linn, S.; Lo, W. D.; Lopez, J. C. F.; Lorkowski, S.; Lotufo, P. A.; Lucas, R. M.; Lunevicius, R.; Mackay, M. T.; Mahotra, N. B.; Majdan, M.; Majdzadeh, R.; Majeed, A.; Malekzadeh, R.; Malta, D. C.; Manafi, N.; Mansournia, M. A.; Mantovani, L. G.; März, W.; Mashamba-Thompson, T. P.; Massenburg, B. B.; Mate, K. K. V.; McAlinden, C.; McGrath, J. J.; Mehta, V.; Meier, T.; Meles, H. G.; Melese, A.; Memiah, P. T. N.; Memish, Z. A.; Mendoza, W.; Mengistu, D. T.; Mengistu, G.; Meretoja, A.; Meretoja, T. J.; Mestrovic, T.; Miazgowski, B.; Miazgowski, T.; Miller, T. R.; Mini, G. K.; Mirrakhimov, E. M.; Moazen, B.; Mohajer, B.; Mohammad Gholi Mezerji, N.; Mohammadi, M.; Mohammadi-Khanaposhtani, M.; Mohammadibakhsh, R.; Mohammadnia-Afrouzi, M.; Mohammed, S.; Mohebi, F.; Mokdad, A. H.; Monasta, L.; Mondello, S.; Moodley, Y.; Moosazadeh, M.; Moradi, G.; Moradi-Lakeh, M.; Moradinazar, M.; Moraga, P.; Moreno Velásquez, I.; Morrison, S. D.; Mousavi, S. M.; Muhammed, O. S.; Muruet, W.; Musa, K. I.; Mustafa, G.; Naderi, M.; Nagel, G.; Naheed, A.; Naik, G.; Najafi, F.; Nangia, V.; Negoi, I.; Negoi, R. I.; Newton, C. R. J.; Ngunjiri, J. W.; Nguyen, C. T.; Nguyen, L. H.; Ningrum, D. N. A.; Nirayo, Y. L.; Nixon, M. R.; Norrving, B.; Noubiap, J. J.; Nourollahpour Shiadeh, M.; Nyasulu, P. S.; Ogbo, F. A.; Oh, I. H.; Olagunju, A. T.; Olagunju, T. O.; Olivares, P. R.; Onwujekwe, O. E.; Oren, E.; Owolabi, M. O.; A, M. P.; Pakpour, A. H.; Pan, W. H.; Panda-Jonas, S.; Pandian, J. D.; Patel, S. K.; Pereira, D. M.; Petzold, M.; Pillay, J. D.; Piradov, M. A.; Polanczyk, G. V.; Polinder, S.; Postma, M. J.; Poulton, R.; Poustchi, H.; Prakash, S.; Prakash, V.; Qorbani, M.; Radfar, A.; Rafay, A.; Rafiei, A.; Rahim, F.; Rahimi-Movaghar, V.; Rahman, M.; Rahman, M. H. U.; Rahman, M. A.; Rajati, F.; Ram, U.; Ranta, A.; Rawaf, D. L.; Rawaf, S.; Reinig, N.; Reis, C.; Renzaho, A. M. N.; Resnikoff, S.; Rezaeian, S.; Rezai, M. S.; Rios González, C. M.; Roberts, N. L. S.; Roever, L.; Ronfani, L.; Roro, E. M.; Roshandel, G.; Rostami, A.; Sabbagh, P.; Sacco, R. L.; Sachdev, P. S.; Saddik, B.; Safari, H.; Safari-Faramani, R.; Safi, S.; Safiri, S.; Sagar, R.; Sahathevan, R.; Sahebkar, A.; Sahraian, M. A.; Salamati, P.; Salehi Zahabi, S.; Salimi, Y.; Samy, A. M.; Sanabria, J.; Santos, I. S.; Santric Milicevic, M. M.; Sarrafzadegan, N.; Sartorius, B.; Sarvi, S.; Sathian, B.; Satpathy, M.; Sawant, A. R.; Sawhney, M.; Schneider, I. J. C.; Schöttker, B.; Schwebel, D. C.; Seedat, S.; Sepanlou, S. G.; Shabaninejad, H.; Shafieesabet, A.; Shaikh, M. A.; Shakir, R. A.; Shams-Beyranvand, M.; Shamsizadeh, M.; Sharif, M.; Sharif-Alhoseini, M.; She, J.; Sheikh, A.; Sheth, K. N.; Shigematsu, M.; Shiri, R.; Shirkoohi, R.; Shiue, I.; Siabani, S.; Siddiqi, T. J.; Sigfusdottir, I. D.; Sigurvinsdottir, R.; Silberberg, D. H.; Silva, J. P.; Silveira, D. G. A.; Singh, J. A.; Sinha, D. N.; Skiadaresi, E.; Smith, M.; Sobaih, B. H.; Sobhani, S.; Soofi, M.; Soyiri, I. N.; Sposato, L. A.; Stein, D. J.; Stein, M. B.; Stokes, M. A.; Sufiyan, M. B.; Sykes, B. L.; Sylaja, P.; Tabarés-Seisdedos, R.; Te Ao, B. J.; Tehrani-Banihashemi, A.; Temsah, M. H.; Temsah, O.; Thakur, J. S.; Thrift, A. G.; Topor-Madry, R.; Tortajada-Girbés, M.; Tovani-Palone, M. R.; Tran, B. X.; Tran, K. B.; Truelsen, T. C.; Tsadik, A. G.; Tudor Car, L.; Ukwaja, K. N.; Ullah, I.; Usman, M. S.; Uthman, O. A.; Valdez, P. R.; Vasankari, T. J.; Vasanthan, R.; Veisani, Y.; Venketasubramanian, N.; Violante, F. S.; Vlassov, V.; Vosoughi, K.; Vu, G. T.; Vujcic, I. S.; Wagnew, F. S.; Waheed, Y.; Wang, Y. P.; Weiderpass, E.; Weiss, J.; Whiteford, H. A.; Wijeratne, T.; Winkler, A. S.; Wiysonge, C. S.; Wolfe, C. D. A.; Xu, G.; Yadollahpour, A.; Yamada, T.; Yano, Y.; Yaseri, M.; Yatsuya, H.; Yimer, E. M.; Yip, P.; Yisma, E.;

Yonemoto, N.; Yousefifard, M.; Yu, C.; Zaidi, Z.; Zaman, S. Bin; Zamani, M.; Zandian, H.; Zare, Z.; Zhang, Y.; Zodpey, S.; Naghavi, M.; Murray, C. J. L.; Vos, T. Global, Regional, and National Burden of Neurological Disorders, 1990-2016: A Systematic Analysis for the Global Burden of Disease Study 2016. *Lancet. Neurol.* **2019**, *18* (5), 459–480.

(20) Maruthi Prasad, E.; Hung, S. Y. Current Therapies in Clinical Trials of Parkinson's Disease: A 2021 Update. *Pharmaceuticals (Basel).* **2021**, *14* (8).

(21) Oliveira, L. M. A.; Gasser, T.; Edwards, R.; Zweckstetter, M.; Melki, R.; Stefanis, L.; Lashuel, H. A.; Sulzer, D.; Vekrellis, K.; Halliday, G. M.; Tomlinson, J. J.; Schlossmacher, M.; Jensen, P. H.; Schulze-Hentrich, J.; Riess, O.; Hirst, W. D.; El-Agnaf, O.; Mollenhauer, B.; Lansbury, P.; Outeiro, T. F. Alpha-Synuclein Research: Defining Strategic Moves in the Battle against Parkinson's Disease. *NPJ Park. Dis.* **2021**, *7* (1).

(22) Fenn, J. B.; Mann, M.; Meng, C. K.; Wong, S. F.; Whitehouse, C. M. Electrospray Ionization for Mass Spectrometry of Large Biomolecules. *Science* **1989**, *246* (4926), 64–71.

(23) Chowdhury, S. K.; Katta, V.; Chait, B. T. Probing Conformational Changes in Proteins by Mass Spectrometry. *J. Am. Chem. Soc.* **1990**, *112* (24), 9012–9013.

(24) Loo, J. A. Observation of Large Subunit Protein Complexes by Electrospray Ionization Mass Spectrometry. *J. Mass Spectrom.* **1995**, *30* (1), 180–183.

(25) Robinson, C. V.; Radford, S. E. Weighing the Evidence for Structure: Electrospray Ionization Mass Spectrometry of Proteins. *Structure* **1995**, *3* (9), 861–865.

(26) Reading, E.; Hall, Z.; Martens, C.; Haghighi, T.; Findlay, H.; Ahdash, Z.; Politis, A.; Booth, P. J. Interrogating Membrane Protein Conformational Dynamics within Native Lipid Compositions. *Angew. Chemie Int. Ed.* **2017**, *56* (49), 15654–15657.

(27) Dixit, S. M.; Polasky, D. A.; Ruotolo, B. T. Collision Induced Unfolding of Isolated Proteins in the Gas Phase: Past, Present, and Future. *Curr. Opin. Chem. Biol.* **2018**, *42*, 93–100.

(28) Vallejo, D. D.; Rojas Ramírez, C.; Parson, K. F.; Han, Y.; Gadkari, V. V.; Ruotolo, B. T. Mass Spectrometry Methods for Measuring Protein Stability. *Chem. Rev.* **2022**, *122* (8), 7690–7719.

(29) Wade, J. H.; Jones, J. D.; Lenov, I. L.; Riordan, C. M.; Sligar, S. G.; Bailey, R. C. Microfluidic Platform for Efficient Nanodisc Assembly, Membrane Protein Incorporation, and Purification. *Lab Chip* **2017**, *17* (17), 2951–2959.

(30) Benesch, J. L. P.; Ruotolo, B. T.; Simmons, D. A.; Barrera, N. P.; Morgner, N.; Wang, L.; Saibil, H. R.; Robinson, C. V. Separating and Visualising Protein Assemblies by Means of Preparative Mass Spectrometry and Microscopy. *J. Struct. Biol.* **2010**, *172* (2), 161–168.

(31) Johnson, G. E.; Hu, Q.; Laskin, J. Soft Landing of Complex Molecules on Surfaces *. *Annu. Rev. Anal. Chem. is online Annu. Rev. Anal. Chem* **2011**, *4*, 83–104.

(32) Ouyang, Z.; Takáts, Z.; Blake, T. A.; Gologan, B.; Guymon, A. J.; Wiseman, J. M.; Oliver, J. C.; Davisson, V. J.; Cooks, R. G. Preparing Protein Microarrays by Soft-Landing of Mass-Selected Ions. *Science* **2003**, *301* (5638), 1351–1354.

(33) Verbeck, G.; Hoffmann, W.; Walton, B. Soft-Landing Preparative Mass Spectrometry. *Analyst* **2012**, *137* (19), 4393–4407.

(34) Longchamp, J. N.; Rauschenbach, S.; Abb, S.; Escher, C.; Latychevskaia, T.; Kern, K.; Fink, H. W. Imaging Proteins at the Single-Molecule Level. *Proc. Natl. Acad. Sci. U. S. A.* **2017**, *114* (7), 1474–1479.

(35) Denisov, I. G.; Makris, T. M.; Sligar, S. G.; Schlichting, I. Structure and Chemistry of Cytochrome P450. **2005**.
(36) Barnaba, C.; Gentry, K.; Sumangala, N.; Ramamoorthy, A.; Denisov, I.; Melacini, G. Open Peer Review The Catalytic Function of Cytochrome P450 Is Entwined with Its Membrane-Bound Nature [Version 1; Referees: 4 Approved]. **2017**.
(37) Cheng, Q.; Sohl, C. D.; Guengerich, F. P. High-Throughput Fluorescence Assay of Cytochrome P450 3A4. *Nat. Protoc.* **2009**, *4* (9), 1258–1261.
(38) Wienkers, L. C.; Heath, T. G. Predicting in Vivo Drug Interactions from in Vitro Drug Discovery Data. *Nat. Rev. Drug Discov.* **2005**, *4* (10), 825–833.
(39) Williams, J. A.; Ring, B. J.; Cantrell, V. E.; Jones, D. R.; Eckstein, J.; Ruterbories, K.; Hamman, M. A.; Hall, S. D.; Wrighton, S. A. Comparative Metabolic Capabilities of CYP3A4, CYP3A5, and CYP3A7. *Drug Metab. Dispos.* **2002**, *30* (8), 883–891.
(40) Barnaba, C.; Sahoo, B. R.; Ravula, T.; Medina-Meza, I. G.; Im, S.-C.; Anantharamaiah, G. M.; Waskell, L.; Ramamoorthy, A. Cytochrome-P450-Induced Ordering of Microsomal Membranes Modulates Affinity for Drugs. *Angew. Chemie Int. Ed.* **2018**, *57* (13), 3391–3395.
(41) Rabuck, J. N.; Hyung, S.-J.; Ko, K. S.; Fox, C. C.; Soellner, M. B.; Ruotolo, B. T. An Activation State-Selective Kinase Inhibitor Assay Based on Ion Mobility-Mass Spectrometry. *Anal. Chem.* **2013**, *85* (15), 6995.
(42) Polasky, D. A.; Dixit, S. M.; Vallejo, D. D.; Kulju, K. D.; Ruotolo, B. T. An Algorithm for Building Multi-State Classifiers Based on Collision-Induced Unfolding Data. *Anal. Chem.* **2019**, *91* (16), 10407–10412.
(43) Im, S.-C.; Waskell, L. The Interaction of Microsomal Cytochrome P450 2B4 with Its Redox Partners, Cytochrome P450 Reductase and Cytochrome B5. *Arch. Biochem. Biophys.* **2011**, *507*, 144–153.
(44) Fernando Estrada, D.; Laurence, J. S.; Scott, E. E. Cytochrome P450 17A1 Interactions with the FMN Domain of Its Reductase as Characterized by NMR *. *J. Biol. Chem.* **2016**, *291* (8), 3990–4003.
(45) Peng, H. M.; Im, S. C.; Pearl, N. M.; Turcu, A. F.; Rege, J.; Waskell, L.; Auchus, R. J. Cytochrome B5 Activates the 17,20-Lyase Activity of Human Cytochrome P450 17A1 by Increasing the Coupling of NADPH Consumption to Androgen Production. *Biochemistry* **2016**, *55* (31), 4356–436

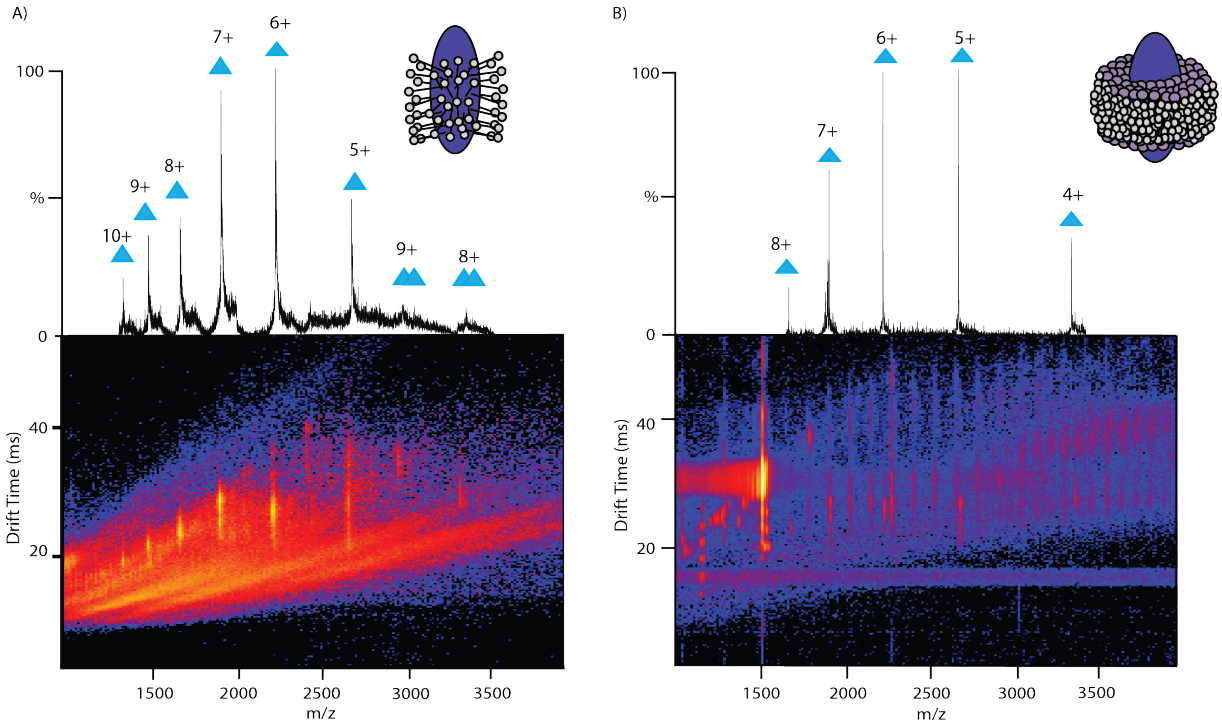

Appendix Figure I-1 GDX MS and drift scope out of DDM and POPC-DDMB bicelles

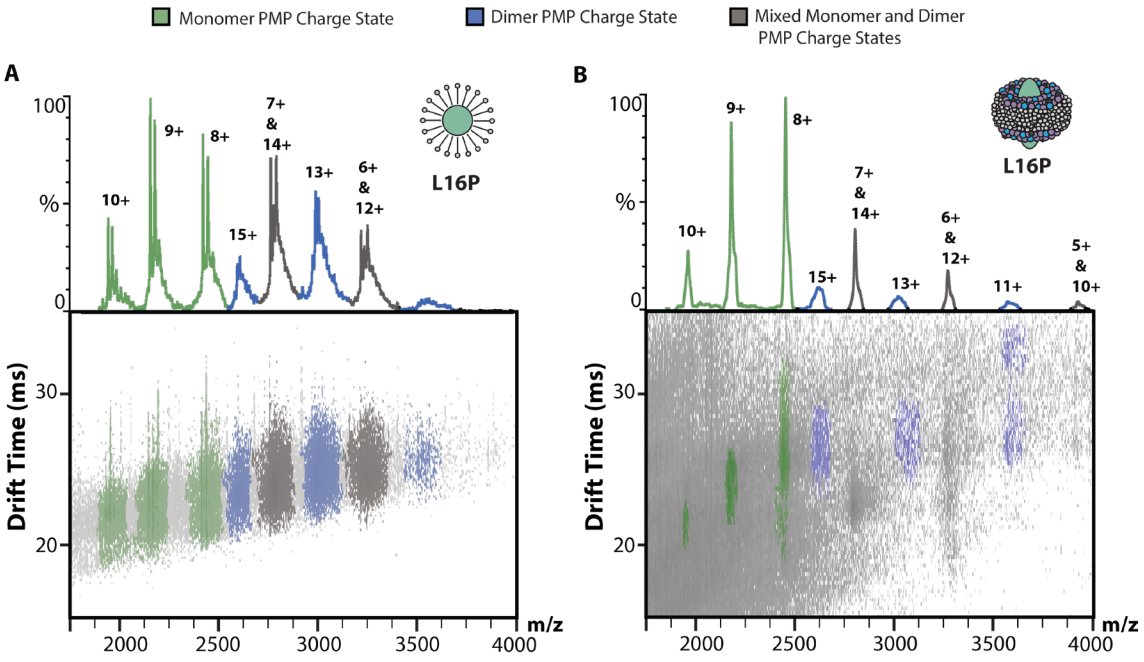

Appendix Figure I-2 Mass spectra and IM-MS datasets of L16P PMP22 liberated from micelles and SCOR bicelles.A, B. When released from C12E8 micelles or SCOR bicelles, monomeric (green), dimeric (blue), and overlapping monomeric and dimeric (gray) charge states of L16P PMP22 can be detected. The 13+ dimeric charge state was chosen for CIU analysis.

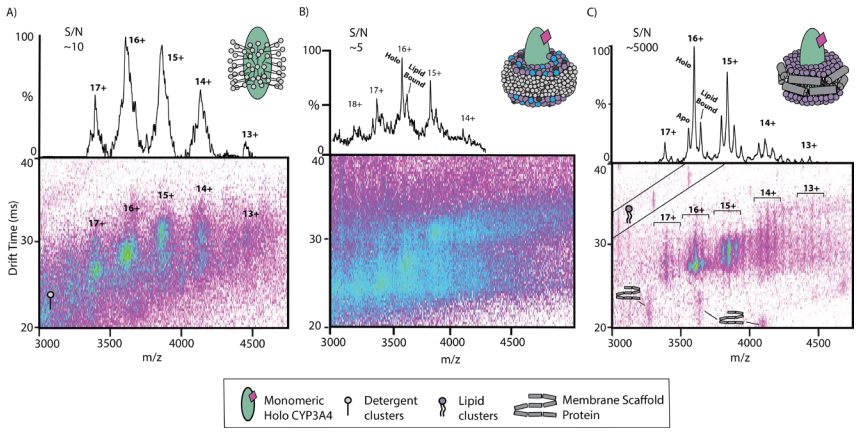

Appendix Figure I-4 Mass spectra and IM-MS datasets of CYP3A4 liberated from micelles, bicelles, and nanodiscs.A). CYP 3A4 can be observed with the charge state distribution of 13-17+ when liberated from OG micelles. These peaks are broad enough that apo and holo protein forms cannot be resolved, however the centroid of the peak aligns well with weight for the holo CYP 3A4. The peak broadness could be caused by detergent adduction. S/N ~10 B) CYP3A4 liberated from SCOR bicelles, charge states 14-18+ observed as well as lipid binding resulting a lower resolution between peaks, S/N~5 C). When liberated from nanodiscs, the apo, holo, and lipid bound peaks of CYP 3A4 can be resolved for the charge states 13-17+ S/N~5,000

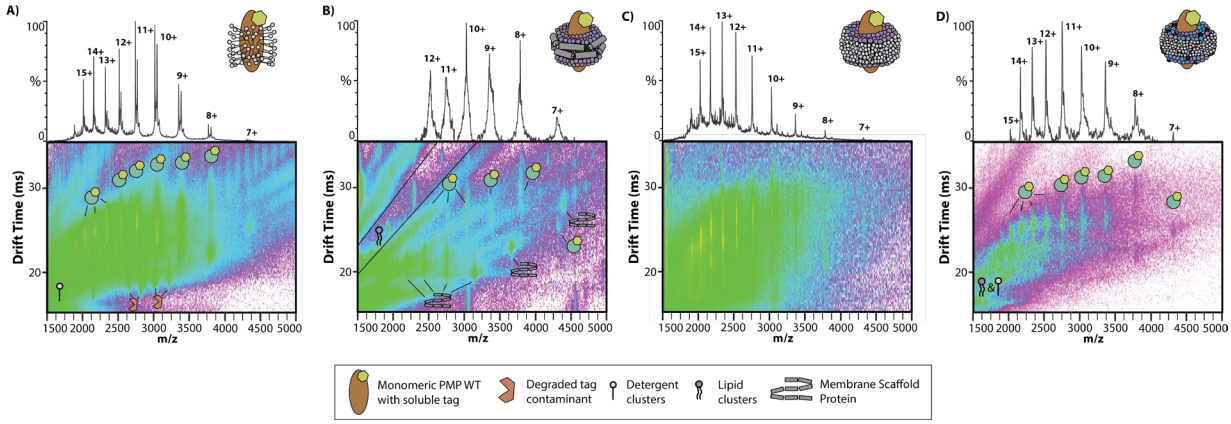

Appendix Figure I-3 Mass spectra and IM-MS datasets of WTtag PMP22 liberated from micelles, SCOR bicelles, and POPC nanodiscs. A. When released from C12E8 micelles monomeric WTtag PMP22 can be observed from 7-15+, along with detergent related noise and a smaller contaminant protein. This contaminant could be related to degraded forms of the 11 kDa soluble tag, but we do not observe it to interact with the protein and the signals do not interfere with the 9+ charge state CIU. ted. The 9+ monomeric charge state was chosen for CIU analysis. B. When released from SCOR bicelles monomeric WTtag PMP22 can be observed from 7-15+, along with detergent and lipid related noise signals. C. When released from POPC nanodiscs, monomeric WTtag PMP22 can be observed from 7-12+, however any higher charge state overlaps significantly with MSP1D1 signals and cannot be distinguished. Some charge states can be separated in IM space from MSP1D1 although they possess significant mass to charge overlap. The 9+ charge state is the most distant in mass to charge space from MSP1D1 signals and was chosen for CIU analysis

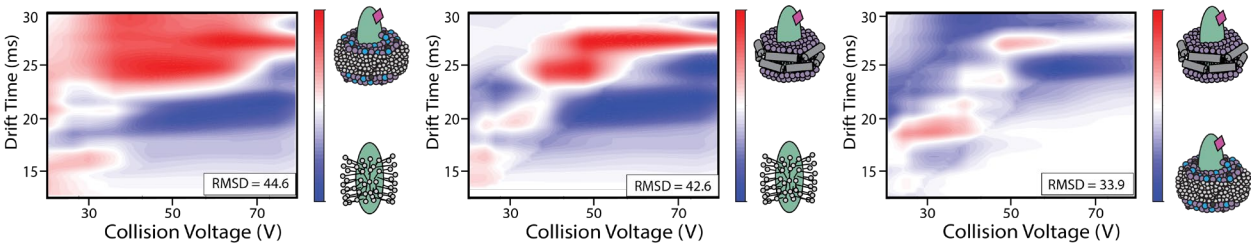

Appendix Figure I-5 RMSD comparisons for PMP22wt across all mimetics

Appendix II Chapter 4 Supporting Information

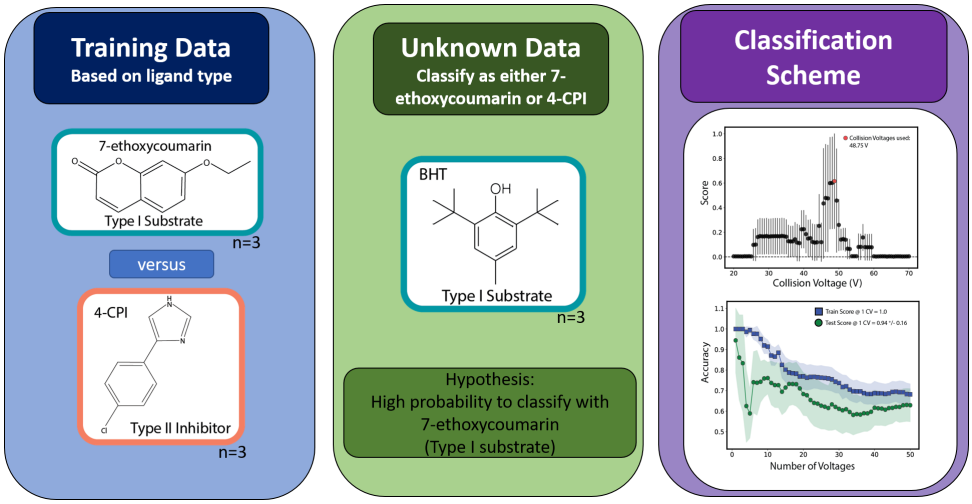

Appendix Figure III-1 Classification scheme for 7-ethoxycoumarin vs 4CPI, unknown BHT

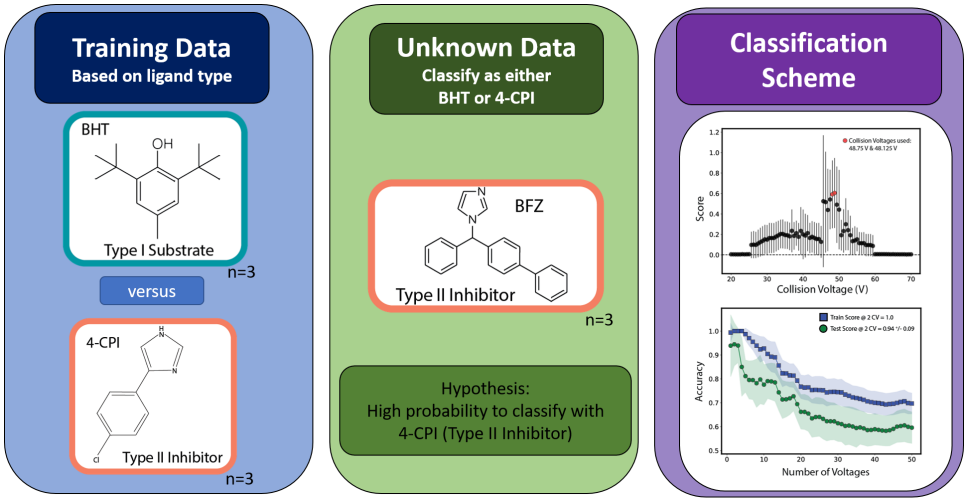

Appendix Figure III-2 Classification Scheme for BHT vs 4-CPI, unknown BFZ

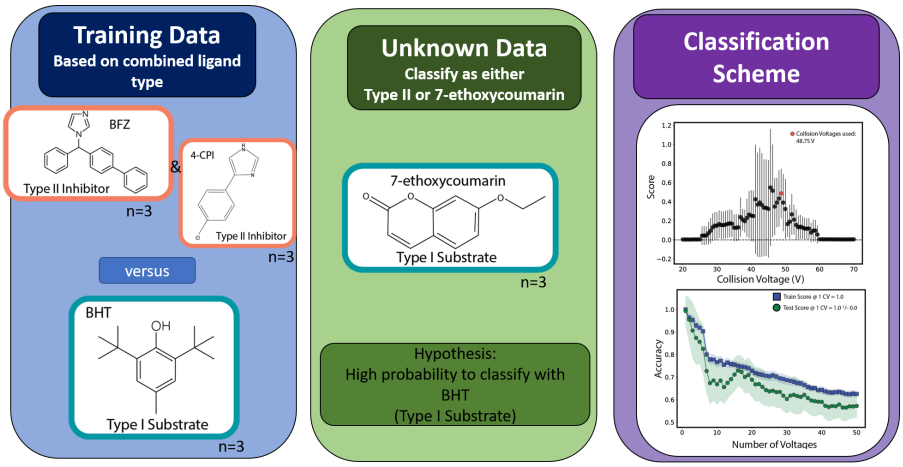

Appendix Figure III-3 Classification scheme for Type II inhibitors vs BHT (TI), unknown 7-ethoxycoumarin

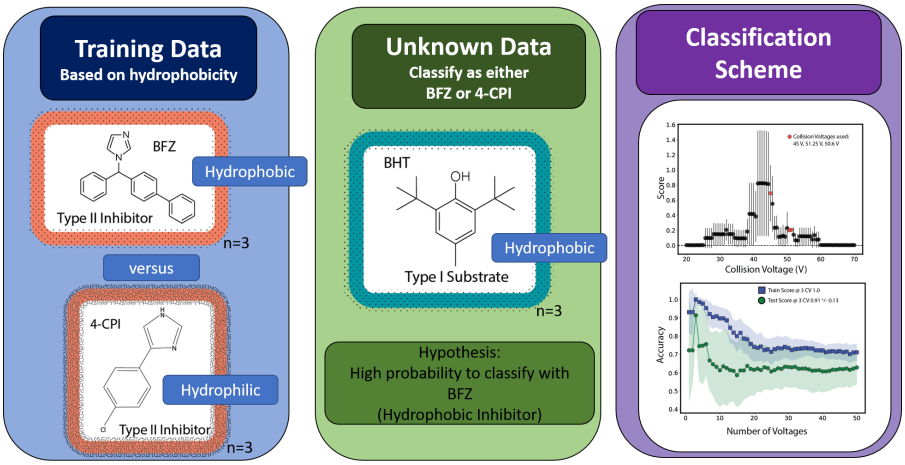

Appendix Figure III-4 Classification scheme for hydrophobic vs hydrophilic, unknown BHT

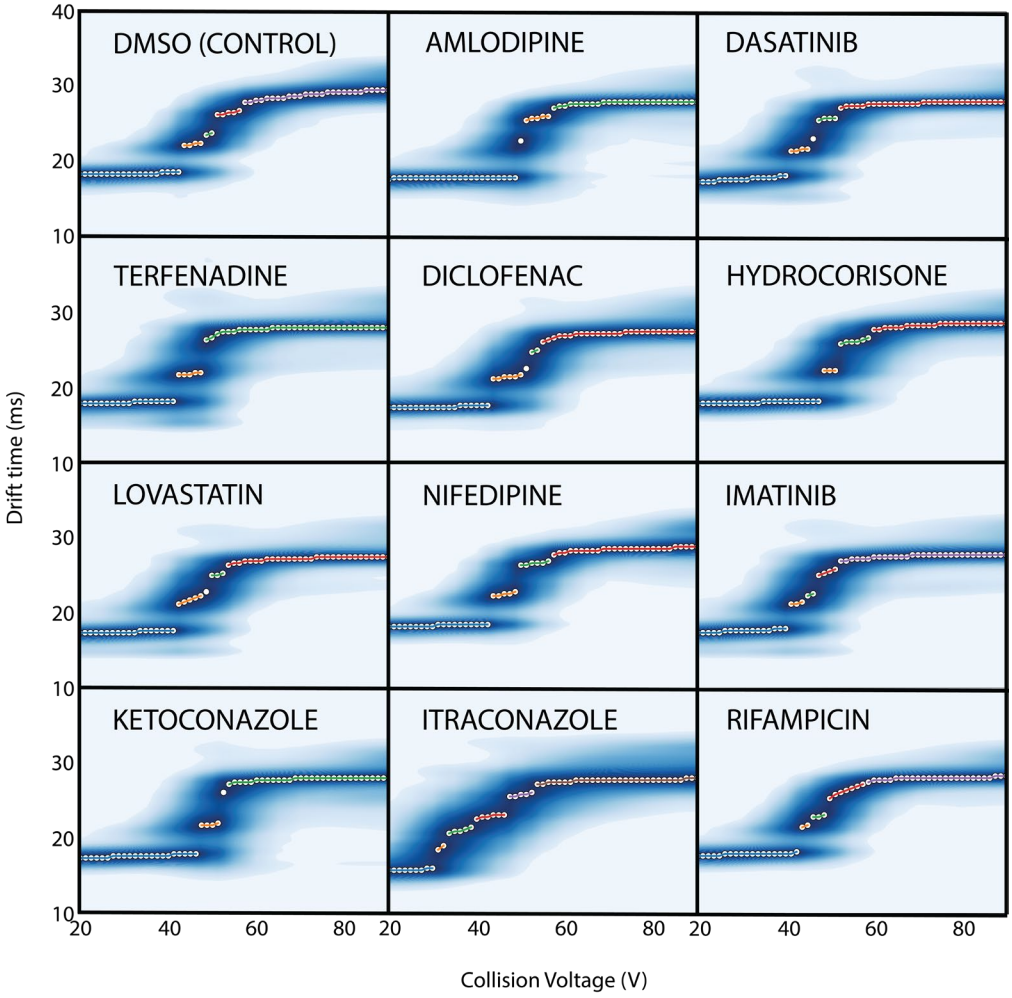

Appendix Figure III-5 CIU fingerprints for all CYP3A4 13+ ligand bound species

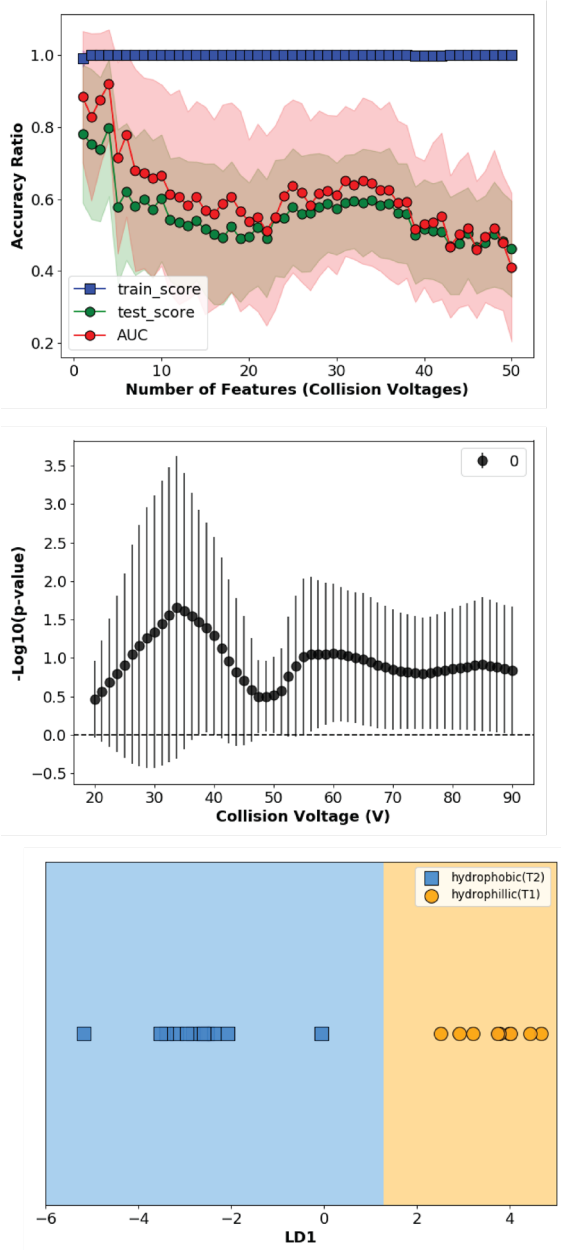

Appendix Figure III-6 Classification Scheme for 2-way classifier for determining CYP3A4 hydrophobicity

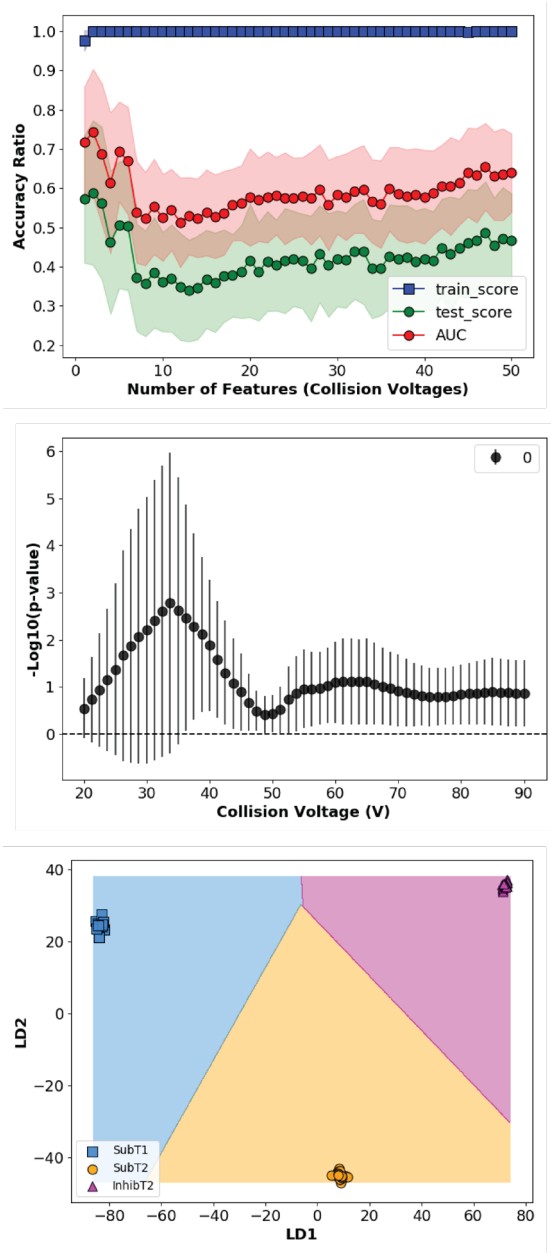

Appendix Figure III-7 Classification Scheme for 3-way classifier for determining CYP3A4 ligand biding types

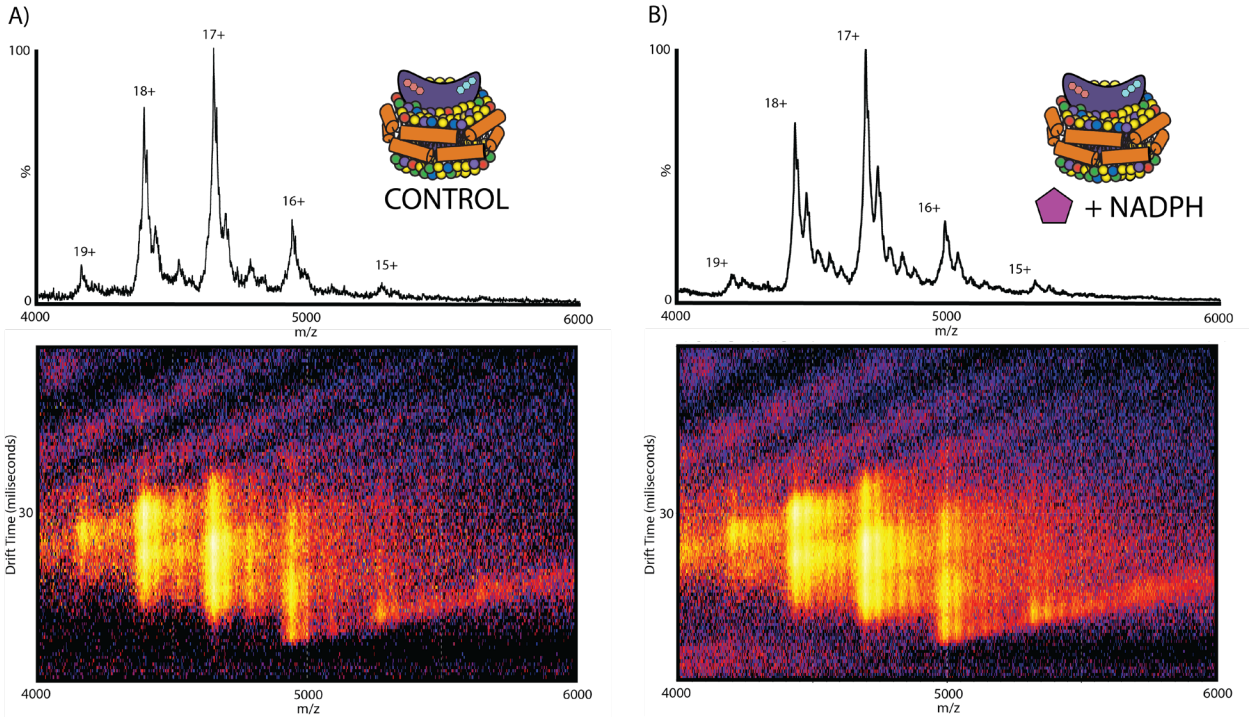

Appendix Figure IV-1 POR liberated from mix ER 4F ND with and without NADPH Mass spectrum with native like charge state distribution of 15-19+ on top and drift scope on bottom **A**) without NADPH, two main peaks present and **B**) with NADPH increased binding effects are observed

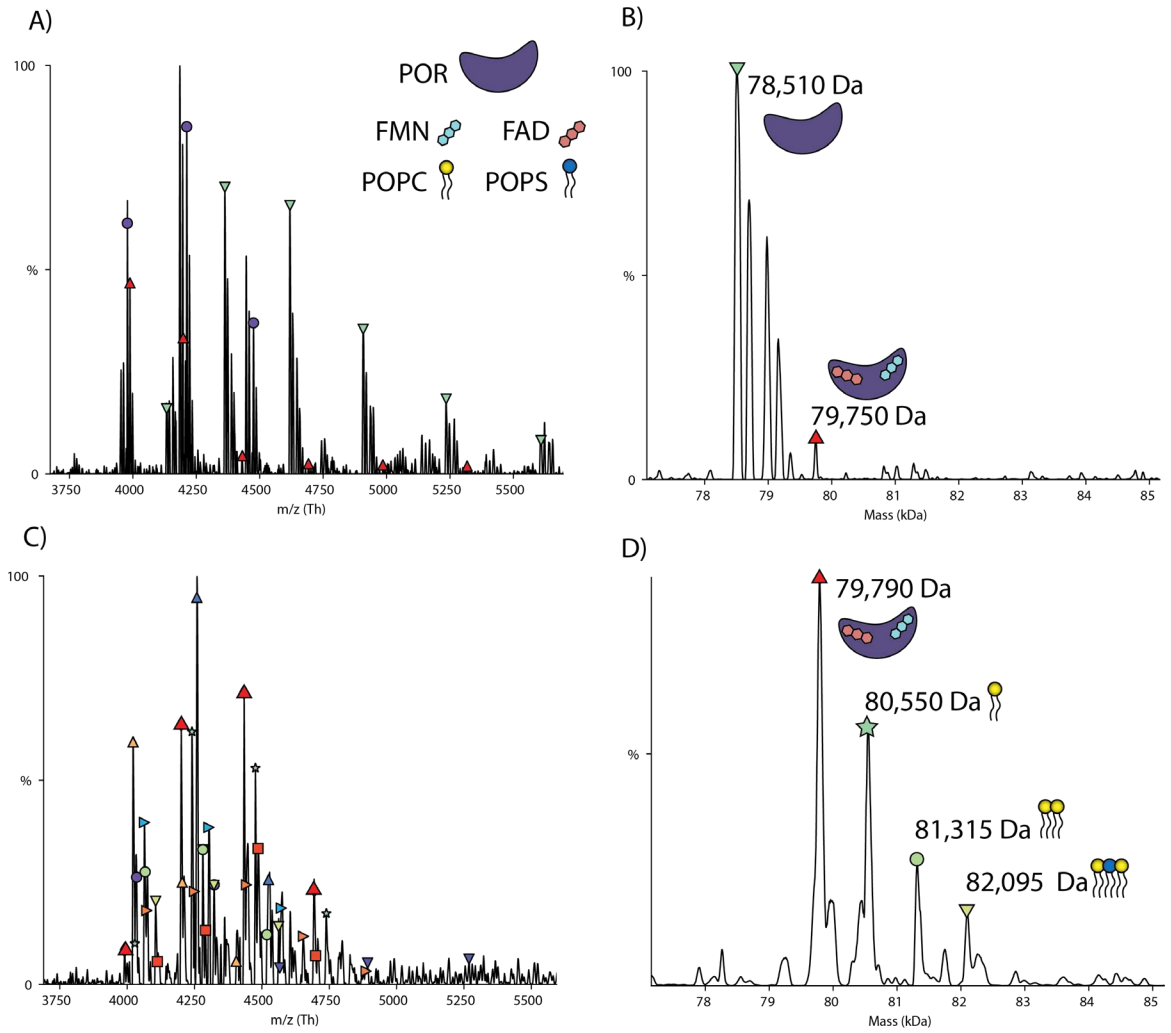

Appendix Figure IV-2 High resolution mass spectrometry data of POR.**A**) POR liberated from mix ER 4F ND without NADPH **B**) deconvoluted mass spectrum indicated masses of the two main observed species **C**) POR liberated from mix ER 4F ND with NADPH **D**) deconvoluted mass spectrum indicated masses of bound peaks and the ID of POPC and POPS lipids